MEASUREMENT OF THE EFFICIENCY OF A FLASHING FLOW NOZZLE

by

Michael P. Alexandrian

Thesis submitted to the Faculty of the
Virginia Polytechnic Institute and State University
in partial fulfillment of the requirements for the degree of
MASTER OF SCIENCE
in
Mechanical Engineering

APPROVED:

_____

Dr. Alan A. Kornhauser, Chairperson

_____ _____

Dr. Thomas E. Diller Dr. Eugene F. Brown, P.E.

September, 1994
Blacksburg, Virginia

MEASUREMENT OF THE EFFICIENCY OF A FLASHING FLOW NOZZLE

by

Michael P. Alexandrian
Committee Chairman: Dr. A. A. Kornhauser
Mechanical Engineering Department

(ABSTRACT)

The efficiency of a flashing flow converging-diverging nozzle was measured. The primary motivation for measurement of nozzle efficiency in this work was to improve the performance of an ejector as a refrigerant expander; previous experimentation has suggested that motive nozzle efficiency is poor.

Measurement of the efficiency was performed using a technique which does not require knowledge of the non-equilibrium nozzle outlet state. This technique is based on the measurement of nozzle thrust and mass flow rate to determine the actual kinetic energy at the nozzle exit. A vapor compression refrigeration cycle using refrigerant R-12 was employed to test the nozzle. Use of a bubble seeding device upstream of the nozzle to provide nucleation sites in the flow was expected to decrease the non-equilibrium, therefore producing an increase in nozzle efficiency.

Experiments were performed at various condenser pressures and mass flow rates. In addition to the efficiency measurement, a parameter to quantify the metastability in the nozzle flow was defined and empirical correlations were developed for both. The experimentation illustrated that the efficiency did indeed increase when flow conditions were closer to equilibrium. Efficiency and metastability parameter results indicate an unexplained dependence on the condenser subcooling. Recommendations were therefore made to investigate this unexpected phenomenon.

ACKNOWLEDGMENTS

I would first like to thank my advisor, Dr. A. A. Kornhauser, for his guidence and insight into this work. I would also like to thank the other members of my thesis committee, Dr. T. E. Diller and Dr. E. F. Brown, for their crucial input for the completion of this work. All the members of the committee were a pleasure to work with.

I would like to thank Calmac, Inc., especially Mr. Richard Hrbeck, for the support and friendship received throughout the duration of this task.

I would also like to thank my fellow students, Greg Harrell, Peter Menegay, Bryan Kafka, Frank Cantelmi, Doug Hudgins, Stephen Canfield, and Jeff Miller, for their support and encouragement for the completion of this work.

TABLE OF CONTENTS

LIST OF FIGURES

LIST OF TABLES

NOMENCLATURE

Variables

COP	Coefficient of Performance
T	Temperature
s	Entropy
C_d	Discharge Coefficient
$\dot{m}$	Mass Flow Rate (lbm/min)
A	Area
ρ	Density
h	Enthalpy
η	Efficiency
F	Thrust
U	Velocity
V	Voltage
ε	Strain
C_g	Gage Factor
Cv	Valve Coefficient
L	Length
OD	Outer Diameter
ID	Inner Diameter
E	Modulus of Elasticity
C_m	Metastability Parameter
σ	Standard Deviation
μ_m	Mean
W	Mass Flow Rate (lbm/hr)
d	Orifice Diameter
K	Flow Coefficient
h_w	Differential Pressure (in. H2O)
Re_D	Reynolds Number based on Flow Meter Piping Inner Diameter
D	Flow Meter Piping Inner Diameter
β	Ratio of Orifice Diameter to Piping Diameter

μ	Viscosity
q	Heat Transfer
w	Work
v	Specific Volume
R^2	Correlation Coefficient
G	Mass Flux
M	Moment
I	Moment of Inertia
x	Quality

Subscripts

act	Actual
e	Exit
i	Inlet
isen	Isentropic
EXP	Experimental
HEM	Homogeneous Equilibrium Model
FROZ	Frozen Model
corr	Corrected
meas	Measured
o	Stagnation
b	Back or Ambient
thr	Throat
1	Upstream of a Shock Wave
2	Downstream of a Shock Wave
c	Critical
1-ϕ	Single Phase

Chapter 1
INTRODUCTION

1.1 Background and Objective

Vapor-compression refrigeration systems are very common in today's society, with small units located in house windows and kitchens all over the world, and very large commercial systems being used for either refrigeration of products or air-conditioning of buildings. With so many systems in use and given the need for energy conservation, refrigeration systems represent a prime candidate for energy savings. By finding ways to increase the *COP* economically, major electricity resource savings can be gained.

One component of vapor compression refrigeration systems that is subject to major losses is the throttling device. Typical throttling mechanisms include capillary tubes and thermostatic expansion valves which work well but waste energy. The constant enthalpy process they follow implies that the kinetic energy gained in the pressure drop is lost. A means for recovering this kinetic energy would be beneficial to the overall efficiency of the refrigeration system.

There are several methods by which this could be accomplished but many are difficult to implement and maintain, such as total flow turbines which can easily become damaged in the two-phase fluid environment.

Another method of utilizing the kinetic energy typically lost in throttling devices is by use of an ejector. Ejectors require no maintenance and are not damaged by the rapidly expanding two-phase fluid. Detailed information concerning the operation and design of ejectors as refrigerant expanders is presented by Menegay [1] and is only briefly outlined below.

Process and *T-s* diagrams [1] for the ejector cycle are shown in Figs. 1 and 2, respectively. Using an ejector as an expander in a refrigeration system serves to decrease the work required by the compressor while also providing additional cooling. This is accomplished through the following processes within the ejector:

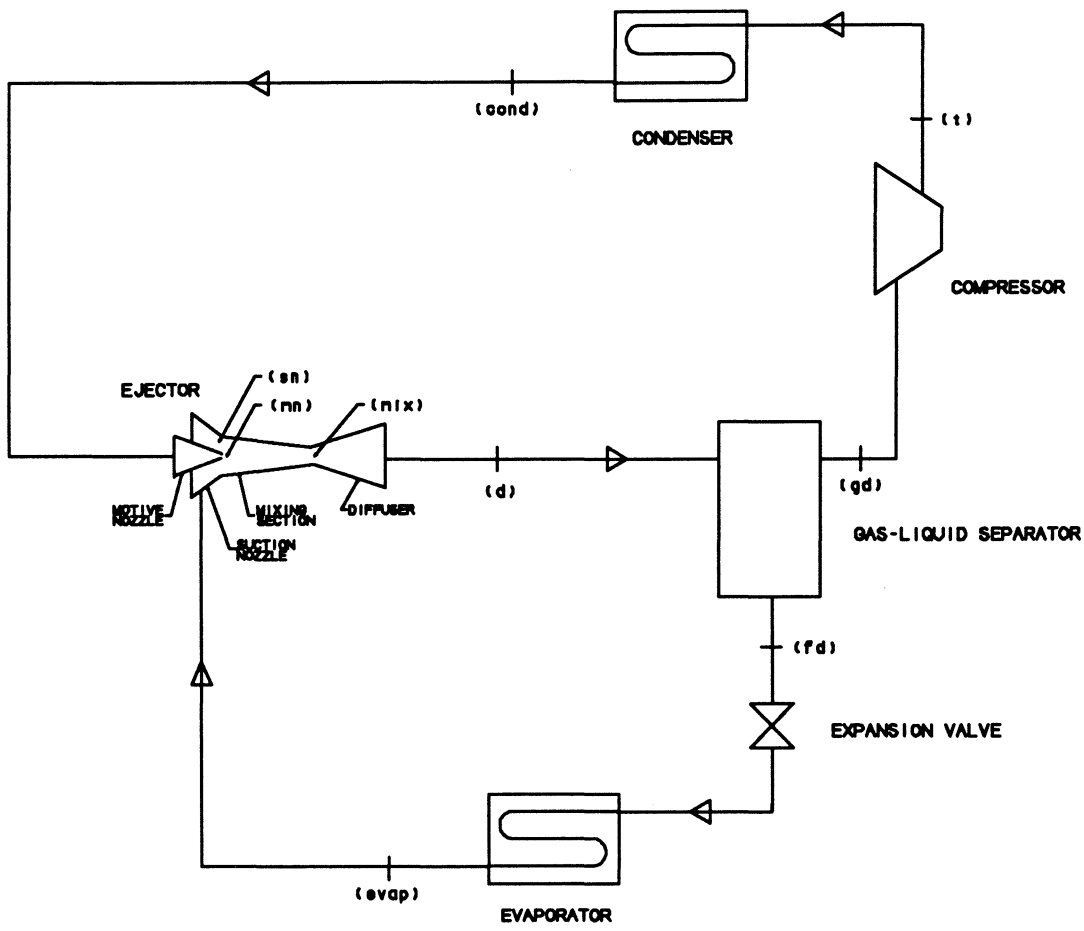

Figure 1 - Schematic of Ejector Cycle

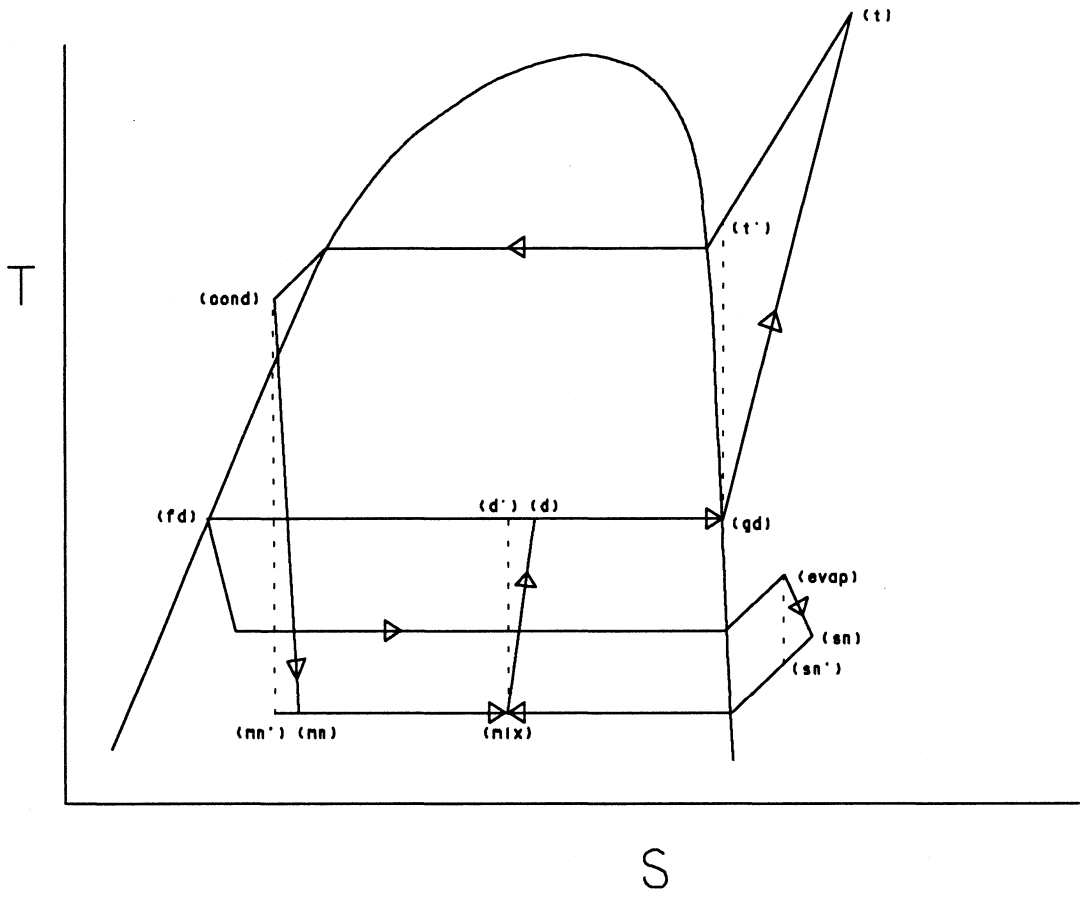

Figure 2 - T-s Diagram of Ejector Cycle

1. A subcooled or low quality fluid from the condenser is expanded in the motive nozzle to produce a low pressure, high velocity two-phase fluid.
2. This high velocity fluid entrains the vapor exiting the evaporator through the ejector suction nozzle.
3. The high velocity stream imparts its momentum to the suction vapor.
4. Kinetic energy in the stream is then converted to pressure energy in the diffuser. This causes the pressure of the fluid exiting to be higher than the evaporator pressure.

By using the kinetic energy of the high velocity fluid from the motive nozzle, some of the compressing work is performed on the fluid. This raises the pressure of the fluid higher than if the compressor were drawing the vapor directly from the evaporator therefore requiring less work of the compressor. More cooling is obtained since the ejector expansion process is closer to an isentropic process than a valve. These two benefits serve to increase the *COP* of a refrigeration cycle.

Menegay's previous research with an ejector was moderately successful, producing approximately a 3% increase in refrigeration cycle *COP* [2]. An idealized analytical computer analysis by Kornhauser [3] predicted a possible 21% increase in cycle *COP*. Poor motive nozzle efficiency is a major reason for the discrepancy between the analytical and experimental results. This reason provides the motivation and justification for this work.

The objective of this project was to design, build, and test an apparatus to measure the efficiency and quantify the metastability of the nozzle. With this knowledge, the nozzle can be re-designed to improve the experimental performance of the ejector as a whole, and a better understanding of the nozzle two-phase flow can be gained.

A method of determining the nozzle efficiency was conceived which required no knowledge of the non-equilibrium thermodynamic outlet state. This method included the measurement of nozzle thrust using a load beam. The derivation showing how the nozzle efficiency was calculated will be detailed in Sec. 1.3.1.2.

In Menegay's and the present work, a bubbly flow valve and tube was installed upstream of the nozzle to increase its efficiency. The bubbly flow valve was used to slightly throttle the subcooled condenser efflux into the saturation region while the tube promoted turbulence in the flow to break up the bubbles created by the valve. This bubbly mixture provided nucleation sites in the nozzle flow therefore decreasing the non-equilibrium.

To quantify this non-equilibrium, a metastability parameter was defined for this work which was based on the experimental, homogeneous equilibrium model, and frozen critical mass flow rates. The procedure for its calculation and the explanation of each of these mass flow rate is provided in Sec. 4.4. Use of the bubbly flow valve and tube was expected to decrease the metastable effects in the nozzle thus increasing nozzle efficiency.

1.2 Previous Work

Little research has been done concerned with efficiency measurement of two-phase convergent-divergent nozzles. The most relevant papers were by Ohta *et. al.* [4] and Akagawa *et. al.* [5] where the authors tested several nozzle geometries with subcooled water as the nozzle inlet fluid. In Ohja's paper, fine wires were placed at the inlet of some of the nozzles to instigate nucleation sites within the subcooled water. It was concluded that the presence of these wires did lower the metastability of the expanding nozzle flow.

The authors of both works defined a parameter, termed the thrust coefficient, which was equal to the square root of the nozzle efficiency calculated here. Thrust measurement was achieved by exhausting the nozzle flow into a wire mesh attached to a load cell. The thrust coefficient of the nozzles with fine wires was increased by a maximum of 10% over identical nozzles without wires, corresponding to an increase of 3.2% in efficiency.

1.3 Theoretical Basis

1.3.1 Nozzle Thrust Measurement

Due to the metastability that was present in the nozzle, typical methods of efficiency calculation were inadequate. A method that would eliminate the dependence on the outlet thermodynamic state was required. The following derivations show the inadequacy of the equilibrium efficiency calculations and how the actual efficiency can be determined with knowledge of the nozzle thrust, mass flow rate, inlet properties, and outlet pressure.

1.3.1.1 Efficiency Calculation for Thermodynamic Equilibrium Nozzles

Calculation of the efficiency of a nozzle is relatively simple when the process fluid is in thermodynamic equilibrium. Assuming 1-dimensional flow, the discharge coefficient can be calculated by determining the nozzle mass flow rate and the inlet and outlet pressures. The nozzle efficiency is then calculated from the discharge coefficient.
By definition of C_d, the actual nozzle flow is

$$\dot{m}_{act} = C_d A_e \rho_{e,isen} \sqrt{2(h_i - h_{e,isen})}, \tag{1}$$

while by the definition of η it is

$$\dot{m}_{act} = A_e \rho_{e,act} \sqrt{2\eta(h_i - h_{e,isen})}. \tag{2}$$

Combining the above equations gives

$$C_d \rho_{e,isen} = \sqrt{\eta}\rho_{e,act}. \tag{3}$$

For incompressible liquids ρ is constant, and this result becomes $\eta = C_d^2$. In the case of thermodynamic equilibrium, $\rho_{e,act}$ can be determined from the outlet conditions and the equation of state; therefore efficiency can be calculated from C_d.

For a two-phase mixture in non-equilibrium, the above method is useless since no equation of state is available for the nozzle exit conditions. An alternate method of calculating the nozzle efficiency is required.

1.3.1.2 Efficiency Calculation for Non-Equilibrium Nozzles

Where metastability is present, the nozzle efficiency can be determined from a combination of nozzle thrust and mass flow rate.

Figure 3 shows a simplified version of the apparatus to complement the discussion below.

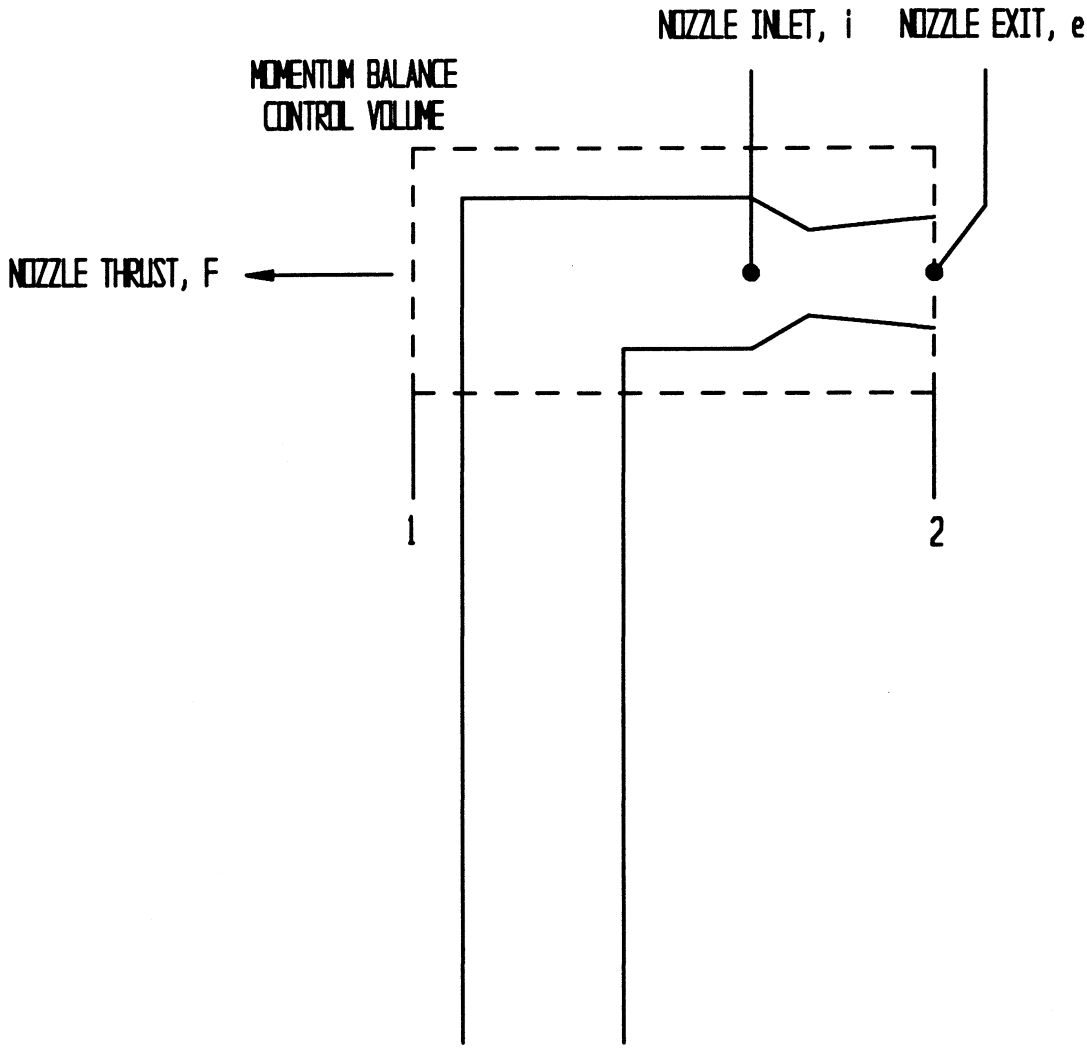

Figure 3 - Diagram of Simplified Thrust Measuring Apparatus

For 1-dimensional flow, the definition of η can be used to write

$$\eta = \frac{U_{e,act}^2}{2(h_i - h_{e,isen})}. \tag{4}$$

The pressure forces along the nozzle axis, at planes 1 and 2 on Fig. 3, balance since the flow enters through a 90 degree upstream bend. The momentum equation therefore gives thrust, F, as

$$F = U_{e,act}\dot{m}. \tag{5}$$

Equation 5 is only accurate if the pressure at the nozzle exit, along plane 2, is constant and the same as the pressure at plane 1. By determining the both the thrust and mass flow rate, the nozzle efficiency is calculated from

$$\eta = \frac{F^2 / \dot{m}^2}{2(h_i - h_{e,isen})}. \tag{6}$$

This result allows the calculation of the motive nozzle efficiency without complete knowledge of the outlet thermodynamic state provided the exit pressure is equivalent to the nozzle ambient pressure. All of the parameters in equation 6, with the exception of the thrust, are readily obtainable from well known methods. In this case an orifice meter is used to measure mass flow rate, as will be discussed in Sec. 2.4.2, and equation of state computer subroutines are used to determine the enthalpy at the inlet and isentropic outlet states of the nozzle. A more detailed development of the efficiency is presented in Sec. 4.3. Another important note was that the above derivation was based on one-dimensional flow. Therefore the efficiency calculation was actually an estimation.

1.3.1.3 Thrust Measurement Using Load Beam

A nozzle test stand was used as a load beam for measurement of the thrust. As shown in Fig. 4, the test stand was equipped with strain gages mounted to the base of the inlet tube. The strain gages measured the force from the bending moment on the tube created by the nozzle flow.

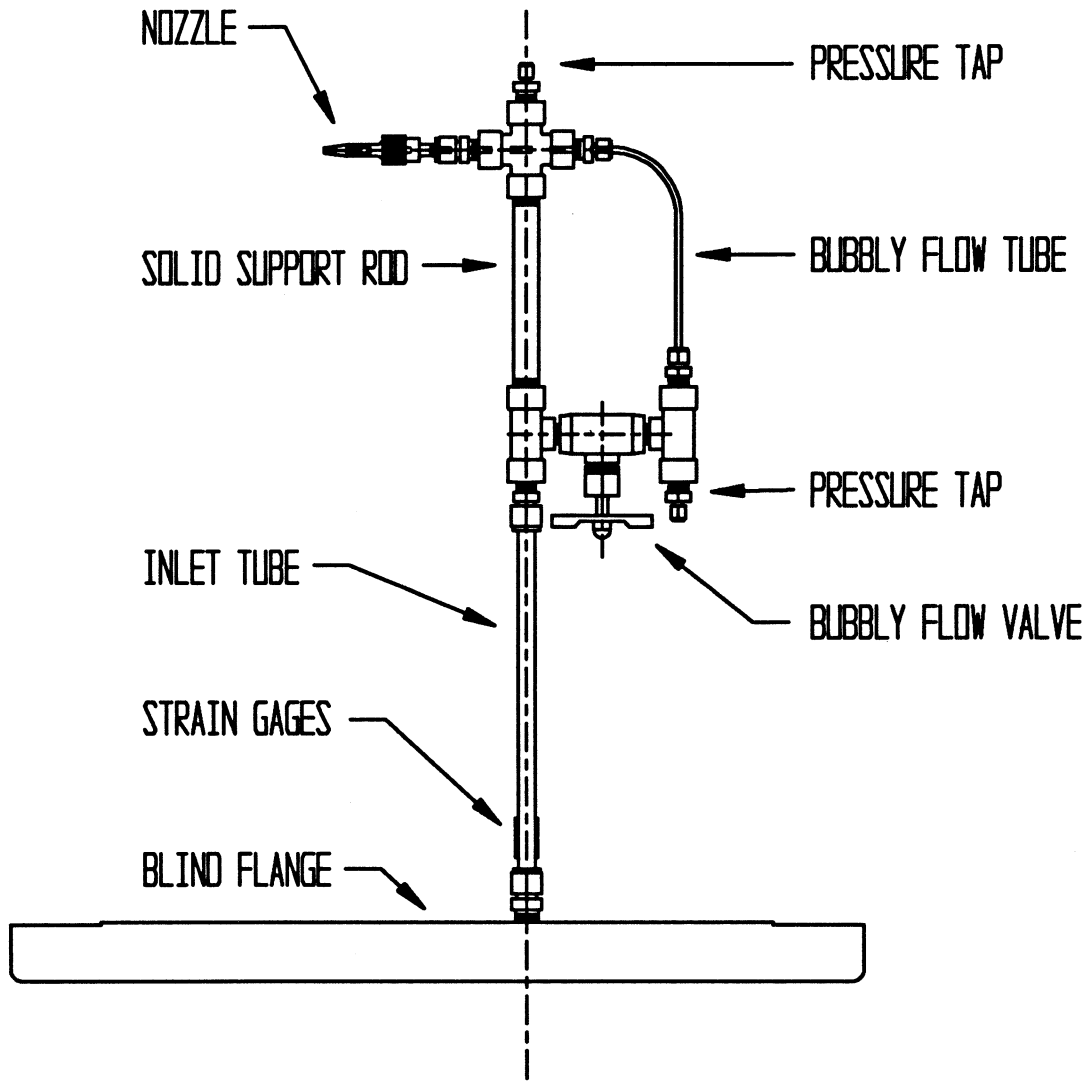

Figure 4 - Diagram of Experimental Nozzle Test Stand

Also shown on the test stand is the bubbly flow valve and tube, and the nozzle. Flow enters the base of the inlet tube, proceeds through the bubbly flow valve and tube, and exits the nozzle. Two pairs of strain gages were mounted opposed to each other in the nozzle plane. Using four strain gages provided two major benefits; an increase of the sensitivity by a factor of two, and the inherent temperature compensation of a full Wheatstone bridge.

The thrust is obtainable from the following parameters:

- output voltage signal from the strain gage bridge,
- geometry of the thrust measuring apparatus such as the gage-to-nozzle moment arm distance, tube moment of inertia, etc.,
- material properties of the inlet tube to which the strain gages are mounted,
- gage factor of the strain gages, and
- the bridge excitation voltage.

Equation 7, derived in Appendix A, shows the relationship between these parameters,

$$V_o = \varepsilon C_g V_i = \frac{16FL_g(OD)}{\pi(OD^4 - ID^4)E} C_g V_i, \tag{7}$$

where F is the thrust, L_g is the moment arm distance, E is the inlet tube modulus of elasticity, C_g is the strain gage factor, V_i is the excitation voltage, and V_O is the output voltage from the strain gage Wheatstone bridge.

While the equation above predicts the thrust, F, for a given output voltage, V_O, several of the parameters are difficult if not impossible to determine precisely. Therefore, the load beam was calibrated with a precision weight set as detailed in Appendix B.

1.3.2 Metastability Measurement

To represent the metastability, the following metastability parameter was defined,

$$C_m = \frac{\dot{m}_{EXP} - \dot{m}_{HEM}}{\dot{m}_{FROZ} - \dot{m}_{HEM}}, \tag{8}$$

where $\dot{m}_{EXP}$ was the experimentally measured critical mass flow rate, $\dot{m}_{HEM}$ was the homogeneous, equilibrium critical mass flow rate, and $\dot{m}_{FROZ}$ was the frozen or constant phase composition critical mass flow rate. The procedure of this calculation and a full explanation of each mass flow rate is provided in Sec. 4.4.

1.4 Shock Analysis

An important justification to the step above involving the momentum balance on the nozzle must be made. By drawing the control volume along the exit of the nozzle, the assumption was made that the exit pressure was equal to the nozzle ambient pressure. This assumption would be incorrect if the nozzle operated in the underexpanded or overexpanded mode.

For a nozzle to be underexpanded, the back pressure must be below that which produces perfect isentropic expansion within the nozzle. Underexpansion leads to the development of expansion waves downstream of the nozzle exit. These waves act to decrease the nozzle exit fluid pressure to the ambient pressure.

An overexpanded nozzle implies that the back pressure is above the perfect isentropic expansion value, but below the pressure for which a standing normal shock wave is produced at the exit plane of the nozzle. Overexpansion leads to the development of oblique and detached shocks at the nozzle exit. These shocks, which exist only outside the nozzle, act to increase the nozzle exit fluid pressure to the ambient pressure.

The existence of either the expansion wave or oblique shock phenomena invalidates equation 5 obtained from the momentum balance control volume in Fig. 3. If the pressure at the nozzle exit is different than that on all sides of the control volume, an additional pressure term representing the actual exit pressure would have to be added complicating the thrust equation. Determination of this actual nozzle exit pressure would be very difficult and probably very inaccurate.

For these reasons, an analysis of the nozzle flow was necessary to reinforce the fluid mechanic foundation of the efficiency calculation. An HEM analysis, which is a method of modeling a two-phase fluid as homogeneous and in equilibrium, was performed on the flow to determine if any shocks were present outside the nozzle. The results of this analysis show that a normal shock wave inside the nozzle was present. The discussion of this analysis is located in Sec. 3.7.

Research on previous work concerned with the existence of shock waves in two-phase fluids was also conducted. The results of this research indicated that the speed of sound for a two-phase fluid is better approximated by its vapor speed of sound. In this experiment, the nozzle outlet velocity was well below the outlet vapor speed of sound. Therefore, the research implied that there were no shocks associated with the nozzle flow. This is discussed further in Sec. 3.7.3.

Chapter 2
EXPERIMENTAL APPARATUS

2.1 Introduction

The experimental apparatus was divided into two principal components: a pressure vessel which housed the bubbly flow valve, tube, and the nozzle, and a vapor-compression refrigeration cycle with its related elements. Figure 5 shows these two components in a schematic of the system used for experimentation.

The pressure vessel served as the housing for the nozzle, nozzle test stand, and bubbly flow elements, while allowing the flow from the nozzle to be viewed through a glass window. A section of 12 in. standard schedule 40 (12 in., 304.8 mm ID) carbon steel pipe served as the pressure vessel. The pipe measured 22 in. (558.8 mm) in length; slip-on flanges were fastened by ASME certified welders to each end of the pipe section. One flanged end was used for a glass window while the other end was closed with a carbon steel blind flange.

The vapor compression refrigeration system, which served as a base for the experimental apparatus, was a Scott Air Conditioning and Refrigeration Education System, Model 9086. This system had been used for previous experimentation and had been modified extensively [2].

The major elements were:

- a 1/2 hp (0.7 kW) hermetically sealed compressor,
- an air cooled condenser,
- a dry expansion evaporator,
- receiver tanks for refrigerant storage,
- an accumulator at the exit of the evaporator which assured that only vapor entered the compressor suction,
- an oil separator, and
- instrumentation.

This chapter is dedicated to the description and explanation of both the pressure vessel hardware and the vapor compression refrigeration system described above, as well as the instrumentation and data acquisition equipment.

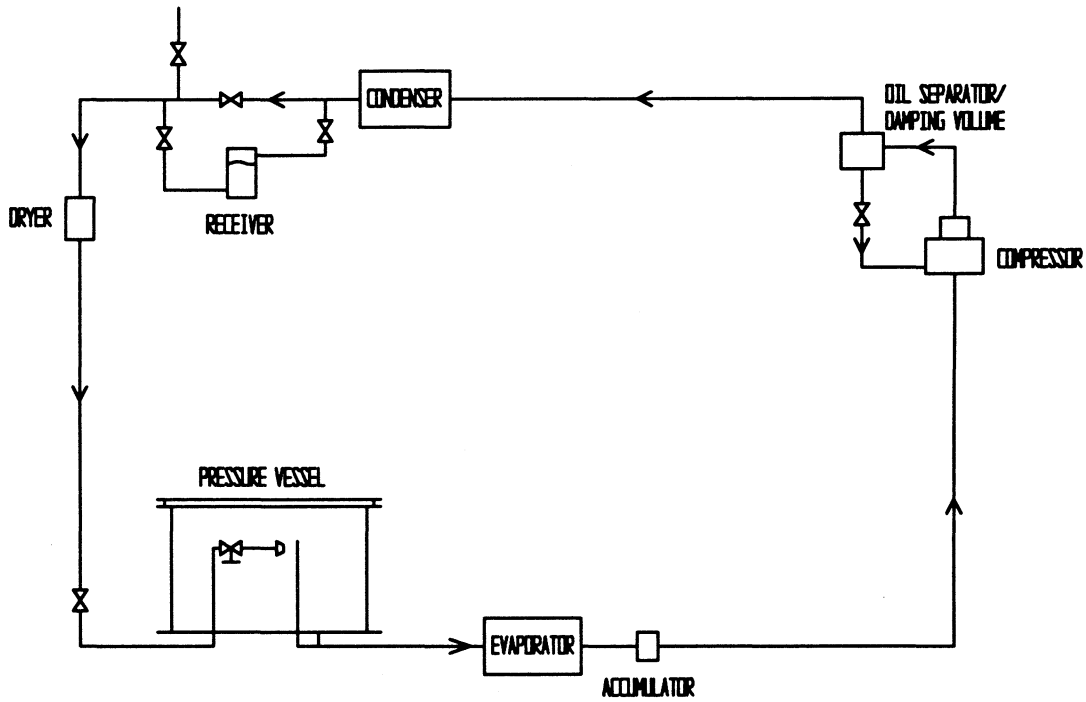

Figure 5 - Process Diagram for Thrust Measuring Apparatus

2.2 Nozzle Test Stand

The nozzle test stand was an innovative tool for determining the efficiency of a nozzle by measuring its thrust. The test stand was made up of several important elements necessary for instrumentation, operation, and control of the nozzle flow parameters.

The features of the stand which will be detailed in the following sections include:

- the nozzle test stand acting as a load beam,
- bubbly flow valve and tube, and
- other pressure vessel components.

2.2.1 Inlet Tube/Load Beam

The test stand is shown in Fig. 6. It consists of compression fittings and NPT (National Pipe Thread) fittings. The innovative mechanism on the test stand was the strain gage mounted to the 3/8 in. (9.53 mm) OD by 8.5 in. (215.9 mm) long stainless steel inlet tube.

As detailed in the previous chapter, the inlet tube with affixed strain gages enabled accurate determination of the efficiency by acting as a load beam for the nozzle thrust. As the inlet tube was bending under the thrust, the strain gage Wheatstone bridge output a proportional voltage. This method eliminated any reliance on the thermodynamic outlet state of the nozzle which contained metastable effects.

Other important features also included on the test stand were two pressure taps mounted up- and down-stream of the bubbly flow tube. The pressure tap lines were constructed from 1/16 in. (1.59 mm) OD by 0.02 in. (0.51 mm) ID stainless steel tubing. Small lines were required to minimize their effect on the sensitivity of the load beam. The pressure taps were required for the following reasons:

1. Determination of the pressure entering the nozzle.
2. To provide further understanding of the bubbly flow elements.

It should be noted that in Fig. 6, the solid rod was designed as a structural unit only and does not allow flow to bypass the valve and tube. Also, the rod carries all of the thrust produced by the nozzle flow to the inlet tube. This was necessary since the bubbly flow tube was not nearly rigid enough to support the nozzle weight or thrust during testing.

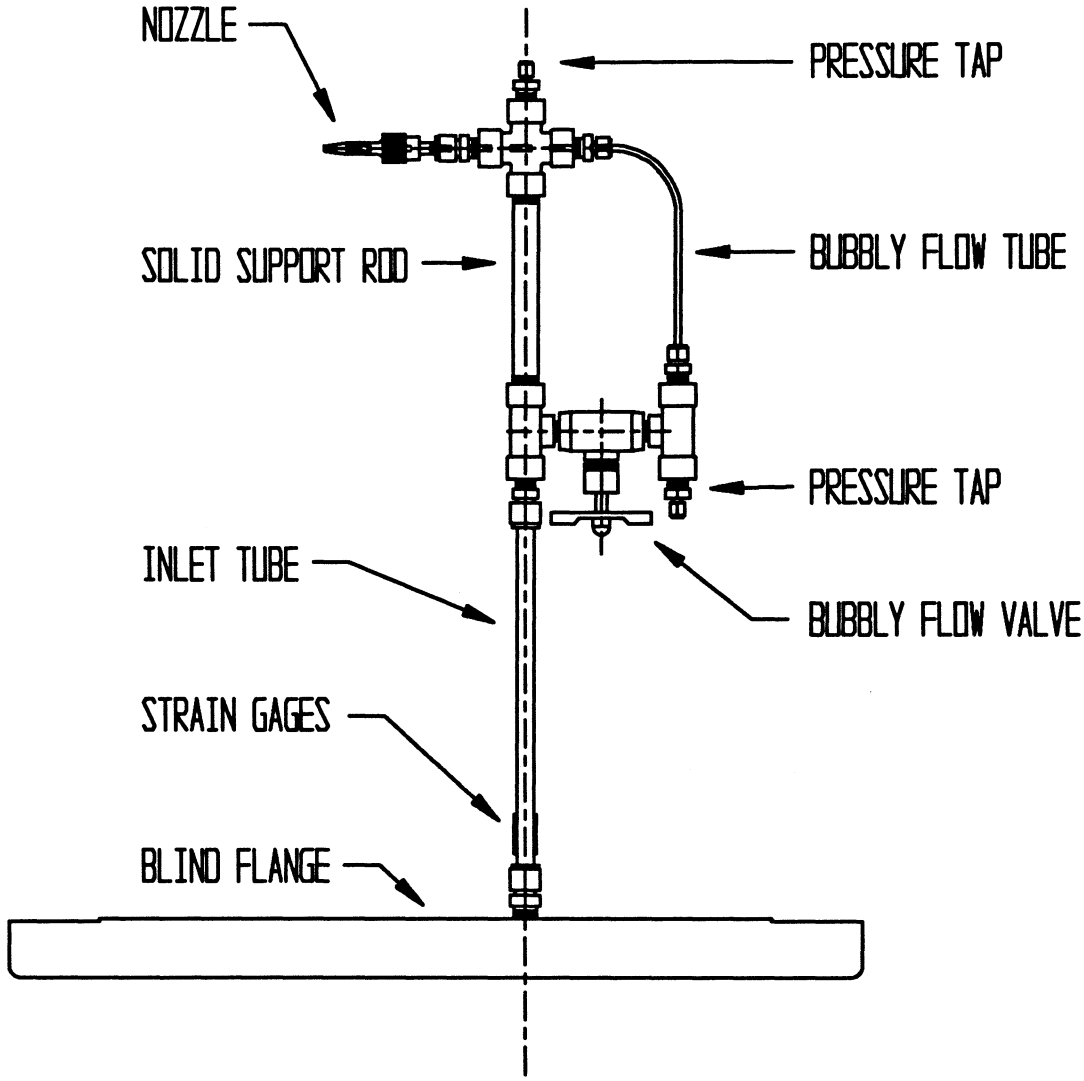

Figure 6 - Diagram of Experimental Nozzle Test Stand

2.2.2 Load Beam Design Considerations

A stainless steel inlet tube was chosen as the strain gage specimen material for its relative smooth surface, good durability and elastic bending properties. The diameter of the inlet tube was a more difficult choice. Mounting the strain gages on a larger inlet tube would have been easier, but the sensitivity of the inlet tube acting as a load beam would have decreased. Using the program in Appendix C which includes an HEM analysis to determine the thrust, and considering the limited sizes available, a 3/8 in. (9.525 mm) outer diameter tube was chosen with a 0.028 in. (0.71 mm) wall thickness. This proved to be a good choice for two reasons:

1. Strain gage installation was relatively easy given the variety of sizes of strain gage widths.
2. The load beam provided a sensitivity of 3.85 mV/lb_f (0.87 mV/N). This was acceptable since the computer program predicted a force of approximately 0.067 lb_f (0.3 N) corresponding to a bridge voltage output of 0.26 mV, which could easily be amplified with the equipment used for this experiment.

Careful design of the strain gage leadwires was also important. They were soldered to 36 AWG, polyurethane enamel insulated, single conductor, copper wire. Insulated wire was required because the gages were in close proximity to each other causing the leadwires to come in contact. The length of the leadwires had to be kept the same ensuring equal resistance in each arm of the full Wheatstone bridge. The Wheatstone bridge configuration is detailed in Sec. 2.4.1.

2.2.3 Nozzle

The nozzle was of the convergent-divergent type with dimensions as shown in Fig. 7, constructed from 316 stainless steel. It was designed by Menegay using the Henry-Fauske model which accounted for the non-equilibrium effects neglected by the HEM analysis. A full account of the nozzle design can be found in Menegay's thesis [1]. The nozzle was manufactured to Menegay's specifications by the Croll-Reynolds Co. [6].

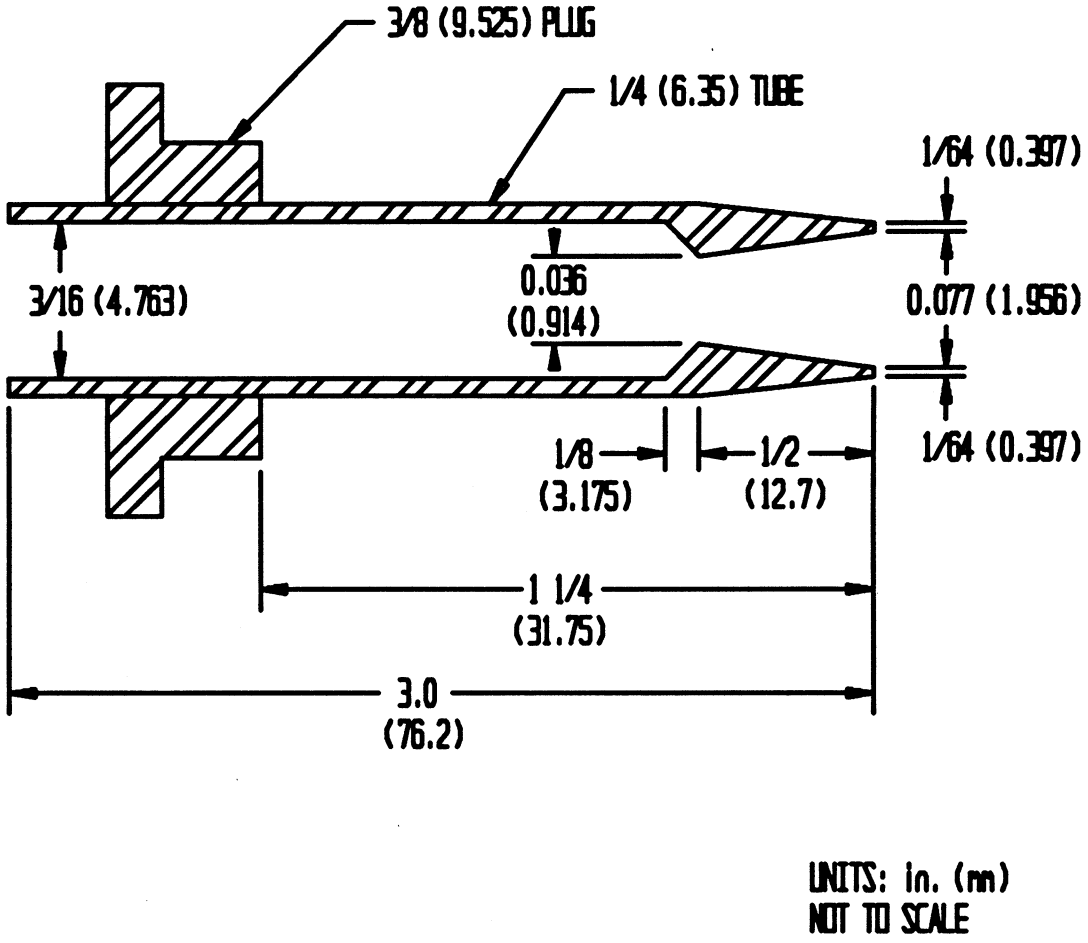

Figure 7 - Schematic of the Nozzle with Dimensions

2.2.4 Bubbly Flow Valve and Tube

The throttling process in a vapor-compression refrigeration cycle, which delivers a low temperature fluid to the evaporator for cooling purposes, is used to control mass flow rate. Two common types of throttling devices are capillary tubes and thermostatic expansion valves. Both of these devices have inherent mass flow rate control abilities which are explained well in general refrigeration equipment handbooks.

In the overall ejector expansion refrigeration cycle, by which this research was motivated, the main flow control mechanism was a convergent-divergent nozzle. Unlike the capillary tube and thermostatic expansion valve, the ejector expansion nozzle could not be adjusted for varying evaporator cooling loads. Without mass flow rate control, the evaporator would be prone to flooding, causing liquid carry-over into the compressor. Therefore another method of mass flow rate control was needed.

Previous experimentation by Menegay [1], with the ejector expansion refrigeration cycle, utilized hot gas bypass as a means of controlling the flow rate through the nozzle. This consisted of a bleed line attached at the outlet of the compressor, delivering high temperature vapor to the motive nozzle inlet. A metering valve was placed in the bleed line to control the amount of hot gas entering the nozzle. The hot gas from the bypass line introduced low density vapor at the nozzle inlet therefore decreasing the flow as the metering valve was opened.

Hot gas bypass was utilized not only for mass flow rate control but also as an instrument to decrease the metastable effects in Menegay's motive nozzle. By introducing nucleation sites in the nozzle inlet, metastable effects are minimized due to the fluids greater ability to change its phase from liquid to vapor. Menegay's experiments with hot gas bypass found that the *COP*, relative to a standard cycle operating without the ejector expansion device, actually decreased. For this reason, hot gas bypass was rejected as a mass flow rate control mechanism.

What was needed was a method of decreasing the metastability in the nozzle while not degrading the overall cycle performance.

The solution was discovered by Kornhauser and Menegay [7]. Their idea was to use a metering valve to slightly throttle the subcooled liquid exiting the condenser, into the two-phase region. This created small vapor bubbles which then enter a tube with a small inner diameter promoting turbulence in the bubbly flow, which is believed to break up the

bubbles in the flow. In addition, the throttling valve acts as a mass flow rate control mechanism. Previous experiments by Menegay [2], using the bubbly flow valve and tube arrangement, have shown increased *COP* results over hot gas bypass as well as non-ejector experiments. Research was continuing to optimize the bubbly flow system for which a patent was pending.

The bubbly flow elements used in this experiment, consist of a Hoke metering valve, model 2RB281 with a C_V of 0.6, and a 1/8 in. (3.175 mm) OD by 0.0715 in. (1.816 mm) ID by 11 in. (279.4 mm) long stainless steel tube. Sizing of the bubbly flow tube was based on Menegay's previous work, while the valve was sized based on the expected valve coefficient, C_V. The bubbly flow tube was inserted into the nozzle to avoid any coalescence of the bubbles before entering the nozzle inlet. Mass flow rate was controlled by adjusting the metering valve which was fully enclosed in the pressure vessel. This adjustment was achieved with a device that could be disengaged from the valve to avoid any interference with the thrust measurement of the test stand as will be explained in Sec. 2.2.5.3.

2.2.5 Pressure Vessel Components

As mentioned previously, the pressure vessel was constructed of a 12 in. standard schedule 40 (12 in., 304.8 mm ID) carbon steel pipe. One hundred and fifty pound slip-on flanges were welded onto each end of the pipe section by certified ASME welders. A diagram of the vessel with it's internal components is shown in Fig. 8.

The pressure vessel housed the following items:

- the entire test stand,
- pressure measurement lines passing through the blind flange,
- a viscous damping mechanism to increase the precision of the thrust data,
- a glass viewing window, and
- the blind flange elements such as refrigerant return lines, pressure tap lines, and bubbly flow valve adjusting handle.

The viscous damping mechanism, glass window, and blind flange elements are detailed next.

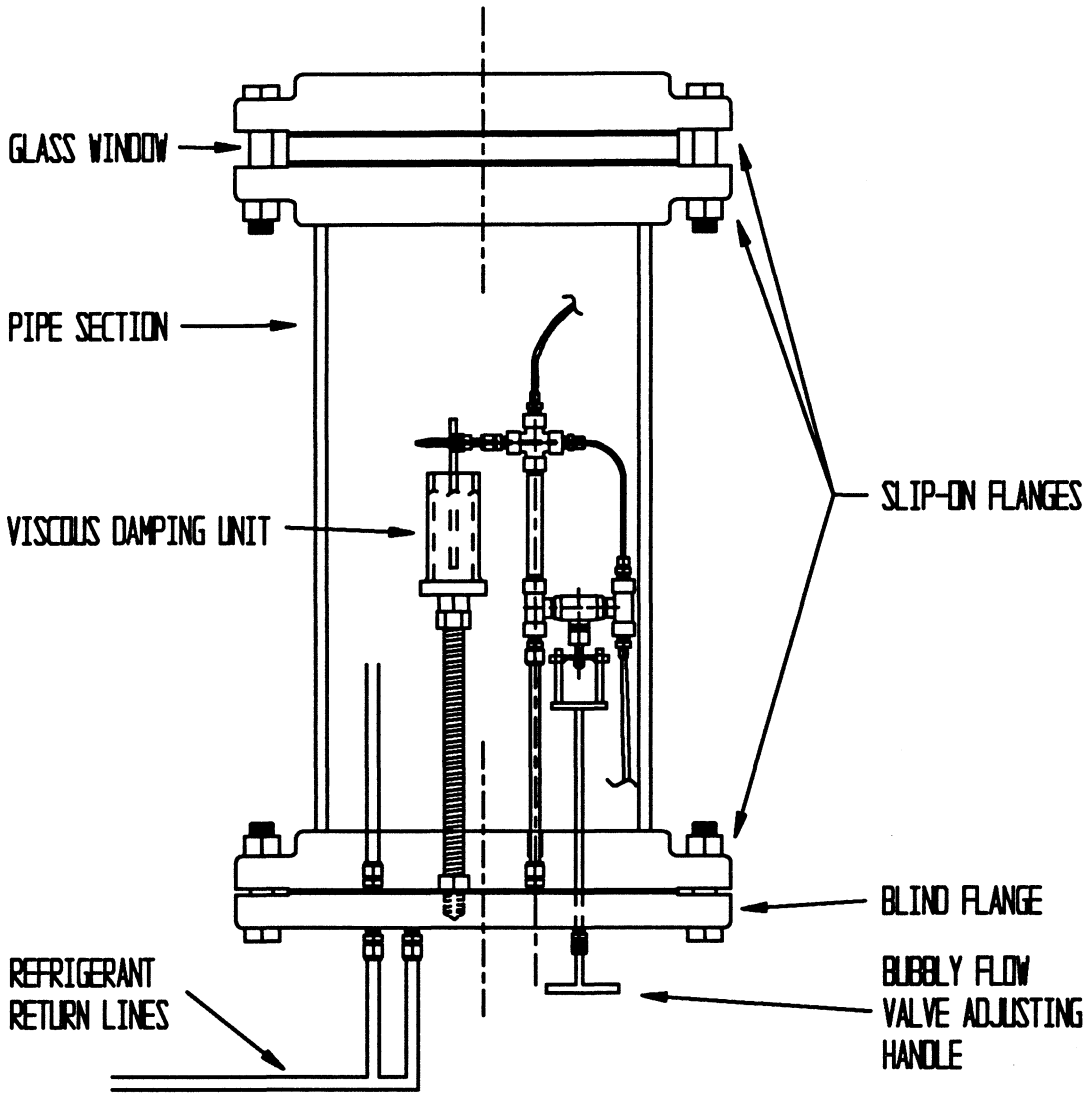

Figure 8 - Pressure Vessel Diagram and Components

2.2.5.1 Viscous Damping Mechanism

Early experimental runs produced a large variation in the thrust signal. This variation, which could be seen with the naked eye as unsteadiness of the nozzle, was caused by the flow exciting the test stand. During operation, the test stand would become unsteady for short periods of time indicating that a possible change in the flow characteristics was exciting the test stand at its natural frequency of approximately 10Hz.

In the efficiency calculation, the thrust variation was squared. The following equation, termed the standard deviation ratio by the present author, was used to quantify the variation in the experimental results:

$$\left(\frac{\sigma}{\mu_m}\right). \tag{9}$$

Where σ was the statistical standard deviation, and μ was the mean value of the efficiency data. The value for the average standard deviation ratio for initial experimental runs was approximately 70%. Clearly this standard deviation ratio was unacceptable.

To decrease the large standard deviation, some sort of damping was needed. The chosen mechanism could not produce any frictional or other forced dead band in the response of the test stand while operating the apparatus in steady state. Therefore, a viscous damper was chosen to provide the necessary damping of the test stand perturbations because it would not act to influence the test stand's equilibrium position.

Figure 9 shows the construction of the viscous damping unit and how it is connected to the test stand. A 7/8 in. (22.225 mm) threaded rod was used to secure the oil container to the blind flange. Such a large rod was used because any flexing of the container and rod would decrease the effectiveness of the viscous damping. The paddle attached to the nozzle was made from aluminum. Its 3/16 in. (4.7625 mm) thickness ensured negligible flexing.

Two important constraints were applied to the design and construction of the viscous damping mechanism:

1. A small clearance between the paddle and container walls was desired since the smaller the clearance, the greater the viscous damping effect. An analogy of this being the flow of viscous fluid through an orifice which is the most common type of damping used in the front suspension of motorcycles.

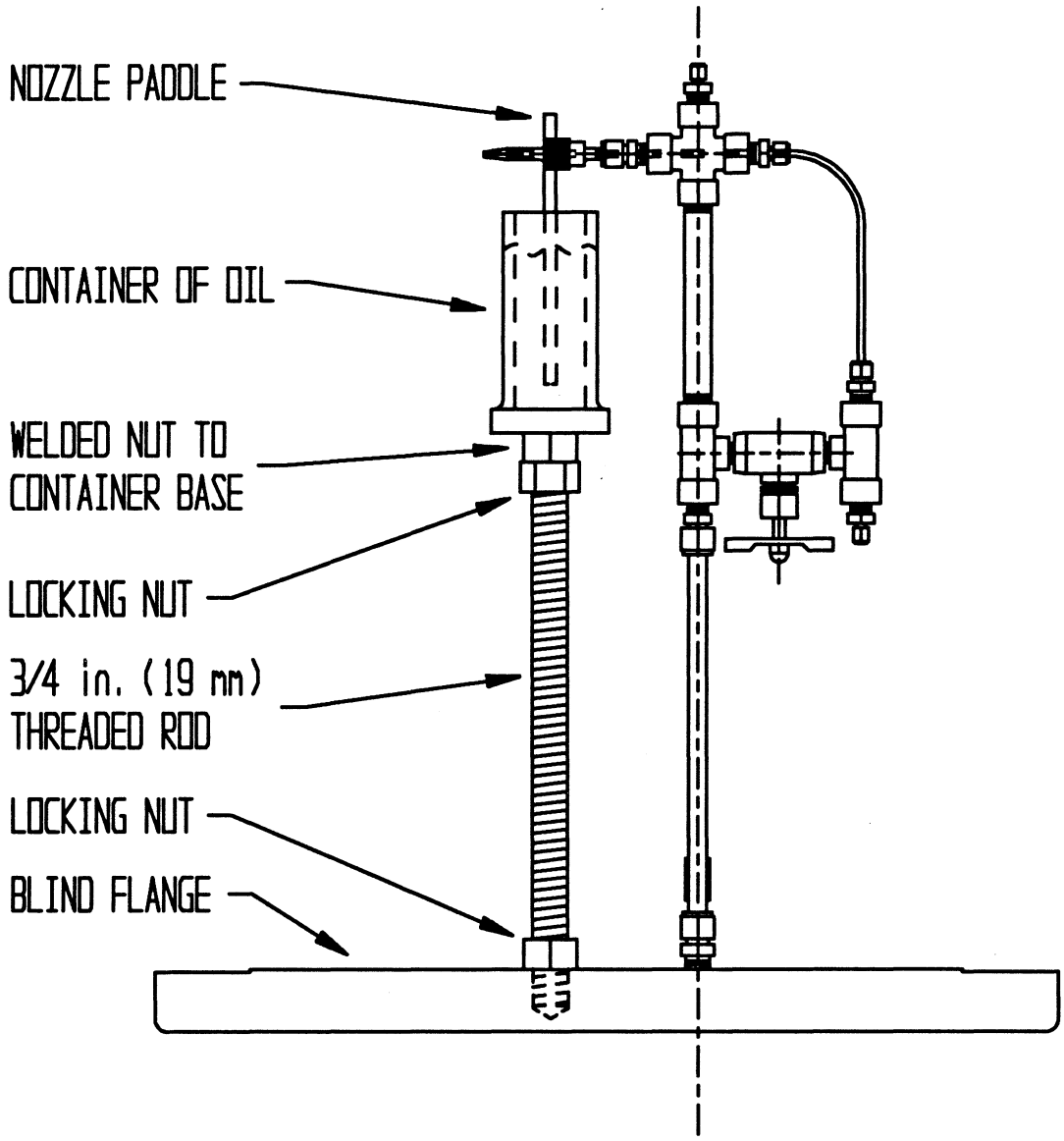

Figure 9 - Diagram of Experimental Test Stand with Viscous Damping Mechanism

2. The paddle could not contact the container walls during its motion in response to the thrust. Any contact between the paddle and container would cause the addition of frictional damping to the mechanism and could introduce undesirable dead band into the system.

The initial oil selection for the damping medium was made from a list of refrigeration lubricants to ensure compatibility with the compressor oil already in the system. The most viscous refrigeration oil found was Suniso 5GS. The average standard deviation ratio for the experimental efficiency results with the Suniso 5GS oil in the damper was reduced to 21%. This was acceptable but it was believed that with better oil selection further reduction in the standard deviation could be obtained.

Relaxing the constraint of considering only refrigerating oils allowed the inclusion of oils with much higher viscosities. Further research led to gear oils as an extremely viscous replacement for the refrigerant compatible lubricants. The gear oil chosen was Chevron's ISO 460 (SAE 140 gear oil equivalent). ISO 460 acting as the damping medium reduced the efficiency average standard deviation ratio to 4.9%.

Table 1 shows how the viscosity in SUS (Saybolt Universal Seconds) compares for the two damping oils. The viscosity of oils at the evaporator temperature have been predicted using an API chart which gives a linear variation of viscosity with temperature [8]. ISO 460 gear oil has a 57% greater Saybolt viscosity than Suniso 5GS refrigeration oil at the evaporator temperature, providing a significant increase in damping.

Table 1 - Comparison of Viscous Damping Oils

Oil Type	@ 100°F	@ 210°F	@ Evaporator Temperature of 43.4°F
Suniso 5GS	525 SUS	55.3 SUS	~21 000 SUS
Chevron ISO 460	2 341 SUS	144 SUS	~33 000 SUS

2.2.5.2 Viewing Window

A glass window was installed on the pressure vessel. Having a view port into the pressure vessel was beneficial for the following reasons:

1. Inspection of the nozzle test stand during operation. This feature of the window provided more advantages to the operation of the experiment than had been

anticipated. The unsteadiness of the nozzle was easily seen and the effect of upgrading the viscous damping mechanism could be quickly assessed qualitatively. The window also aided in determining the position of the bubbly flow valve adjusting mechanism to ensure that it was not in contact with the valve. This mechanism will be discussed in Sec. 2.2.5.3.

2. Examination of the nozzle fluid outflow. The window can also provide a means of determining the qualitative and quantitative nature of the jet which was beyond the scope of this work.

The window was relatively easy to install because of the flange affixed to the top of the vessel. This flange allowed the glass to be held between itself and another slip-on flange, leaving the ID of the flanges open for an obstructionless view into the vessel.

A 1 in. (25.4 mm) thick by 15 in. (381 mm) OD glass disk served as the window. It was constructed of tempered, Corning 7740 Pyrex. The vendor quoted an 80 psia (551.6 kPa) pressure limit for the glass which was well above the expected operational pressure of 55 psia (379.2 kPa).

Twelve 7/8 in. (22.2 mm) flange bolts were used to secure the glass between the two slip-on flanges. Neoprene gaskets with a 12.875 in. (327.03 mm) ID by 15.875 in. (403.23 mm) OD were used to avoid any high stress points caused by the rough flange surfaces and prevent any glass to metal contact.

A bolt torque calculation was necessary to prevent the any leaks from the window mating surfaces without overstressing the glass. From the determination of several constants based on the gasket characteristics from Spotts [9], and an equation for the bolt torque from Deutschman *et. al.* [10], a torque requirement of 73.0 ft·lb$_f$ (99.0 N·m) was calculated.

Other precautions taken with the glass window were as follows:

- Careful installation between the flanges. A criss-cross pattern with small torque increments was used to tighten the bolts securing the window.
- Installation of a pressure relief valve. The valve, set at 65 psia (448.2 kPa), was placed in the outlet line of the pressure vessel to avoid over pressuring the glass window. As mentioned, the operational pressure of the vessel was 55 psia (379.2 kPa); within glass disk capabilities. A possible problem would occur if any liquid were left in the vessel at shutdown since the vapor pressure of R-12 at a typical ambient temperature of 70°F is 84.9 psia (585.4 kPa); beyond glass capabilities.

Equipment failure could also cause the pressure in the vessel to reach the maximum allowable pressure of the glass.

- A cover was kept over the glass during down time for safety reasons.

2.2.5.3 Blind Flange Elements

The blind flange was bolted to the bottom slip-on flange opposite the viewing window. The same type of gasket and torque value described above was used to assure a leak free mating surface.

The following elements were supported by the blind flange:

- the nozzle test stand/refrigerant supply line,
- refrigerant return lines,
- pressure tap lines,
- Wheatstone bridge circuit wires in pass through, and
- the bubbly flow valve adjusting handle.

The nozzle test stand, which was previously described, and the refrigerant lines were passed through the blind flange by compression fittings attached to the flange with NPT fittings.

Two refrigerant return lines were used; one for liquid, and another for vapor. This was done since the extent of a liquid level developing at the bottom of the vessel was not known initially and the exclusion of the vapor in the return line would have been detrimental to the experiment.

As mentioned in Sec. 2.2.1, two pressure tap lines were used to measure the pressure across the bubbly flow valve and tube. These lines simply passed through the flange using compression fittings as all the other lines did.

A pass through rated at 1000 psia (6894.73 kPa) with temperature limits of -328°F to 392°F (-200°C to 200°C) was fixed to the blind flange using a jam nut/o-ring type body with straight 1/2-20 threads. The pass through's nine wires were 24 AWG, Teflon insulated, stranded silver-plated copper. Four wires of the pass through were used; two to deliver the excitation voltage to the Wheatstone bridge, and the other two to measure the output voltage of the bridge. The unused wires were coiled and left in the pressure vessel.

Another important feature required by the internal test stand design was the bubbly flow valve adjusting handle. This handle was a convenient method for changing the position of the valve since it required frequent adjustment during experimental operation.

The adjusting handle was a simple design with two fingers that engaged the valve handle. A drilled through compression fitting was used to secure the handle in the blind flange. By loosening the fitting, the handle could be turned with minimal refrigerant loss since it took a short time to adjust the valve. During measurement of the thrust from the test stand, the bubbly flow valve adjusting handle was disengaged from the valve.

2.3 System Components and Piping

With most of the important refrigeration elements already described in this chapter, this section will detail the following other essential components that play small roles in the experimentation:

- The receiver was used for holding refrigerant when the system was not in operation. During operation, the receiver was kept open and a liquid level was maintained to ensure that only subcooled liquid entered the bubbly flow valve.
- A dryer was installed downstream of the receiver to remove any water from the liquid refrigerant.
- An accumulator was located at the outlet of the evaporator to separate the liquid and vapor. Only the vapor phase exiting the evaporator was allowed to enter the compressor suction port to avoid damaging the compressor.
- The oil separator was located directly downstream of the compressor to remove oil from the refrigerant. Oil droplets entrained in the high temperature vapor leaving the compressor collect at the bottom of the separator, where they are returned to the compressor suction line through a globe valve. This was done to avoid any effects the oil may have had on the nozzle flow.
- Extensive re-piping was required. The system was dismantled to the base refrigeration elements and then reassembled to suit this experiment's goal.

The experimental apparatus was designed and controlled for the sole purpose of testing the nozzle. All processes, with the exception of the throttling process, were the same as found in typical vapor compression refrigeration cycles.

2.4 Instrumentation and Data Acquisition

Computerized data acquisition was used to collect and articulate the data from the apparatus instrumentation. Pressure transducer and thermocouple signals were obtained to evaluate the refrigerant properties at certain points in the system.

Each instrument signal was sent to a PC based data acquisition board. The data acquisition system required voltage input signals for A/D (Analog to Digital) conversion. Figure 10 shows the electrical schematic for the all signal generating instrumentation.

Important measurements, such as the nozzle thrust with the strain gage Wheatstone bridge, and the mass flow rate measurement are discussed in this section as well as the following instrumentation:

- strain gages,
- gage pressure transducers,
- differential pressure transducers/transmitter,
- thermocouples and the cold reference junction box,
- other instrumentation, and
- signal conditioning equipment.

Figure 11 shows the process diagram and the relative location of the instrumentation. The symbols given in the process diagram serve to label the instrumentation. The letters represented the type of instrument; *P* for pressure transducer, *DP* for differential pressure transducer, *T* for thermocouple, and *SG* for strain gages. The numbers were used only to differentiate instrumentation of the same type.

Also discussed is a procedure employed for control of the evaporator and condenser pressures by use of the data acquisition equipment.

2.4.1 Strain Gages for Thrust Measurement

The strain gages and adhesive required careful selection. The gages had to be small enough for mounting on the inlet tube, able to withstand the refrigerant environment, and have the same thermal expansion properties as the inlet tube to which they were bonded.

Measurements Group model WK-09-125AD-350 strain gages used for this experiment had the required specifications [11] given below:

1. full encapsulation with glass-fiber-reinforced epoxy-phenolic resin,

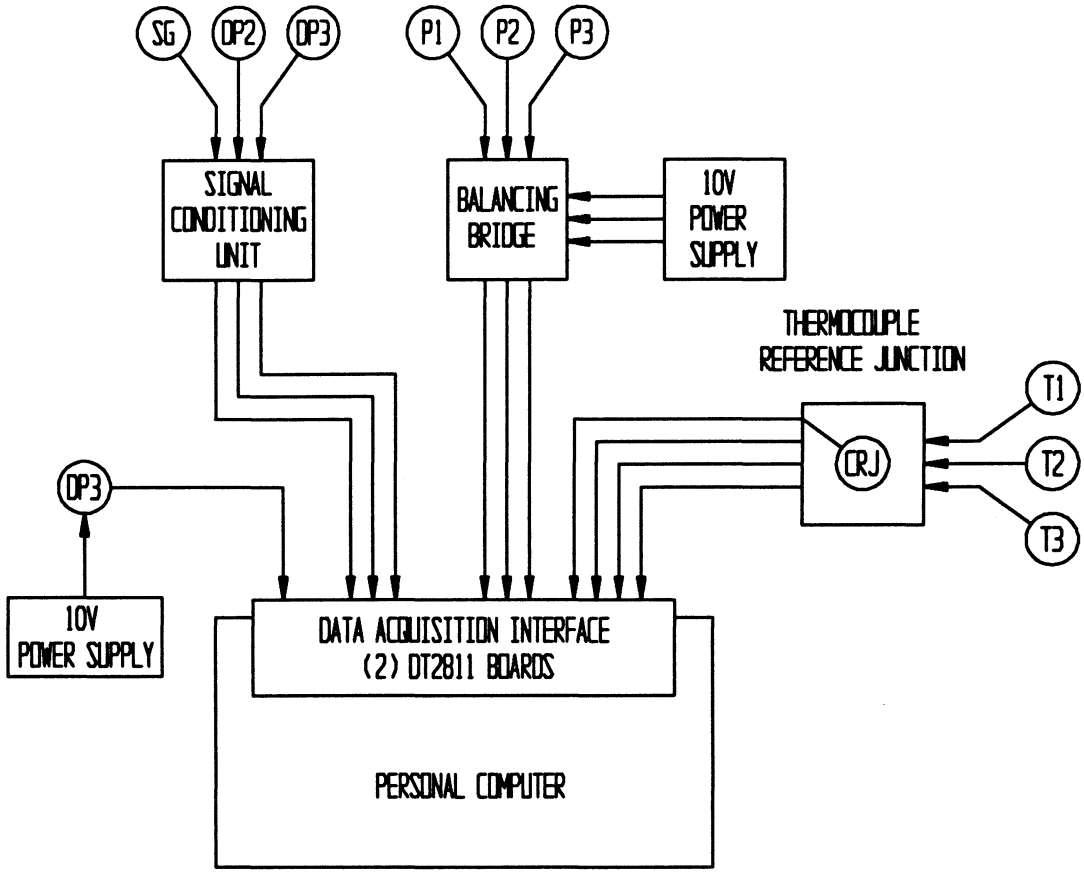

Figure 10 - Schematic for Instrumentation to Data Acquisition Electrical Connections

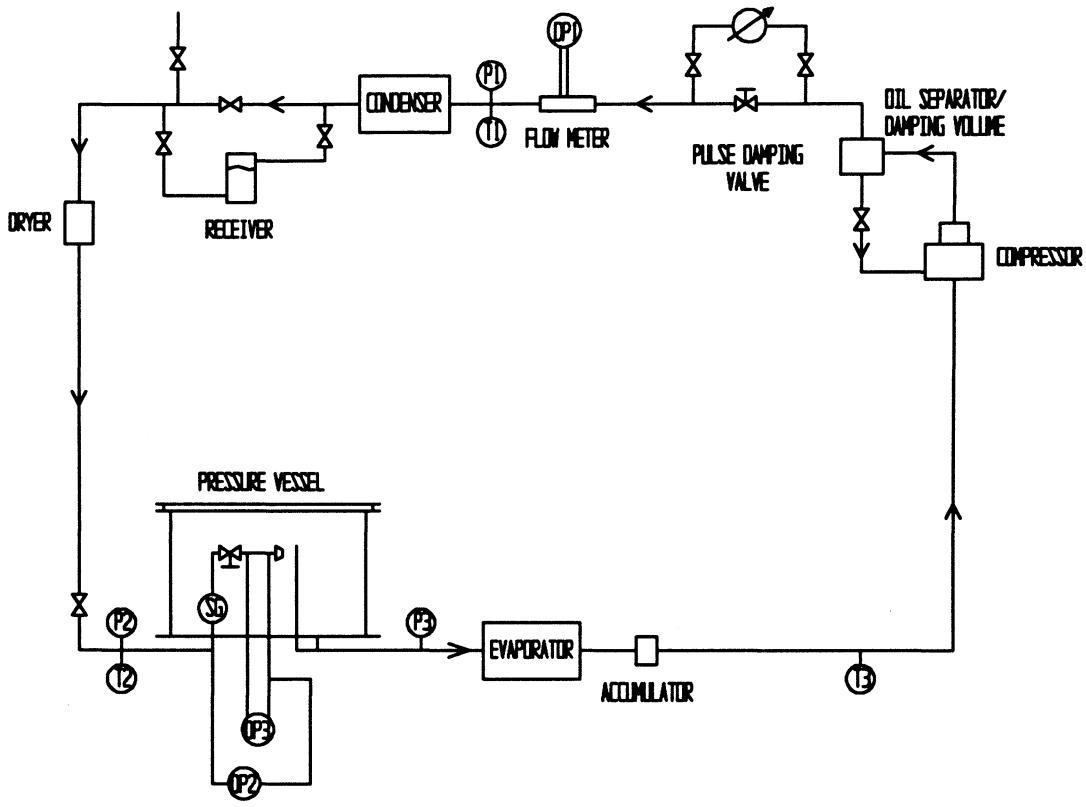

Figure 11 - Process Diagram with Instrumentation

2. nickel-chromium alloy foil,
3. thermal expansion coefficient of 9.0 ppm/°F (16.2 ppm/°C) matched as closely as possible to the 304 stainless steel coefficient of 9.6 ppm/°F (17.28 ppm/°C),
4. active gage length of 0.125 in. (3.175 mm), width of 0.125 in. (3.175 mm), and
5. a gage resistance of 350Ω.

The type of adhesive used, also available from the strain gage manufacturer, was an epoxy-phenolic type; M-BOND 600.

Figure 12 shows the full Wheatstone bridge configuration of the strain gages used on the inlet tube. Gages 2 and 4 were located on the compressive side of the inlet tube while gages 1 and 3 were on the tensile side. The pairing of the gages yielded greater sensitivity while providing temperature compensation.

Once the gages and adhesive had been obtained, the gages were mounted on the inlet tube. The manufacturer instructions [12] were carefully followed for surface preparation of the stainless steel inlet tube and mounting of the gages. Properly cleaning the gage specimen was a crucial step in ensuring successful strain gage bonding, therefore appropriate cleaning solutions and equipment were also purchased from the manufacturer. Mounting the gages also required care and patience [13]. The adhesive used to bond the gages was a high temperature curing epoxy resin and required a temperature controlled oven for proper curing. The manufacturer also specified that 15-70 psi (103.4-482.6 kPa) be applied to the gages while curing.

After mounting, the strain gages were soldered into the full Wheatstone bridge configuration, and the output voltage signal was wired to an amplifier via the pass through. From there, the signal was sent to data acquisition system for sampling. The amplifiers also provided the excitation voltage for the bridge.

To eliminate errors in the theoretical equation for output thrust from the bridge, the strain gages were calibrated. By placing the test stand in the horizontal plane, masses could be used to simulate force on the nozzle. A detailed explanation of the calibration procedure and calibration FORTRAN program can be found in Appendix B.

2.4.2 Flow Meter

An orifice meter was used for mass flow measurement in this experiment. Orifice meters are well understood and are used for many mass flow applications in industry.

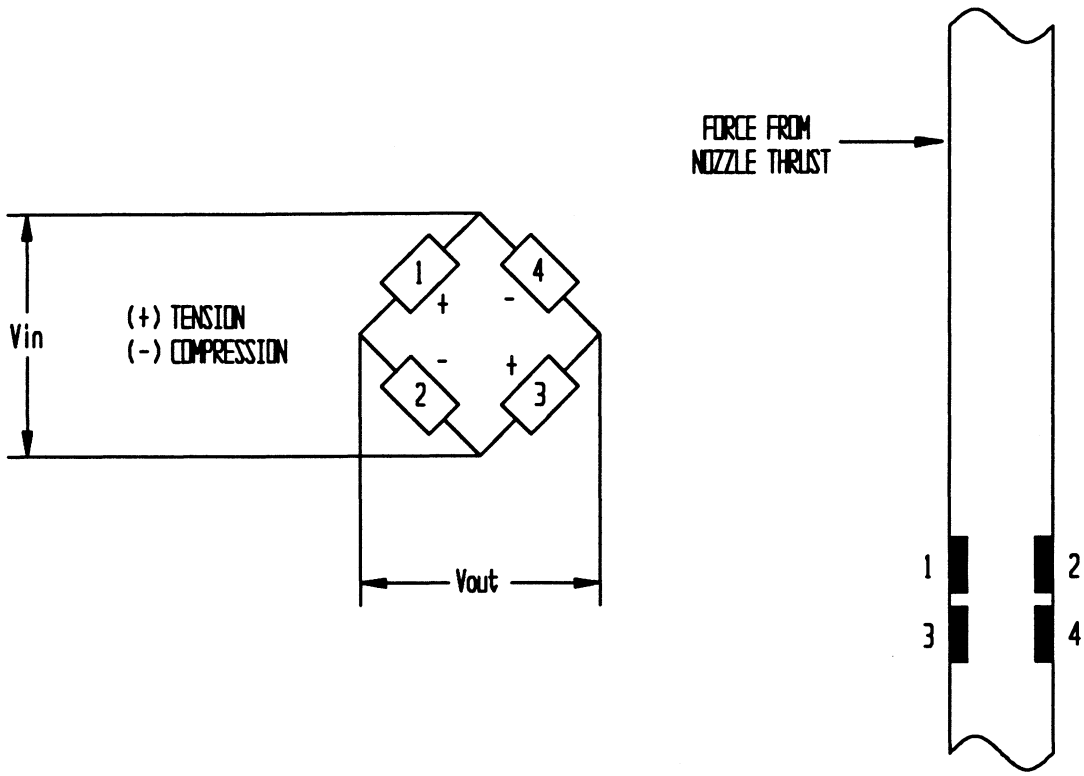

Figure 12 - Schematic of Wheatstone Bridge Configuration

Two important potential problems had to be addressed in the construction and analysis of the flow meter for this experiment:

1. orifice up- and down-stream piping, and
2. pressure pulsation's from the single piston, single acting compressor.

2.4.2.1 Piping Requirements and Other Elements

Orifice flow meter products by Asea Brown Boveri [14] and Daniel [15] both used 0.5 in. (12.7 mm) ID honed piping with 12 in. (304.8 mm) upstream and 6 in. (152.4 mm) downstream of the orifice. Their products were honed to a surface roughness of 5-10 microinches (0.127-0.254 micrometers). These products were expensive and had long lead times. Therefore, construction of the orifice mass flow meter was done in-house in less time and at less cost.

For this experiment, a 24 in. (609.6 mm) section of 0.5 in. (12.7 mm) ID, welded seam, 304 stainless steel piping was used for the orifice piping. An internal surface roughness of 5-10 microinches (0.127-0.254 micrometers) was obtained by mechanical honing and electro-polishing of the pipe [16]. Mechanical honing was required only to remove the welded seam on the ID of the pipe, while electro-polishing was used to yield the desired surface roughness.

ASME guidelines [17] on orifice meters were also consulted to ensure accurate mass flow measurements. These guidelines recommended that the fluid enter the orifice plate with a fully developed velocity profile since pits or scores in the upstream piping can greatly decrease the accuracy of an orifice flow meter. Table 2 compares the ASME requirement with that used for this experimentation.

Table 2 - Comparison of Orifice Piping Requirements Between ASME and the Present Experiment

Flow Meter Characteristic	ASME Requirement	Present Experiment
Straight Upstream Piping-	4.6 in. (116.8 mm)	18 in. (457.2 mm)
Straight Downstream Piping-	1.4 in. (35.6 mm)	6 in. (152.4 mm)
Surface Roughness-	350 μin. (8.9 μm)	5-10 μin. (0.127-0.254 μm)
Honed Upstream Piping-	2.22 in. (56.4 mm)	18 in. (457.2 mm)
Honed Downstream Piping-	1.11 in. (28.2 mm)	6 in. (152.4 mm)

Comparison of the above values show that the ASME requirements were substantially exceeded for each characteristic specified. An important note was that the above recommendations given by ASME considered pipes of at least 2 in. (50.8 mm) ID.

Daniel 0.5 in. (12.7 mm), Class 300 orifice flanges were used with NPT female connections for the NPT pipe sections. The pressure taps located on the flanges required drilling through the honed pipe. A 13/64 in. (5.16 mm) orifice plate was sized based on the past mass flow rate in experiments conducted by Menegay [2]. Appendix D contains the orifice sizing procedure.

Hard composition gaskets received with the Daniel flanges were difficult to seal under the experiment operational pressure of the flow meter (180 psia, 1241.1 kPa). A much softer material, neoprene, was used instead with good results.

The orifice flanges had NPT equipped pressure taps. A Rosemount differential pressure transmitter measured the pressure drop across the orifice. Also required was an gage pressure transducer and thermocouple to measure gage pressure and temperature at the orifice. With these data, the following equation [18] was used to calculate the mass flow rate:

$$W = 359.1\left\{\frac{\mathrm{lb_m}}{\mathrm{in^2\ hr}}\left[(\mathrm{in.H_2O})\frac{\mathrm{lb_m}}{\mathrm{ft^3}}\right]^{\frac{1}{2}}\right\} d^2 K\sqrt{h_w \rho}\,, \tag{10}$$

where W was the mass flow rate (lb_m/hr), d was the orifice diameter (in.), K was the flow coefficient, h_w was the pressure drop across the orifice (in.H2O), ρ was the upstream density (lb_m/ft^3), and the constant serves to correct for the units. The definition of the parameters in Eq. 10 are fully explained in Sec. 4.2. The units correction was so complex because the parameters used in the equation had typical units. For example, the orifice diameter is usually small, therefore inches were used, while units for density were lb_m/ft^3.

2.4.2.2 Pulse Damping System

The Tecumseh compressor on the experimental apparatus was of the single piston, single acting, reciprocating type. This results in large volume flow rate variations per cycle of the compressor. Mass flow rate is proportional to the square root of the pressure

drop across the orifice. For this reason the average signal of the varying pressure drop is not accurate when used to calculate the average mass flow rate.

To dampen the variations, a large volume with a downstream valve was modeled along with an equation for the compressor mass flow. As previously shown in Fig. 11, the oil separator served as a convenient volume for the pulse damping system. The details of this model can be found in Appendix E.

From the model, smaller mass flow variations required larger pressure drops. A valve pressure drop was chosen that served two purposes:

1. an acceptable decrease in the mass flow variation, and
2. a valve differential pressure that would not overload the compressor.

The chosen value was 12 psid (82.74 kPa) across the valve yielding a mass flow fluctuation of ±0.37%, and not demanding an excessively high pressure from the compressor outlet.

2.4.3 Pressure Transducers

Three gage pressure transducers and three differential pressure transducers were used for pressure measurement on the apparatus.

All of the gage units were of the full bridge strain gage, voltage output type. An excitation voltage of approximately 10 Volts was used for the transducers.

A Teledyne model 226-SA (*P1* on the Fig. 11) pressure transducer was used to measure the condenser inlet pressure. This transducer was capable of measuring pressures of 0-300 psia (0-2068.4 kPa).

Measuring the pressure entering the pressure vessel was a Statham Laboratories model P24a-300A-350 transducer (*P2* on the Fig. 11). This unit was also capable of measuring pressures of 0-300 psia (0-2068.4 kPa).

For measurement of the evaporator pressure, a Flader type PSH S was used (*P3* on the Fig. 11). The Flader unit was capable of measuring pressures of 0-100 psia (689.5 kPa).

Each of the gage pressure transducers was balanced using a balancing bridge shown in Fig. 13. The bridge consisted of a potentiometer in the signal output line of the instrument. To correctly balance them, piping was installed to open the transducers to atmospheric pressure through a container of oil, thus avoiding air contamination of the

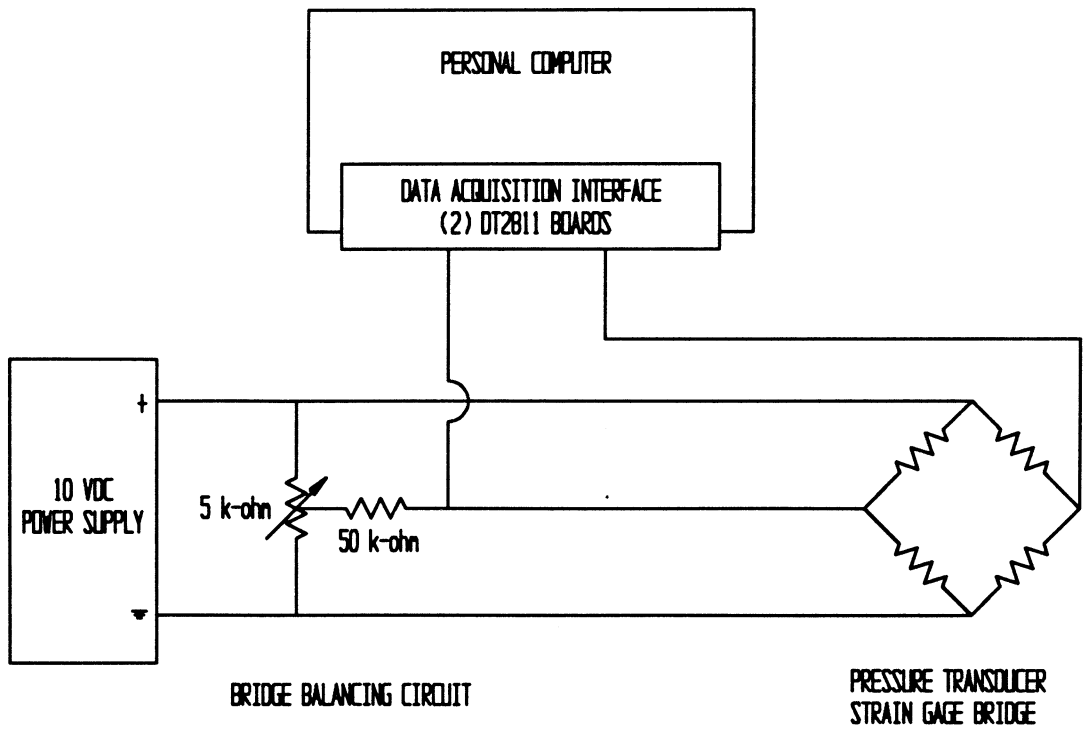

Figure 13 - Balancing Bridge Diagram for Gage Pressure Transducers

system. A FORTRAN program was written to show the voltage out of each transducer to properly balance them. This program is located in Appendix F.

Three differential pressure transducers were used to measure differential pressure across the bubbly flow valve and tube, tube alone, and mass flow meter orifice.

Differential pressure measurement of the bubbly flow elements was handled by two Statham Laboratories P80fTC-50D-350 transducers (*DP2* and *DP3* on the Fig. 11). These transducers were capable of measuring pressures of 0-50 psid (0-344.74 kPa). Excitation was provided by the amplifiers and balancing was accomplished with the amplifier potentiometric LED null indicators which are detailed in Sec. 2.4.6, through similar piping to atmospheric pressure as described above.

The other differential pressure sensor, used with the mass flow meter, was a Rosemount model 2024 with a variable capacitance sensing element (*DP1* on the Fig. 11). This transmitter had a usable differential pressure range adjustable from 0-50 in. H_2O (0-1270 mm H_2O) to 0-250 in. H_2O (0-6350 mm H_2O). Due to the expected pressure drop of approximately 25 in. H_2O (635 mm H_2O), the transmitter was configured for the 0-50 in. H_2O (0-1270 mm H_2O) range. The output of this transmitter was 4-20 mA. High precision resistors were used to convert the current output to voltage before being sampled by the data acquisition board. Balancing on the Rosemount flow meter differential transducer was done with the zero adjust on the transducer itself and no amplifier channel was used. Excitation was provided with a 10V power source.

All pressure sensors with the exception of the Rosemount differential pressure transducer were calibrated in-situ with a dead weight tester. The Rosemount transmitter was calibrated in-situ using a 60 in. (1524 mm) manometer which allowed a much smaller pressure range. A FORTRAN computer program was written for the above instrumentation calibration. The calibration techniques and program are located in Appendix B.

Two methods of liquid pressure line piping were used to avoid liquid head effects on the pressure measurements:

1. The sensing line was fixed to the top, and elevated from, the desired pressure line before entering the transducer port. This caused vapor to fill the sensing line entering the transducer.
2. The transducer was located at the same level as the desired pressure line creating no static liquid head.

2.4.4 Thermocouples

Type-T thermocouples with 0.125 in. (3.18 mm) stainless steel sheaths were used. A thermocouple accompanies each gage pressure transducer in the locations described above. Thermocouple correlation constants from the manufacturer [19] were used to convert the millivolt output signal to temperature in degrees Celsius; this procedure is located in Appendix G. A Hy-Cal Engineering thermocouple reference junction was used to condition the temperature signal before sampling with the data acquisition system.

Two methods were used to increase the accuracy of the temperature measurements:

1. Insertion of the thermocouples into tee junctions to promote turbulence in the flow.
2. Insulation of the thermocouple sheaths to reduce convective and radiative heat transfer to the surroundings.

Due to the importance of the pressure and temperature measurements made at the inlet of the pressure vessel, the thermocouple (*T2* on Fig. 11) was calibrated against the pressure transducer. A metering valve placed upstream of the two instruments throttled the flow into the two-phase region therefore fixing the temperature of the fluid with knowledge of the pressure. A FORTRAN computer program located in Appendix H was used to store the measured temperature, measured pressure, and the calculated temperature from refrigerant property subroutines based on the measured pressure. A small eye-glass moisture indicator between the metering valve and instruments provided a method of ensuring that two phase flow was present. The results of the calibration are shown graphically in Sec. 5.4.

From these results a small linear correction was made to the thermocouple reading:

$$T2_{corr} = T2_{meas} + (0.1137 * T2_{meas} - 10.7334), \tag{11}$$

where the temperatures were in degrees F. This resulted in a correction of less than 2.7°F during normal operation of the experiment, while the average $T2_{meas}$ was approximately 111°F.

2.4.5 Other Instrumentation

Two analog pressure gauges were mounted on the system. One was used for the in-vessel pressure to monitor the pressure on the glass window. The other was used in conjunction with the pulse damping system detailed previously.

The chosen pressure drop across the pulse damping valve was maintained with a piping scheme that allowed the pressure on each side of the valve to be checked separately, thereby eliminating any accuracy problems associated with the analog gauge since the error would be applied to both readings. The differential pressure across the valve was small in relation to the line pressure, approximately 8%, and a Freon compatible differential pressure gauge was not readily available.

2.4.6 Amplifiers

The output voltage from three instruments were fed into the amplifiers:

1. the strain gage Wheatstone bridge, and
2. both Statham Laboratories differential pressure cells.

To amplify these signals, a Measurements Group Strain Gage Conditioner and Amplifier System were used. The model 2110A Power Supply Module provided the excitation voltages. In addition, a 2120A Conditioner Module was used to amplify the above voltage output signals.

The Conditioner Module components included a ten-turn potentiometer for balancing with LED null indicators and an adjustable gain ranging from 1 to 2100. The gain was chosen based on the maximum signal expected from the instrument during operation. Adjustment of the excitation voltage was also provided on this unit but supplied by the Power Supply Module.

Both the Strain Gage Conditioner and Power Supply Module worked as an integral unit. With the Conditioner providing controls for the individual channels or instruments, the Power Supply unit could serve several of them at once.

2.4.7 Fan Speed Control

To maintain desired pressure in the condenser and evaporator, two variable speed electric fans were employed. A PID control system was used to control the fans' speed. This system was developed by Menegay [2] and was not modified for the present experimentation.

The data acquisition hardware was equipped with Digital/Analog converters to allow for DC voltage output determined from the PID control routine. The computer was capable of outputting a voltage of -5 Volts to +5 Volts. This voltage was then amplified where it was converted to a corresponding AC voltage to power the electric fan motors.

2.4.8 Data Acquisition Hardware

Data acquisition was achieved with the use of a JDR Microdevices 286 personal computer with two Data Translation DT2811 boards installed.

The DT2811 boards each allowed eight differential input signals. Differences in the boards configuration was confined to the available gain settings. One board handled the higher voltage input signals such as those from the amplifiers, while the other had the capability of amplifying lower signals. These gain settings were defined by the software; each board was physically identical. Referred to as Board 1 and Board 2, Table 3 outlines the available gains and allowable input voltages [20].

Table 3 - Available Gains for DT2811 Data Acquisition Boards

	Board 1	Board 2
Available Gain	1,2,4,8	1,10,100,500
Input Voltage Range	-5V,+5V	-2.5V,+2.5V

Two D/A channels were also available on each board for output voltage signals as with the fan-speed control scheme. All D/A channels were configured for -5V,+5V output.

The actual data taking program was written in FORTRAN and linked with the data acquisition routines from Data Translation and FORTRAN R-12 refrigerant subroutines. This program can be found in Appendix H.

2.4.9 Experimental Procedure

Development of the testing schedule began well before the system was operable. The original hope was to complement previous experimentation. This was found to be impossible with the given apparatus because of equipment limitations.

The objective of this experiment was to measure the efficiency of the nozzle and to gain a better understanding of the bubbly flow tube process. To this end, experimental variables were chosen that would allow complete characterization of the nozzle performance. These parameters included the condenser pressure and mass flow rate.

The superheat of the vapor leaving the evaporator provided a convenient control for the mass flow rate. Changes in the position of the bubbly flow valve caused changes in the superheat of the evaporator out flow and hence, the mass flow rate. For various condenser pressures, the above method was used to vary the mass flow rate while the superheat value was used as a gauge of steady state in the system.

The procedure used to achieve the objective of this experimentation follows:

1. The system was charged with refrigerant to approximately 40 psia (275.8 kPa). This was done so that the pressure transducers could be zeroed by relieving their pressure into a can of oil ensuring no air contamination of the system.
2. The pressure transducers were balanced using the appropriate means; balancing bridge, amplifier potentiometer, or zero adjust on the instrument itself. At this point, a reading of atmospheric pressure was taken to be input into the data acquisition program.
3. After re-valving the instrumentation back into the system, the compressor was started. The receiver was opened to allow the system to fully charge. Since it was not large enough to hold all the liquid refrigerant required for the system to operate properly, another tank of refrigerant was connected to the suction side of the compressor to complete the charging of the system.
4. At this point, the system was left to reach thermal equilibrium. Two important notes were that the system must be monitored to avoid any flooding of the

evaporator leading to liquid carry-over to the compressor and the evaporator set point should be reached before the execution of the next step. Both of these concerns were controlled via the bubbly flow valve. Closing the valve caused the superheat to increase and the pressure of the evaporator outlet fluid to decrease. Opening the valve produced the opposite effects.

5. Once the system had reached thermal equilibrium, and the evaporator pressure reached the desired set point, the strain gages were re-zeroed. This was accomplished by shutting the bubbly flow valve, which stopped the flow through the nozzle. When the thrust signal was no longer driven by the flow, the remaining voltage signal was adjusted to zero using the amplifier balance bridge.
6. Data was taken provided the system was in steady state. As described previously, the instrumentation signals were collected by a data acquisition program which is reported in Appendix H. A minimum of 120 data points were taken during each run; this corresponds to at least 100 seconds of data storage at steady state.
7. Once enough data was obtained, the program was terminated and either the bubbly flow valve was adjusted to obtain a different mass flow rate, or a new condenser pressure was chosen.
8. Again, steady state was achieved and step 6 was repeated.
9. When testing was completed, the compressor was shut down and the refrigerant removed from the system in accordance with current laws regarding R-12 refrigerant reclamation established by the Environmental Protection Agency.

After shutting down the system, the data was analyzed to confirm that it was indeed taken at steady state. All transient data was rejected and the remaining data averaged to produce one set of data. This set of data was then used for the overall analysis of the experiment. The full data sets can be found in Appendix I.

Chapter 3
Error Analysis

3.1 Introduction

An error analysis was performed to determine the maximum possible error on the efficiency and metastability parameter. This was done to define the accuracy of the calculations.

The efficiency error was especially important since its calculation utilized nine of the eleven pieces of experimental apparatus instrumentation, possibly allowing errors to accumulate.

A simulation of the classical error analysis as explained by Schenck [21] was performed using a FORTRAN computer program, located in Appendix J, to compute the error in four experimental measurements:

1. thrust, F,
2. mass flow rate, $\dot{m}$,
3. efficiency, η, and
4. metastability parameter, C_m.

The errors for these measurements are detailed in the following sections.

Throughout this chapter, the terms low and high will be used as modifiers for the error values. They refer to the value of the measurement which was lower or higher than the actual measurement. The reason for this separation was that the low and high error were significantly different, and it was believed that each should be reported.

The development of the error analysis computer program was initially difficult since it was not always intuitively obvious which instrumentation error, the low or the high, would yield the low or high error of the experimental measurements. The coupling of the instrumentation signals with the above measurements through refrigerant properties was oftentimes complicating.

The computer program utilized sections of the data acquisition program allowing all refrigerant properties and system parameters to be calculated in exactly the same manner as in the data analysis routine, thereby eliminating the chance of introducing additional errors. All data generated by the program is stored in Appendix K.

The errors in the measurements will be explained by presenting the actual average error value. In addition, the deviation of this value will be expressed by reporting the mimimum and maximum percentage that the error comprises of the actual measurement. This is done to indicate the constancy of the error. In some of the following cases, the error of the measurement increases substantially as the measurement increases.

Since several of the calculations shared the same instrumentation, a brief section on instrumentation error will precede the discussion of experimental measurement error.

Another source of possible error was the existence of shocks outside the nozzle exit. A brief discussion concerning the implication of oblique or detached shocks and expansion waves outside the nozzle was given in Sec. 1.4. The procedure and results of a shock analysis are presented as well as relevant research of literature concerning shock waves in two-phase flow.

3.2 Instrumentation Error

The error in the experimental apparatus instrumentation was carried into each calculation for which it was used. The following was the source or method used to determine the error for each type of instrumentation:

- Thermocouples: The published limit of error given by the manufacturer for Type-T thermocouples was ±1°C(K) or ±1.8°F(R) [19].
- Thermocouple Reference Block: The published limit of error given by the manufacturer for the thermocouple compensation reference junction was ±0.05°C(K) or ±0.09°F(R) [22].
- Gage and Differential Pressure Transducers: Since all pressure cells used for this experiment were calibrated in-situ, reliance on transducer error limits, amplifier errors, and data acquisition errors were eliminated. Instead, the standard deviation from the calibration curve was used to determine the overall error for both the absolute and differential pressure transducers.
- Strain Gage Wheatstone Bridge: The same error determination method was applied to the thrust measuring strain gages as was used for the pressure transducers. Again, the standard deviation from the calibration of the Wheatstone bridge eliminated the need to combine the errors of each of the experimental data acquisition equipment separately.

Calibration correlations for all instrumentation can be found in Appendix B.

Table 4 shows the error associated with each instrument and is used for reference throughout the remaining sections of this chapter.

Table 4 - Instrumentation Error

Type of Instrument	Symbol	Standard Deviation or Error
Thermocouples	*T1, T2, T3*	±1.8°F (±1.0°C)
Thermocouple Reference Block	*CRJ*	±0.09°F (±0.05°C)
Absolute Pressure Transducer	*P1*	±0.0063 psia (0.0435 kPa)
Absolute Pressure Transducer	*P2*	±0.0205 psia (0.1415 kPa)
Absolute Pressure Transducer	*P3*	±0.0167 psia (0.1150 kPa)
Differential Pressure Transducer	*DP1*	±0.0012 psid (0.0083 kPa)
Differential Pressure Transducer	*DP2*	±0.0005 psid (0.0037 kPa)
Differential Pressure Transducer	*DP3*	±0.0006 psid (0.0041 kPa)
Wheatstone Bridge for Strain Gages	*SGT*	±0.0031 lb_f (0.0135 N)

The symbols can be found on Fig. 11 in Sec. 2.4.1 for a graphical illustration of the location of each instrument.

By estimating the error in each calibrated instrument to be twice the standard deviation, a confidence interval of 95.44% was achieved for the error in each of the measurements examined in this chapter. The simple relation for the confidence interval as a function of the standard deviation can be found in any statistics text.

3.3 Thrust Measurement Error

Calculation of the thrust error (*SGT* in Table 4) was trivial. It was simply equal to twice the standard deviation from the calibration curve for the strain gage Wheatstone bridge.

Table 5 shows the values derived from the computer program for the thrust error.

Table 5 - Thrust Error Analysis Results

Error (lb_f)	% Minimum Thrust	% Maximum Thrust
±0.0061	±6.14%	±7.91%

Figure 14 shows the thrust with limits of error graphically.

3.4 Mass Flow Rate Measurement Error

Determination of the mass flow rate error was much more difficult than the thrust. Even though the mass flow calculation was a function of only three separate error contributing instrumentation signals, the relatively complex procedure used for its determination in the data acquisition program made its error calculation a complicated procedure. Recalling Eq. 10 to illustrate the parameters involved in the calculation of the mass flow rate,

$$W = 359.1\left\{\frac{\mathrm{lb_m}}{\mathrm{in^2\ hr}}\left[(\mathrm{in.H_2O})\frac{\mathrm{lb_m}}{\mathrm{ft^3}}\right]^{\frac{1}{2}}\right\} d^2 K\sqrt{h_w \rho}, \qquad (10)$$

where W was the mass flow rate (lb_m/hr), d was the orifice diameter (in.), K was the flow coefficient, h_w was the pressure drop across the orifice (in. H2O), and the constant serves to correct for the units.

All errors for the factors determined by experimental instrumentation in the mass flow rate equation were incorporated into the error analysis program. These are discussed below. The mass flow rate calculation procedure is detailed in Sec. 4.2.

An equation for the flow coefficient, K, was obtained. This equation was a function of the flow Reynolds number which itself was a function of the mass flow rate, implying that the mass flow equation could not be solved explicitly. The dynamic viscosity term in the Reynolds number required measurement of the process fluid temperature (*T1* in Table 4) of the flow meter. See Eq. 18 in Sec. 4.2 for the flow coefficient relation. Orifice pressure drop, h_w, was measured with a differential pressure transducer (*DP1* in Table 4).

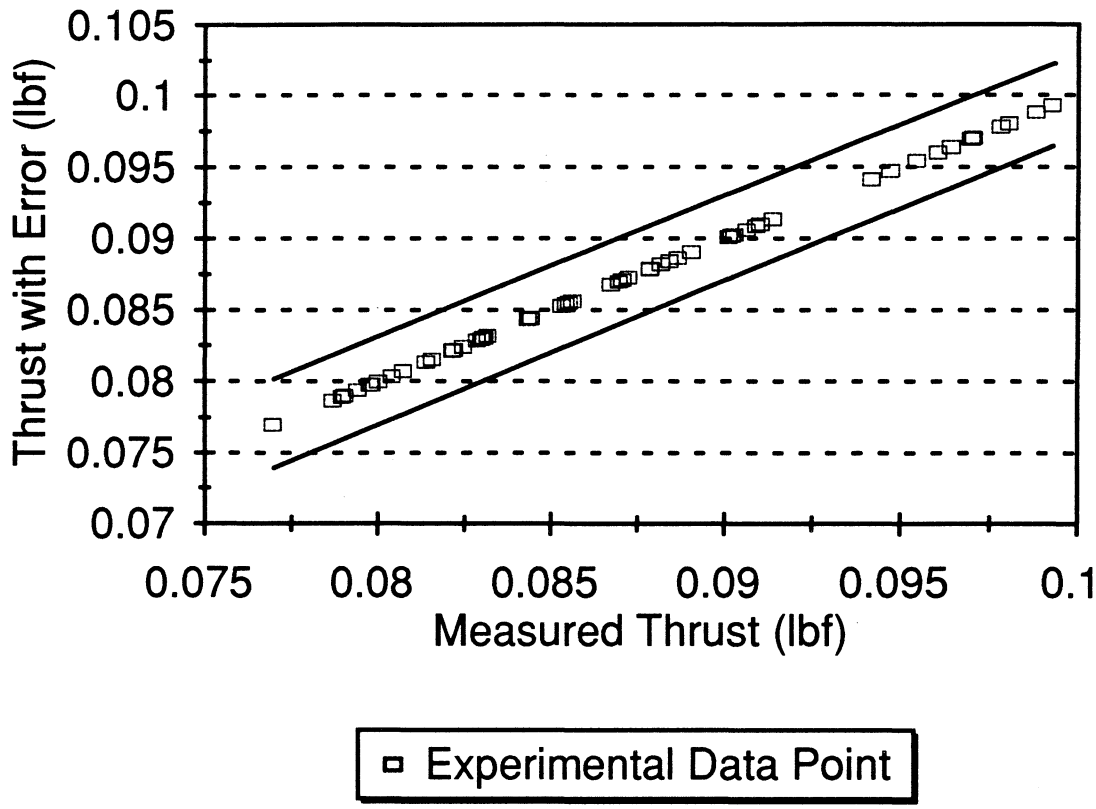

Figure 14 - Thrust with Limits of Error

Calculation of the density from computer subroutine equations of state required both the pressure and temperature (*P1* and *T1* in Table 4) since the process fluid was superheated vapor.

In addition to the above sources of instrumentation error in the mass flow rate calculation, an inaccuracy was used for the orifice flow meter acting as a unit. This inaccuracy, 0.75%, was determined from a manufacturer [15] of an orifice plate, flanges, and honed pipe similar to those used in this experiment.

Table 6 shows the computer program derived values for the average low and high mass flow rate error and the standard deviation ratio:

Table 6 - Mass Flow Rate Error Analysis Results

	Error (lb_m/min)	% Minimum Mass Flow	% Maximum Mass Flow
Low	-0.0165	-1.00%	-1.25%
High	0.0169	1.16%	1.40%

Figure 15 shows the mass flow rate with limits of error graphically.

Factors not considered in this error analysis were the following:

- difference in orifice diameter, *d*, from the design size,
- error in convergence of mass flow iteration, (less than 1.0E-6 lb_m/min),
- orifice thermal expansion area multiplier at operating temperature (less than 1.001 [18]), and
- vapor compressibility effects since the pressure drop across the orifice was 0.6% of the line pressure.

3.5 Efficiency Measurement Error

Equation 6, as in the Introduction chapter, shows the parameters used in the calculation of the efficiency,

$$\eta = \frac{F^2 / \dot{m}^2}{2(h_i - h_{e,isen})}. \qquad (6)$$

Attention Patron:

Page 49 is missing
from all copies

Both the thrust and mass flow rate errors in the efficiency measurement have been addressed in this chapter. The remaining parameters in the efficiency calculation, the enthalpy of the fluid entering the nozzle and the enthalpy exiting the nozzle for isentropic expansion, utilized several more instruments.

For the enthalpy entering the nozzle, h_i, pressure and temperature measurements entering the pressure vessel (*P2* and *T2* in Table 4) were used. Also needed was the differential pressure measurement across the bubbly flow elements (*DP2* in Table 4) for the calculation of the nozzle inlet fluid pressure.

For the isentropic expansion enthalpy, the nozzle exit pressure was required (*P3* in Table 4). During the initial experimental testing, there was some concern that the pressure drop in the two-phase fluid exiting the vessel was substantial since it had to flow along approximately 15 ft (4.57 m) of 0.375 in. (9.525 mm) copper tubing before arriving at the transducer. The analog pressure gauge that was placed on the fluid line exiting the pressure vessel was located about 2 ft (0.61 m) from the vessel along this same line. To determine the pressure drop in the two-phase fluid, the analog gauge was calibrated against the pressure transducer at a static pressure approximately equal to the operating pressure. It was determined that there was an approximately 1.66 psi (11.4 kPa) pressure drop between the vessel refrigerant line exit and the location of the pressure transducer. All relevant data, including the nozzle efficiency, were adjusted for this difference.

Table 7 shows the computer program derived values for the average low and high efficiency error:

Table 7 - Efficiency Error Analysis Results

	Error	% Minimum Efficiency	% Maximum Efficiency
Low	-0.0533	-18.46%	-19.81%
High	0.0632	21.81%	23.58%

One important note is that the reported error is based on a percentage of the efficiency measurement (i.e., high error $\eta = \eta + \eta * 0.2181$). The difference between the low and high errors seems to be attributed to the refrigerant properties which are highly non-linear.

Figure 16 shows the efficiency with limits of error graphically.

More information on the calculation of the efficiency is presented in Sec. 4.3.

3.6 Metastability Parameter Measurement Error

For the metastability parameter errors, which were also calculated in the computer program, the mass flow rate was again needed. Equation 8, repeated below, shows the factors that were calculated for determination of the metastability parameter, C_m,

$$C_m = \frac{\dot{m}_{EXP} - \dot{m}_{HEM}}{\dot{m}_{FROZ} - \dot{m}_{HEM}}. \tag{8}$$

Errors in the experimental mass flow rate have previously been explained. The remaining parameters were the HEM and frozen critical mass flow rates. Section 4.4 fully details the procedure used to determine both critical mass flow rate values. For the determination of these flow rates, the pressure and quality of the fluid entering the nozzle were needed. As in the efficiency calculation, pressure and temperature measurements of the fluid entering the pressure vessel were used (*P2* and *T2* in Table 4).

Table 8 shows the computer program derived values for the average low and high metastability parameter error:

Table 8 - Metastability Parameter Error Analysis Results

	Error	% Minimum Metastability Parameter	% Maximum Metastability Parameter
Low	-0.0214	-11.04%	-14.03%
High	0.0235	12.82%	14.21%

Again, the reported error is based on a percentage of the metastability parameter measurement.

Figure 17 shows the metastability with limits of error graphically.

Any variation in the nozzle throat and exit areas from that given by the manufacturer were not considered in this analysis.

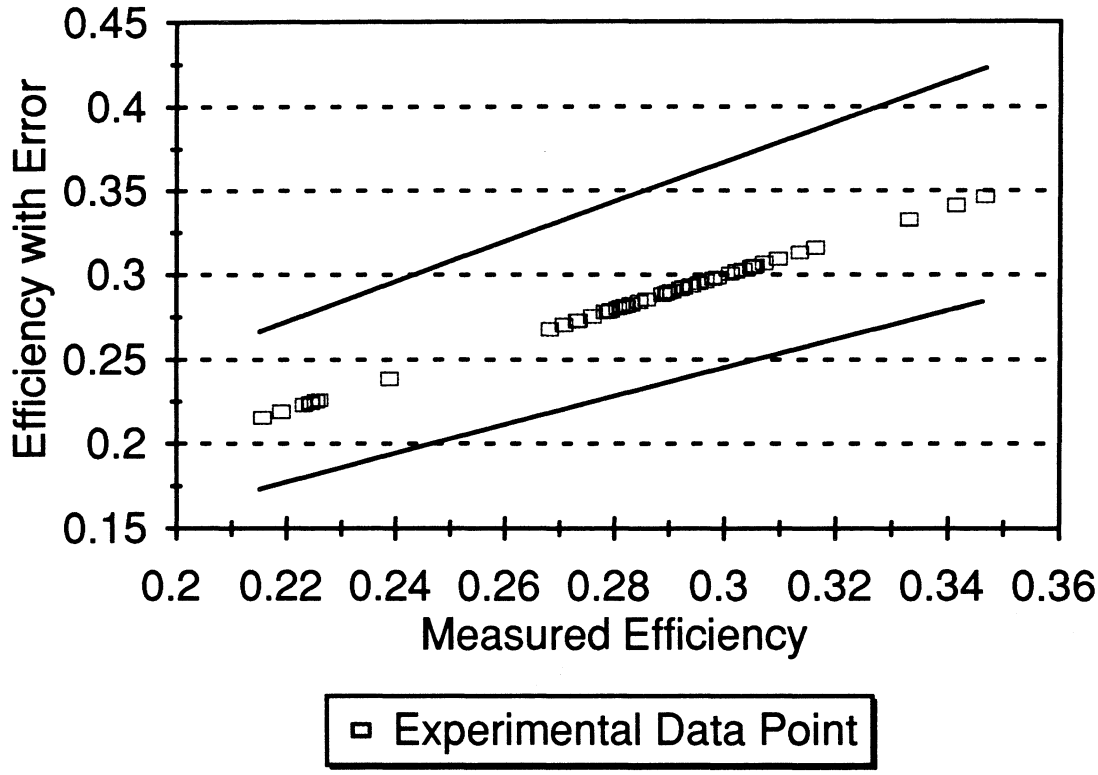

Figure 16 - Efficiency with Limits of Error

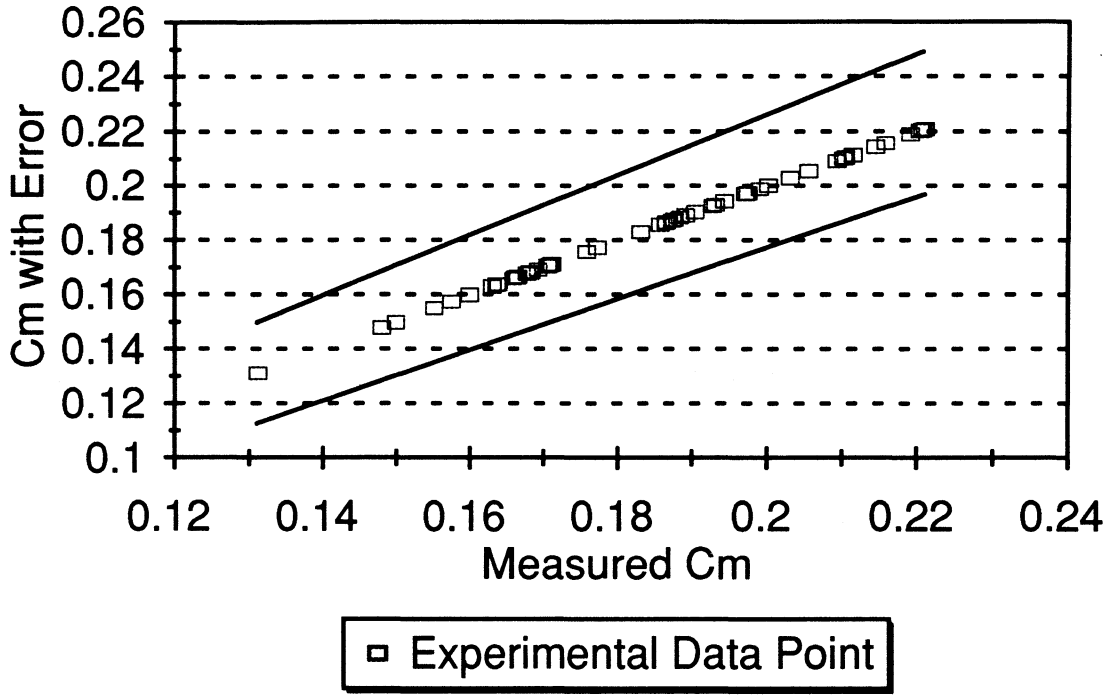

Figure 17 - Metastability Parameter with Limits of Error

3.7 Shock Analysis Results

As mentioned in Sec. 1.4, an analysis on the existence of shocks was necessary to prove that the momentum balance on the nozzle was accurate.

The investigation of the nozzle flow is divided into three sections:

1. An ideal gas example to illustrate a graphical method for determination of shock existence.
2. A simplified analysis using the HEM to model the fluid processes through the nozzle.
3. A discussion of previous research concerning shock waves in two-phase flow and the implications for the present experimentation.

3.7.1 Ideal Gas Example

An ideal gas example will first be presented to illustrate a graph that will allow determination of the nozzle ambient pressure required for pressure discontinuities in the nozzle flow.

From convergent-divergent nozzle compressible flow theory, a graph of the exit to stagnation pressure ratio, P_e/P_o, versus the back to stagnation pressure ratio, P_b/P_o, will illustrate the required back pressure of the nozzle for the following phenomena:

- critical flow,
- subsonic isentropic expansion,
- a standing normal shock wave at the nozzle exit,
- the inception of oblique shocks outside of the nozzle,
- supersonic isentropic expansion, and
- the inception of expansion waves outside the nozzle.

Since the subject of compressible nozzle flow is well known, a general discussion will not be presented here.

With knowledge of the nozzle geometry, and inlet and ambient pressures, the results presented in Fig. 18 can be determined from common isentropic and normal shock tables [23] found in any compressible flow text. A discussion on the development of each point and the physical condition represented by each segment of the line is provided in Table 9.

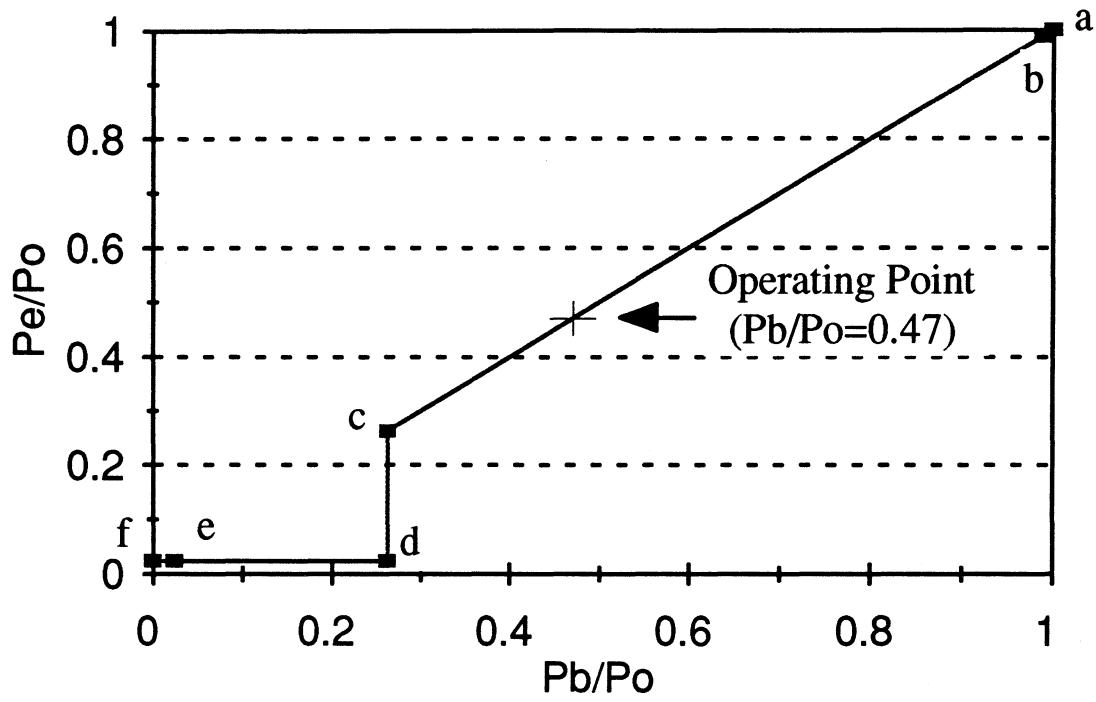

Figure 18 - Ideal Gas Graphical Shock Solution

Table 9 - Point and Segment Description for Graphical Shock Solution

Point or Segment	Description
Point *a*	This point represents the point of no-flow because there is no pressure differential across the nozzle to cause flow.
Segment *a-b*	No shock waves inside or outside the nozzle.
Point *b*	The back pressure which causes the nozzle mass flow rate to become critical. At this pressure, the flow through the nozzle is expanded isentropically, and subsonically.
Segment *b-c*	Standing normal shock inside of the nozzle.
Segment *c-d*	Standing normal shock at the exit plane of the nozzle (not a continuous segment or process line).
Point *c, d*	A standing normal wave at the nozzle exit is formed.
Segment *d-e*	Oblique shock waves outside of the nozzle.
Point *e*	At this back pressure, the flow through the nozzle is expanded isentropically, and supersonically.
Segment *e-f*	Expansion waves outside of the nozzle.
Point *f*	The back pressure is reduced to zero absolute pressure.

The stagnation pressure used to determine these results was the average nozzle inlet pressure from experimentation; 120.2 psia (828.75 kPa). The above example was presented only to illustrate the convenient graph used for determining the nozzle conditions necessary for pressure discontinuity phemonena.

3.7.2 HEM Analysis

Figure 19 shows the same graph used in the section above to determine the existence of shocks in the nozzle with the important difference of the nozzle fluid. This analysis assumes that the two-phase fluid in the nozzle is homogeneous and in equilibrium. The HEM analysis is intended to be an approximation of the actual process for two-phase fluid flow.

A FORTRAN computer program, located in Appendix L, was written to calculate the critical mass flow rate, and the isentropic subsonic and supersonic expansion back pressures. The procedure for back pressure calculation is shown below.

For critical mass flow rate:

1. Input nozzle inlet pressure and quality.
2. Use refrigerant property subroutines to determine the enthalpy and entropy of the nozzle inlet state.
3. Guess a throat pressure lower than the inlet pressure.
4. With the same entropy as the calculated inlet value, determine the enthalpy and density of the fluid.
5. Calculate the velocity using

$$U_{thr} = \sqrt{2(h_{in} - h_{thr})}. \tag{12}$$

6. Calculate the mass flow rate using

$$\dot{m}_c = \rho_{thr} A_{thr} U_{thr}. \tag{13}$$

7. Iterate steps 3. through 6. until the mass flow rate reaches a maximum, this is the critical mass flow rate.

For the isentropic subsonic expansion case (point *b*):

8. Guess an exit pressure higher than the throat pressure.
9. With the same entropy as the calculated inlet value, determine the enthalpy and density of the fluid.
10. Calculate the velocity again using Eq. 12.
11. Calculate the nozzle exit area with the mass flow rate determined above in step 7. using

$$A_e = \frac{\dot{m}_c}{\rho_e U_e}. \tag{14}$$

12. Iterate steps 8. through 11. until the calculated area equals the actual nozzle exit area at which point the guessed back pressure is equal to the isentropic, subsonic expansion exit pressure.

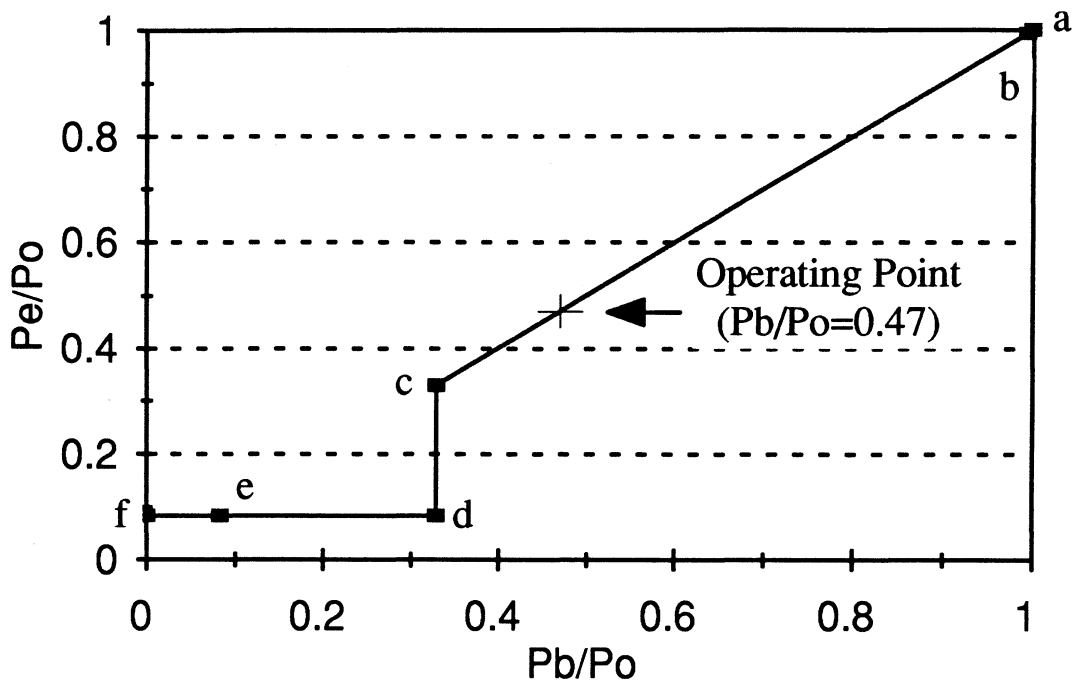

Figure 19 - HEM Two-Phase Graphical Shock Solution

For the isentropic supersonic expansion case (point *e*):

8. Guess an exit pressure lower than the throat pressure.
9. With the same entropy as the calculated inlet value, determine the enthalpy and density of the fluid.
10. Calculate the velocity using Eq. 12.
11. Calculate the nozzle exit area with the mass flow rate determined above in step 7. using Eq. 14.
12. Iterate steps 8. through 11. until the calculated area equals the actual nozzle exit area at which point the guessed back pressure is equal to the isentropic, supersonic expansion exit pressure.

In addition to the critical mass flow, isentropic sub- and supersonic expansion back pressures, Fig. 19 also required the determination of the back pressure required for a normal shock at the nozzle exit plane (points *c* and *d*).

This value was determined from the following forms of the governing equations:
Conservation equation -

$$\rho_1 u_1 = \rho_2 u_2, \tag{15}$$

Momentum equation -

$$P_1 + \rho_1 u_1^2 = P_2 + \rho_2 u_2^2, \tag{16}$$

Energy equation (assuming adiabatic) -

$$h_1 + \tfrac{1}{2} u_1^2 = h_2 + \tfrac{1}{2} u_2^2. \tag{17}$$

Where the subscripts 1 and 2 represent the fluid properties up- and downstream of the shock wave located at the nozzle exit plane. The area terms are left out of the governing equations since the area is constant for this analysis.

The procedure for calculation of this back pressure was as follows:

1. Input results from isentropic, supersonic expansion iteration; P_1, u_1, ρ_1, and h_1.
2. Guess a value for P_2 which is greater than P_1.
3. Calculate u_2 from the conservation and momentum equations.
4. Calculate h_2 from the energy equation.
5. Use the conservation equation to calculate u_2 again.
6. Compare the u_2 calculated from step 3. and 5.
7. Iterate steps 2. through 6. until the u_2 terms are equal.

Another FORTRAN program, also located in Appendix L, was written to iterate this procedure.

The procedures above determined the locations of points *b* through *e* on Fig. 19. The remaining points, *a* and *f*, were trivial since they do not rely on the process fluid or analysis method.

The following results were obtained from the computer programs:

Table 10 - HEM Shock Analysis Results

Isentropic, Subsonic Expansion Back Pressure	119.5 psia (823.6 kPa)
Isentropic, Supersonic Expansion Back Pressure	10.1 psia (69.3 kPa)
Back Pressure for Normal Shock at Nozzle Exit Plane	39.6 psia (272.8 kPa)

The inputs used to determine the above data were the average nozzle inlet pressure, 120.2 psia (828.75 kPa), and the average inlet quality, 0.081936.

The HEM analysis results show that there is no oblique shocks or expansion waves outside of the nozzle since the back pressure required for a standing normal shock wave at the nozzle exit is 39.57 psia (272.82 kPa). This value is less than the experimental back pressure of 56.66 psia (390.66 kPa), indicating that there is a normal shock wave inside the nozzle. Though only the average nozzle inlet property results are presented in this paper, all the data was found to yield this same conclusion.

The HEM results therefore verify the momentum analysis used for this experiment.

3.7.3 Previous Research on Shock Propagation in Two-Phase Fluids

For two-phase fluids, which certainly are poorly modeled by the ideal gas law, an HEM analysis can be an inadequate approximation. For this reason, further research was conducted on two-phase fluid shock propagation. Extensive work has been completed on this subject, but only the relevant and consistent information is reported here.

Homogeneous theory stipulates that when the velocity of the fluid equals the speed of sound in the fluid, critical mass flow has been reached. In a shock wave analysis paper, Moody [24] states that the critical mass flow rate/sonic velocity relation is less clear for a two-phase fluid.

Collingham and Firey [25] also did research on sound velocity in steam-water. They concluded that "the velocity of sound was found to be independent of the quality of the wet steam and approximately equal to the velocity in dry, saturated steam". This statement was also verified empirically in the paper.

The same conclusions were made by DeJong and Firey [26]; mainly that in a vapor-continuous medium, the liquid droplets have a negligible reaction to a shock wave. Hence, the fluid sound speed was best represented by the speed of sound in the vapor phase alone.

Applying the research above on this experiment indicated that the nozzle flow did not include shock waves of any kind and that expansion waves were also not possible given that the experimental back pressure was well above that required for isentropic, supersonic expansion. As the flow expanded and increased velocity in the nozzle, the speed of sound for the fluid also increased. Calculating the velocity from the momentum equation gives an average of 120.8 ft/sec (36.8 m/sec) for all data points taken in this work. The saturated vapor speed of sound for the exiting nozzle fluid was 447.1 ft/sec (136.3 m/sec). Assuming insignificant slip between the phases, comparison of these numbers indicated that the actual flow velocity was well under that required for a shock wave.

Therefore, the research done on two-phase shock propagation also verifies the momentum analysis used for the efficiency calculation.

Chapter 4
Data Analysis

4.1 Introduction

This chapter outlines the equations and procedures used to determine the following experimental quantities:

1. mass flow rate,
2. efficiency, and
3. metastability parameter.

Both the mass flow rate equation and the critical mass flow rates in the metastability parameter calculation can be found in the literature while the calculation of the efficiency was derived specifically for this experiment.

4.2 Mass Flow Rate Procedure

The mass flow rate procedure was located in the data acquisition program. As mentioned in the Experimental Apparatus chapter, an orifice type flow meter was used. Equation 10, repeated here, was the basic mass flow rate measurement formula for an orifice meter;

$$W = 359.1\left\{\frac{\mathrm{lb_m}}{\mathrm{in^2\,hr}}\left[(\mathrm{in.H_2O})\frac{\mathrm{lb_m}}{\mathrm{ft^3}}\right]^{\frac{1}{2}}\right\} d^2 K\sqrt{h_w \rho}\,. \qquad (10)$$

In the data acquisition program, the mass flow rate equation shows up looking quite different. The reason for this was that the flow coefficient was substituted into the mass flow equation.

Calculation of the flow coefficient, K, was achieved with Eq. 18 [17].

$$K = [0.5991 + \frac{0.0044}{D} + \left(0.3155 + \frac{0.0175}{D}\right)(\beta^4 + 2\beta^{16})] + [\frac{0.00052}{D} - 0.000192 + \left(0.01648 - \frac{0.00116}{D}\right)(\beta^4 + 4\beta^{16})]\lambda \quad (18)$$

where: D = the inner diameter of the upstream and downstream piping, (in.),
β = the ratio of the orifice diameter to the piping inner diameter,
λ = $1000 / \sqrt{Re_D}$,
Re_D = pipe Reynolds number.

This equation was valid when: 0.5 in. (12.7 mm) ≤ D ≤ 1.5 in. (38.1 mm),
$0.1 < \beta < 0.8$, and
$Re_D > 1000$.

For this experiment, d = 0.203125 in. (5.16 mm),
D = 0.556 in. (14.12 mm),
$\therefore \beta = (d/D) = 0.3653$, and

$$Re_D = \frac{4\dot{m}}{\pi D \mu}.$$

From Jung and Radermacher's paper on transport properties of pure refrigerants [27], the dynamic gas viscosity for R-12 can be represented by the following equation after substitution of R-12 thermophysical constants and units of viscosity conversion:

$$\mu = [1.9636E-11*(T) - 1.3730E-9]^{0.82}, \quad (19)$$

where the units for μ were slug/(ft·sec), and the absolute temperature in Rankine.

Using average properties for the Reynolds number calculation such as $\dot{m}_{ave}$ = 1.393 lb_m/min (0.632 kg/min), and substituting T_{ave} = 605.5 R (336.4 K) into the gas viscosity equation, the calculation for Reynolds number yielded 59081. Therefore, all the constraints on equation 18 for the flow coefficient were met.

When the flow coefficient relation was substituted into Eq. 10, the mass flow rate could not be determined explicitly. Instead an iteration was used in the data acquisition program to converge on the correct mass flow rate. The accuracy of this convergence was 1.0E-6 lb_m/min.

Initially, the variation of the flow coefficient was unknown since the mass flow rate could only be approximated with previous work [1]. After operating the apparatus, it was determined that the mass flow rate variation between runs was small yielding a maximum flow coefficient variation of only ±0.08%. Hence, the inclusion of the equation for K was unnecessary but not deleterious to the overall mass flow calculation. Equation 20 shows the final version of the mass flow computation used in the data acquisition program:

$$\dot{m} = 0.7967\left\{\frac{lb_m}{min}\sqrt{\frac{in.^2\,ft^3}{lb_f lb_m}}\right\}\sqrt{\Delta P\,\rho} + 0.1677\left\{\frac{lb_m in.ft^2}{lb_f min^2}\sqrt{\frac{lb_f min}{ft}}\right\}\sqrt{\frac{\Delta P\,\rho}{\dot{m}}}\left(5.1655E-7\left\{\frac{1}{°F}\right\}*T-3.6119E-5\right)^{0.41}. \quad (20)$$

Where $\dot{m}$ was the mass flow rate (lb_m/min), ΔP was the pressure drop across the orifice (psid), ρ was the upstream density (lb_m/ft^3), and T was the downstream temperature (R).

The time for each iteration of the data acquisition program was important since it was directly related to the condenser and evaporator fan speed control performance. The less time for each iteration, the better the pressure control of the condenser and evaporator. Adding the internal iteration for mass flow rate to the data acquisition program may have compromised the control procedures; therefore it was optimized to use the least amount of time as possible. An insightful choice of initial conditions for the mass flow calculation limited the number of iterations to 3-5. This was adequate to maintain stability of the control procedures.

All refrigerant properties used in the mass flow rate calculation were obtained from refrigerant subroutine equations of state. A detailed explanation of the instrumentation used to determine the necessary refrigerant properties can be found in Sec 3.4.

4.3 Efficiency Procedure

The efficiency calculation was also located in the data acquisition program. Being a function of the thrust and mass flow rate, which were calculated in the program, the efficiency can be readily obtained by Eq. 6:

$$\eta = \frac{F^2 / \dot{m}^2}{2(h_i - h_{e,isen})}, \tag{6}$$

To describe the origins of Eq. 6, the basis for the efficiency must be explained. Jones and Hawkins [28] does an excellent job of defining nozzle efficiency as follows:

> "Nozzle efficiency η_N is defined as the ratio of the kinetic energy at the nozzle outlet to the kinetic energy that would result at that section if the flow through the nozzle were isentropic between the same initial conditions and the same final pressure."

The denominator of the efficiency equation was obtained from the first law of thermodynamics as derived below.

For open systems such as the nozzle, the first law is written as

$$q - w = \Delta h + \Delta ke + \Delta pe. \tag{21}$$

By neglecting potential energy changes throughout the nozzle, and assuming no heat transfer or work into or out of the nozzle,

$$0 = \Delta h + \Delta ke = (h_i - h_e) + \left(\frac{U_i^2}{2} - \frac{U_e^2}{2} \right), \tag{22}$$

assuming that the inlet velocity was negligible,

$$\frac{U_e^2}{2} = (h_i - h_e), \tag{23}$$

and finally, solving for the exit velocity,

$$U_e = \sqrt{2(h_i - h_e)}. \tag{24}$$

Returning to the definition of the efficiency of a nozzle, which was the kinetic energy ratio between the actual process and the isentropic process,

$$\eta = \frac{\Delta ke, act}{\Delta ke, isen} = \frac{U_{e,act}{}^2}{U_{e,isen}{}^2}. \tag{25}$$

Then, substituting Eq. 24 into Eq. 25, with the appropriate subscripts, the following relation was obtained,

$$\eta = \frac{2(h_i - h_e)_{act}}{2(h_i - h_e)_{isen}}. \tag{26}$$

From Eq. 26, the efficiency can be calculated regardless of non-equilibrium fluid conditions which most certainly exist at the exit of the nozzle. This can be done if the necessary parameters could be determined. Unfortunately the actual exit fluid properties cannot be determined with typical instruments as used in this project because the fluid was in a metastable state.

Therefore, the method of using the thrust and mass flow rate as defined by Eq. 5 to calculate the exit velocity was employed as shown:

$$F = U_{e,act}\dot{m}, \tag{5}$$

solving for U_e, and substituting into Eq. 5 gives Eq. 6 repeated below from the Introduction,

$$\eta = \frac{F^2 / \dot{m}^2}{2(h_i - h_{e,isen})}. \tag{6}$$

This was the final version for the efficiency equation used in the data acquisition program, not including the necessary units conversions.

4.4 Metastability Parameter Calculation

Calculation of the metastability parameter, which will be referred to as C_m, was much more complex in procedure than either the mass flow rate or efficiency. A more time consuming iteration was required, making addition of the C_m calculation procedure detrimental to the overall data acquisition programs performance. Two separate programs, located in Appendix M, were written to calculate the necessary nozzle properties to compute the C_m value.

The following two analyses were used in the C_m calculation;

1. HEM, or constant entropy nozzle flow, and
2. frozen, or constant quality nozzle flow.

These two methods represent extreme opposites in critical mass flow rate calculation. The HEM yields the lowest possible mass flow rate and frozen flow yields the maximum possible.

As introduced in Sec. 1.3.2, the following parameter was devised to represent the metastability,

$$C_m = \frac{\dot{m}_{EXP} - \dot{m}_{HEM}}{\dot{m}_{FROZ} - \dot{m}_{HEM}}, \tag{8}$$

The C_m as defined includes the friction within the nozzle in addition to the metastability. A theoretical parameter which incorporates only the metastability cannot be accurately proposed with the apparatus for the present research.

A physical interpretation of the variables in the metastability parameter follows.

Critical mass flow is obtained when the mass flow rate increases to a maximum as the back pressure is continually reduced. When the nozzle flow does reach the maximum, further reduction in the back pressure no longer affects the mass flow through the nozzle.

The physical affect at work here is that the velocity of the fluid at the nozzle throat becomes equal to the speed of sound in the fluid. At this point, the downstream pressure can continue to decrease having no effect on the mass flow rate.

The HEM critical mass flow rate represents the minimum critical flow rate possible of a two-phase fluid through the nozzle. For the flow to be in equilibrium, phase change must be performed infinitely fast as the pressure decreases within the nozzle. HEM allows for this phase change, producing the maximum vapor quantity. This corresponds to the minimum mass flow rate.

The frozen critical mass flow rate represents the maximum flow rate possible of a two-phase fluid through the nozzle. This method assumes no phase change, or that the phase change takes an infinite amount of time within the nozzle. Physically this means that the fluid remains at the low quality at which it entered or that there is a maximum amount of liquid present in the flow corresponding to the maximum mass flow rate.

As can be seen, these calculations will bound the experimental mass flow rate with a value of zero for C_m meaning homogeneous, equilibrium critical flow and a value of one for C_m meaning frozen critical flow. Neither of these types of flow are possible for obvious reasons.

Deviation of the metastability parameter from zero indicates three possibilities of fluid characterization:

1. Non-homogeneity of the fluid. The bubbly flow elements purpose is to provide a well dispersed bubbly fluid, approximating homogeneous flow. If the bubbles or droplets get larger and deform, the fluid can no longer be represented as single-phase.
2. Non-equilibrium or metastability of the fluid. Metastability results from the quality's inability to react quickly enough to changing pressure and temperature to maintain equilibrium, introducing mechanical and thermal non-equilibrium.

All of the above represent factors causing the metastability parameter to deviate from zero. It can also be stated that non-homogeneity promotes non-equilibrium to some degree, so these two factors are not completely independent. In any case, the role of the bubbly flow tube was to reduce metastability by ensuring that dispersed bubbly flow entered the nozzle. The C_m parameter may also be useful in determining the best characteristics of the bubbly flow tube such as the construction material or surface roughness, the inner diameter, and the length; a concept beyond the scope of this project.

4.4.1 Homogeneous Equilibrium Critical Mass Flow Rate Calculation

The HEM mass flow rate calculation is well known and can be found in many two-phase flow texts. As the name implies, this procedure assumes the flow to be homogeneous, or single phase, and in equilibrium throughout the nozzle flow process. This amounts to isentropic, or constant entropy, nozzle flow.

With knowledge of the nozzle inlet state, the HEM critical mass flow can be calculated. Nozzle inlet properties were obtained from the actual data points.

The procedure for HEM critical nozzle flow used in the metastability parameter computer program was as follows:

1. Input the nozzle pressure and quality to determine the stagnation enthalpy and entropy of the refrigerant.
2. Guess the pressure at the choking point; the nozzle throat.
3. Calculate the resulting quality assuming the flow to be constant entropy.
4. With the quality, calculate the specific volume and specific enthalpy.
5. Compute the velocity of the fluid through the nozzle throat with Eq. 27,

$$U_{thr} = \sqrt{2(h_i - h_{thr})}. \tag{27}$$

6. Calculate the mass flow rate with Eq. 28,

$$\dot{m} = \frac{A_{thr} U_{thr}}{v_{thr}}. \tag{28}$$

7. Iterate steps 2. through 6. until the maximum mass flow rate is found. This is the HEM critical mass flow rate.

4.4.2 Frozen Critical Mass Flow Rate Calculation

The frozen mass flow rate procedure was very similar to the HEM calculation except that where the HEM was an isentropic process, frozen flow assumes constant phase composition (i.e., constant quality).

Again, from the actual nozzle inlet properties obtained from the experimental results, the following procedure was used in the metastability parameter calculation program to compute the frozen critical mass flow rate:

1. Input the nozzle inlet pressure and quality to determine the stagnation enthalpy.
2. Guess pressure at choking plane.
3. Calculate the specific volume and enthalpy assuming that the quality was equal to the inlet quality.
4. Compute the fluid velocity at the throat again using Eq. 27.
5. Calculate the mass flow rate using Eq. 28.
6. Iterate steps 2. through 5. until the maximum mass flow rate was found. This was the frozen critical mass flow rate.

Chapter 5
Results

5.1 Introduction

As stated in the Introduction, this project was originally conceived in order to measure the efficiency of a flashing flow nozzle. To this end, the apparatus was designed, built, and tested. The physical apparatus having previously been discussed, this chapter details the following results of the experimental testing:

- nozzle efficiency and metastability measurement results,
- effect of subcooling on these results,
- nozzle effficiency and metastability parameter correlations, and
- re-design of nozzle throat area using experimental results.

Before these results are discussed, an overview of the experimental data organization is provided.

5.2 Organization of Experimental Data

As mentioned in the experimental procedure, two refrigeration system variables were used to fix the experimental state of the refrigeration cycle; the condenser pressure, and the mass flow rate. Control of the condenser pressure was relatively simple since a PID controller was used to run the variable speed condenser fan. The mass flow rate, on the other hand, could not be directly controlled with the apparatus as structured. Mass flow rate was varied using the bubbly flow valve.

A range of condenser pressures was chosen based on the previous experimentation [1] done with the system. The data acquisition program was configured so that the condenser pressure could be input as desired and the fan speed control hardware would regulate the pressure. Sec. 2.4.7 contains further information on the condenser pressure controller hardware.

Experimental runs were conducted at condenser pressures of 150-180 psia (1034.2-1241.1 kPa). The evaporator pressure was maintained at 56.7 psia (390.9 kPa). For each condenser pressure, a number of differing mass flow rate runs were performed. An

orderly experimental matrix cannot be presented here since data for several condenser pressures and mass flow rates were collected. Appendix I contains all the run data obtained in this experiment.

Each run consisted of average properties taken from many data points. The minimum number of data points used for a run was 120. All instrumentation signals were allowed to steady before the data was recorded.

After all the data was recorded, it was further analyzed by spreadsheet software. To ensure that the data was steady, the mass flow rate signal was checked for any overall increasing or decreasing trends. Also, due to the early problem of thrust unsteadiness, the thrust signal and efficiency calculations were analyzed. Table 11 shows the calculations for the average standard deviation and standard deviation ratio to illustrate the steadiness of the thrust, mass flow rate, and efficiency measurements during each run of data.

Table 11 - Evaluation of Measurement Steadiness for Each Run

Measurement	Standard Deviation	Standard Deviation Ratio
Thrust (lbf)	0.0019	±2.22%
Mass Flow Rate (lb_m/min)	0.0090	±0.65%
Efficiency	0.0137	±4.91%

The above calculations for all data is reported in Appendix I.

5.3 Efficiency and Metastability Measurement Results

The most important nozzle properties for which this experiment was conceived was the measurement of the efficiency and the calculation of the nozzle flow metastability.

Figure 20 shows the efficiency as a function of the nozzle inlet quality. The points on the graph represent the subcooling rounded to the nearest degree F. Figure 21 shows the efficiency as a function of the subcooling in degrees F (subcooling refers to the number of degrees the fluid is below the saturation temperature at its pressure). The points on this graph represent the quality percentage rounded to the nearest percent.

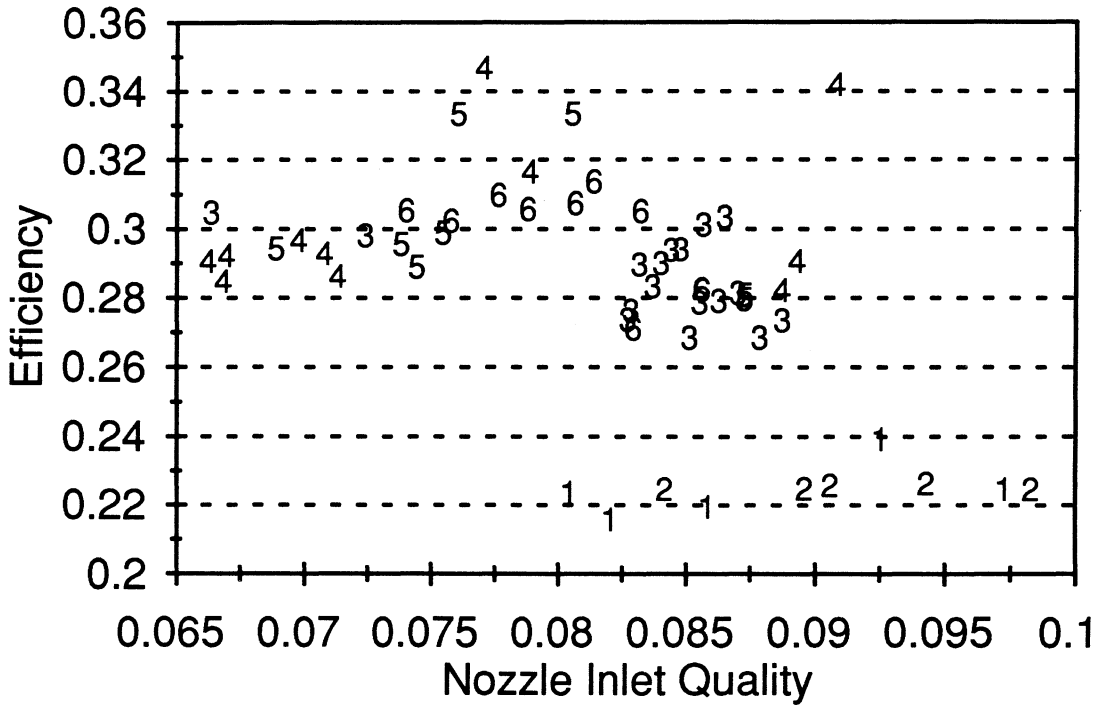

Numbers on Graph are Rounded Subcooling

Figure 20 - Efficiency vs. Nozzle Inlet Quality

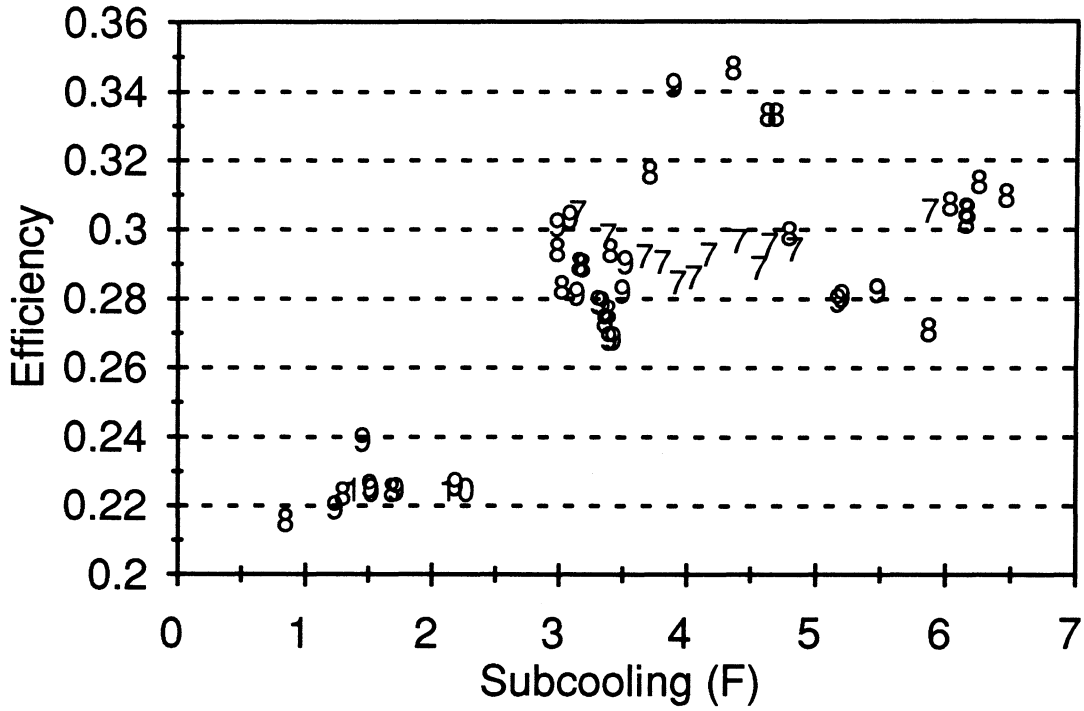

Numbers on Graph are Rounded Nozzle Inlet Quality (%)

Figure 21 - Efficiency vs. Subcooling

Figures 22 and 23 show the same graphs as for the efficiency but with the metastability parameter as the dependent variable.

The nozzle inlet pressure effect on the efficiency and metastability parameter was negligible.

These graphs show that nozzle inlet quality and subcooling were certainly influencing the efficiency and metastability parameter. Nozzle inlet quality was initially anticipated to be the important factor of the flow determining the nozzle performance as explained in Sec. 5.4. The dependence of the efficiency and metastability on the subcooling was unexpected since the bubbly flow valve upstream of the nozzle was expected to erase the history of the fluid. It seems from the experimental data that to achieve the same quality at the nozzle inlet, the amount of throttling, or pressure drop of the fluid, was important. One possibility for this unexpected dependence was that the metastability in the two-phase fluid exiting the bubbly flow valve may have been affecting the bubbly flow tubes performance.

Figure 24 is presented to show the trend of the efficiency to decrease as the metastability of the flow increases. Another interesting, although intuitive, correlation worthy of note was that of the C_m as a function of the mass flow rate as shown in Fig. 25. The general trend was for the metastability to increase with increased mass flow rate. This was expected because as the flow velocity increased, less time was available for phase change, causing further deviation from equilibrium. Increased friction of the nozzle flow was also a result of the increase in flow velocity.

5.4 Effect of Subcooling on Efficiency and Metastability Parameter

Initially it was assumed that the efficiency and metastability parameter would be predicted by the properties at the inlet of the nozzle. This assumption was arrived at by considering that the efficiency was primarily a function of the nozzle inlet state and outlet pressure, while the metastability parameter was a function of the nozzle inlet state and geometry. It was also expected that quality would be the most important nozzle inlet state for each measurement since the flow pattern was directly related to the metastability, and hence, the efficiency.

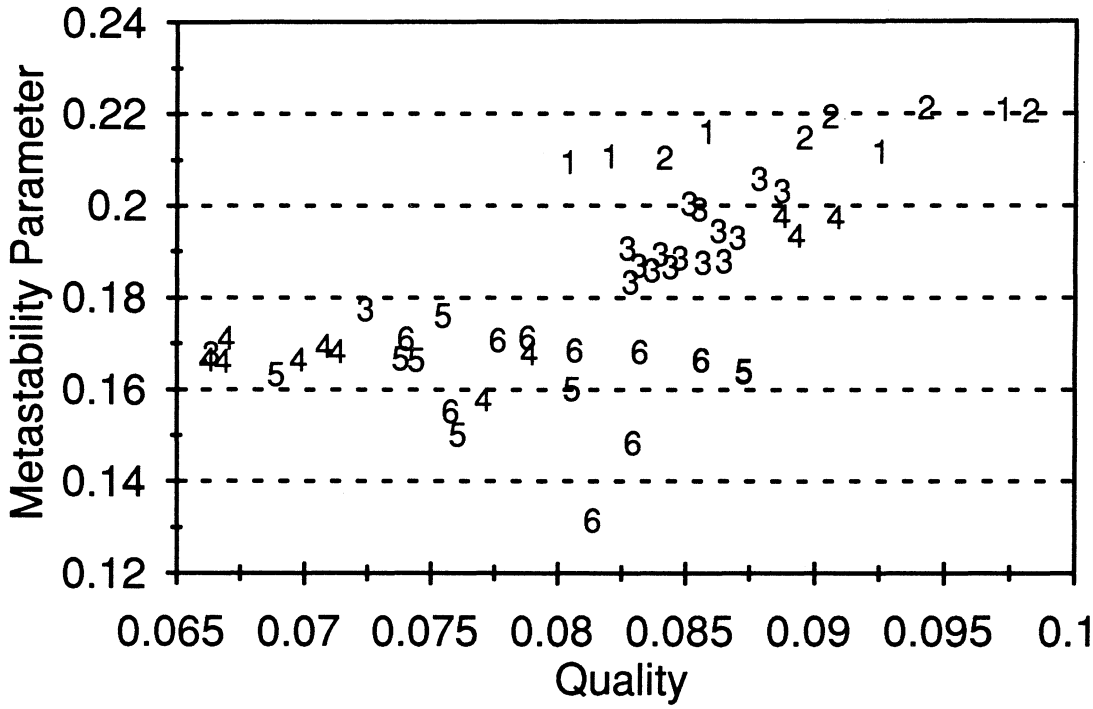

Numbers on Graph are Rounded Subcooling

Figure 22 - Metastability Parameter vs. Nozzle Inlet Quality

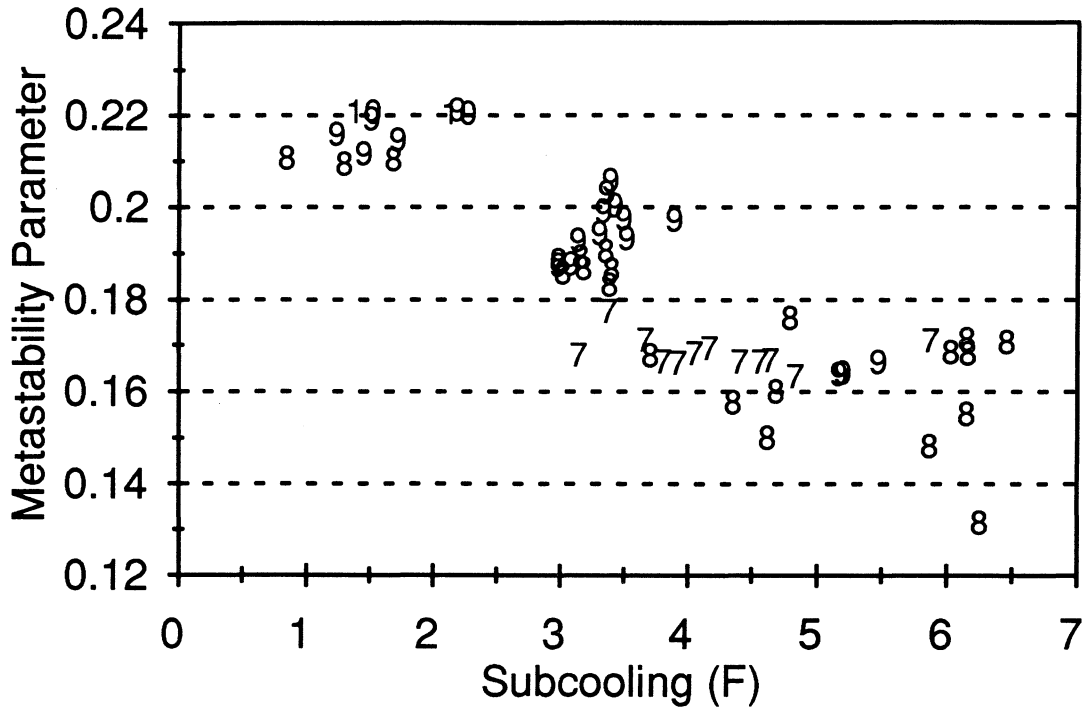

Numbers on Graph are Rounded Nozzle Inlet Quality (%)

Figure 23 - Metastability Parameter vs. Subcooling

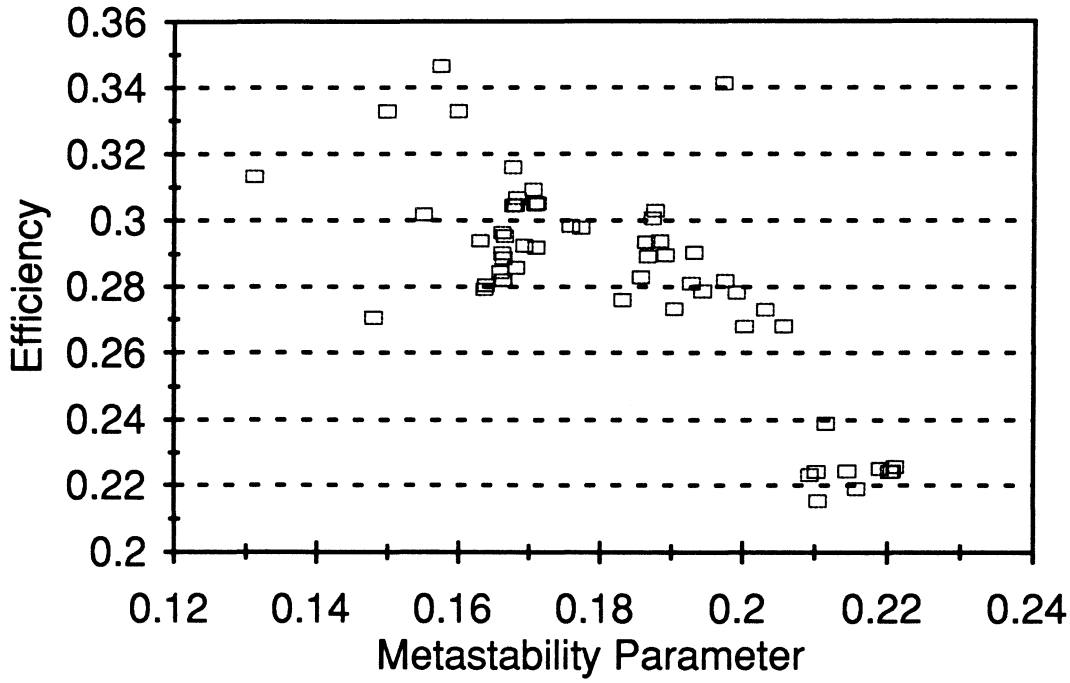

Figure 24 - Efficiency vs. Metastability Parameter

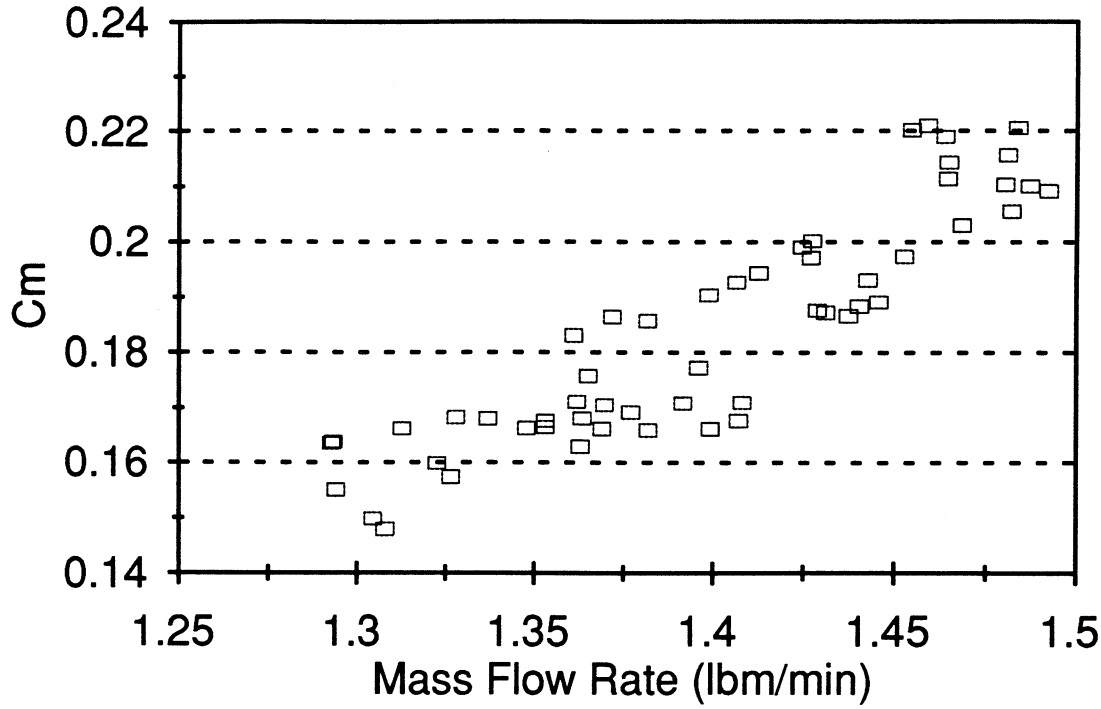

Figure 25 - Metastability Parameter vs. Mass Flow Rate

Unfortunately, the efficiency and metastability parameter proved not to be a function of these properties alone. Only when the subcooling was introduced to the correlation were the measurements adequately predicted with linear regression.

The physical interpretation of the subcooling's effect on the efficiency was unknown at the time of this papers completion. However, one contributing possibility may have been that the thermocouple measuring the subcooling was imprecise and inaccurate; therefore producing incorrect quality calculations.

In Sec. 2.4.4 of this paper, a correction was given for the thermocouple measuring the subcooled temperature leaving the receivers from its calibration. This correction was applied to all the data which was used for analysis. Calibration of the thermocouple was performed several times with small but significant differences each time. One important factor in the calibration results was that the error was approximately equal to the limit of error for a Type-T thermocouple.

An analysis was performed on the effect of the thermocouple on the nozzle inlet quality if the thermocouple was in error an amount equal to its limit of error; 1.8°F (1°C). The results of this analysis are shown in Fig. 26.

This graph shows that the Type-T thermocouple limit of error was significant since the average error of the re-calculated quality was ±9.4% of the original quality. These results alone cannot explain the subcoolings influence since correcting the quality calculation with its error cannot eliminate the subcoolings effect on both the efficiency or metastability parameter.

Fig. 27 shows the calibration graph. The data of the thermocouple clearly indicates the imprecision in its readings; varying by plus and minus the limit of error (±1.8°F) in some cases.

5.5 Efficiency and Metastability Parameter Correlation Results

The nozzle efficiency and metastability parameter were correlated as functions of the nozzle inlet quality and condenser subcooling. This was done to determine, quantitatively, how well the quality and subcooling were predicting the measurements. The results are presented below.

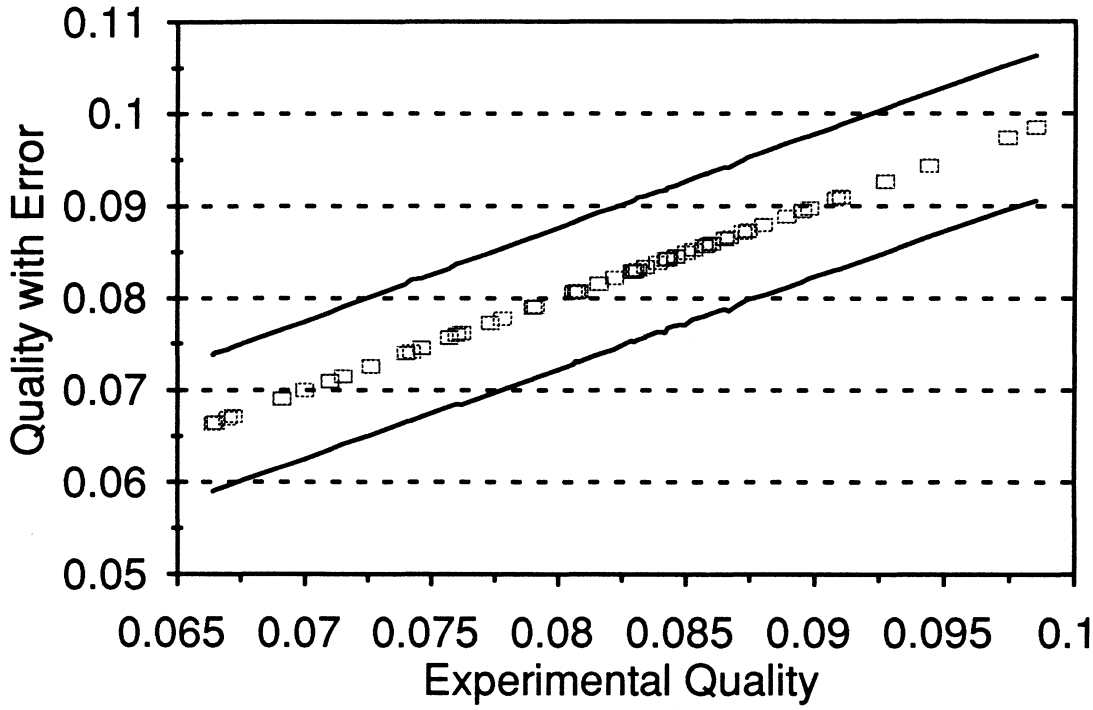

Figure 26 - Error on Quality Due to Thermocouple Temperature with Limit of Error

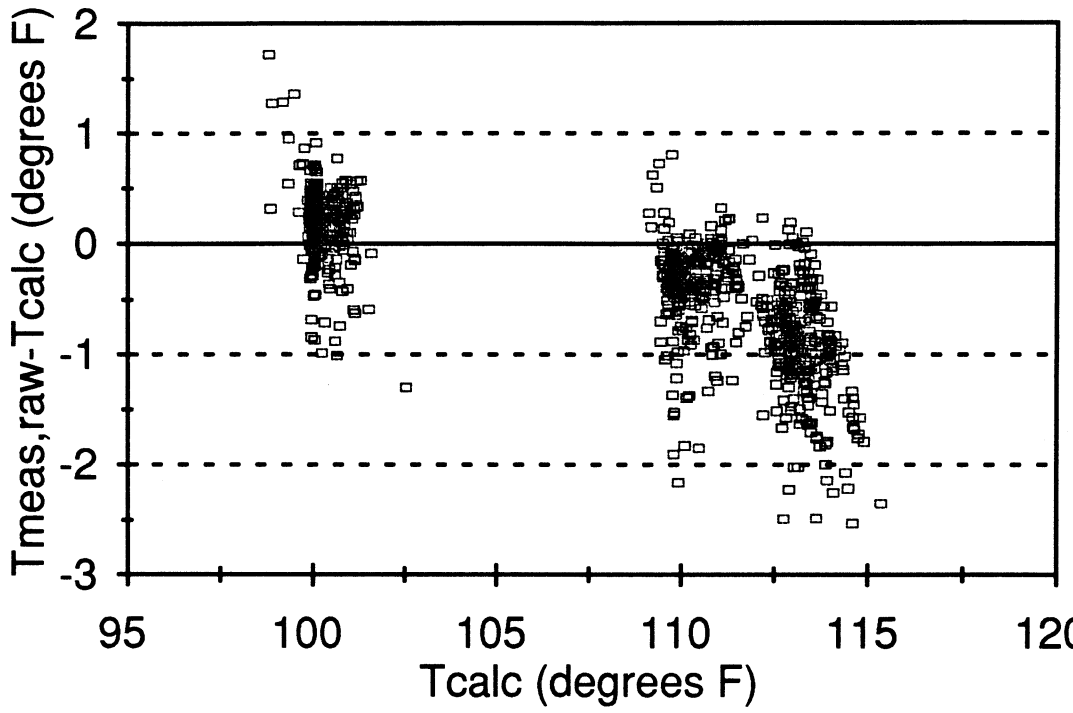

($T_{calc} = T_{sat}$ (@ Measured Pressure))

Figure 27 - Raw Data for Thermocouple Correction

As previously mentioned, the linear regression correlation for the nozzle efficiency and metastability parameter were poor until the subcooling parameter was included. Figures 28 and 29 contain the linear regression graph for the efficiency as a function of the nozzle inlet quality and the subcooling. The correlation equation and statistical methods of determining 'goodness of fit' such as the correlation coefficient, R^2, and the standard deviation, σ, are included on the graph. In the correlation, x_i represents the nozzle inlet quality.

The correlation data points are also shown in the graphs. These points fall within the error limits calculated in Sec. 3.5 and 3.6. This inferred that the correlations were a good estimate of the efficiency and metastability within their respective measurement error.

5.6 Design of Nozzle Using Experimental Data

Using an HEM analysis and a correlation by Henry and Fauske, as Menegay [1] did in his thesis, yielded an oversized nozzle. Another method of nozzle design was proposed. In this case the nozzle inlet fluid properties and discharge coefficient from this experiment were used to design a new nozzle.

As will be discussed in Chapter 6 on recommendations, one modification that will be made to the experimental apparatus after this work is the replacement of the R-12 refrigerant with R-134a. The modifications required for typical vapor compression systems when replacing R-12 with R-134a include mainly the replacement of the compressor lubricant. In addition to this modification, the experimental apparatus will require one important additional change; the nozzle throat area.

The positive displacement compressor used for this experiment inherently delivers a constant mass flow rate given the inlet fluid properties are equivalent. The very reason R-134a was a designated replacement for R-12 was that their thermodynamic properties were very similar. Therefore, the mass flow rate in the system was expected to remain the same for both refrigerants.

To perform an HEM analysis on a nozzle with unknown throat area, the critical mass flow rate must be known. Therefore, the coefficient of discharge, C_d, was assumed equal for each refrigerant. This is a reasonable assumption because of the interchangability of the refrigerants.

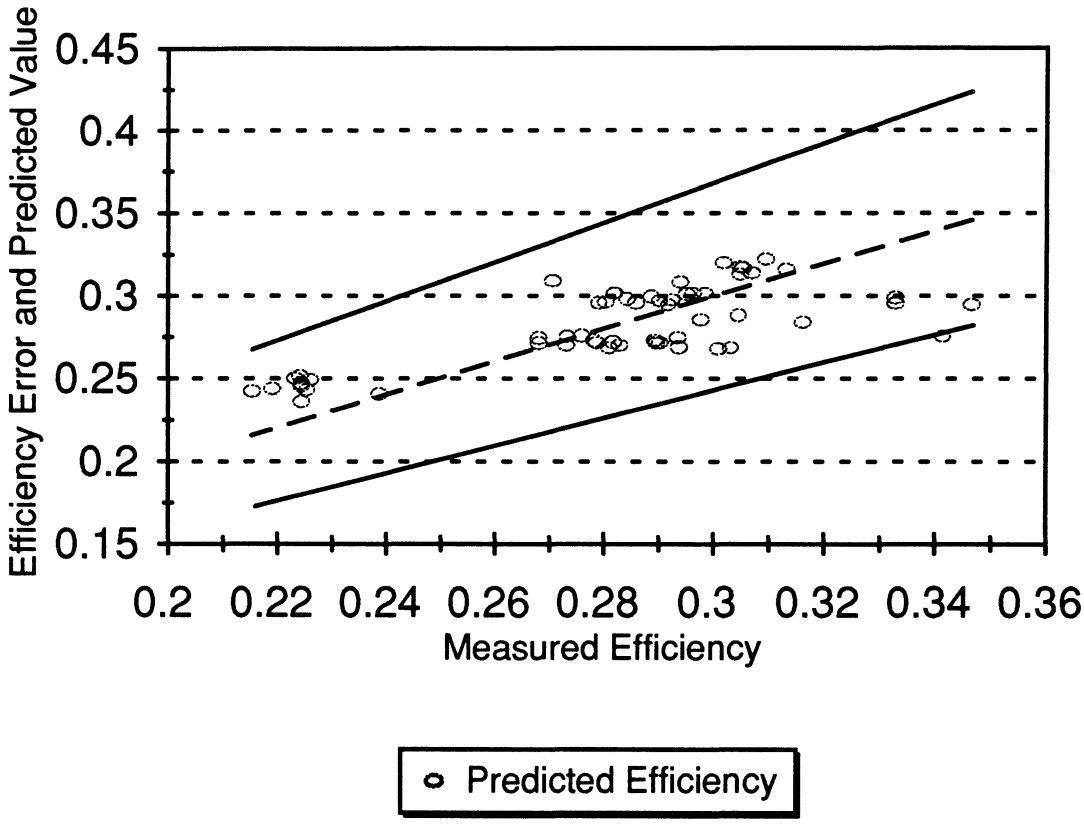

Efficiency Correlation: $\eta = 0.3076 - 0.9411 * x_i + 0.0135\left\{\frac{1}{^\circ F}\right\} * T_{subcooling}$

$R^2 = 0.548, \sigma = 0.0219$

Figure 28 - Efficiency Correlation with Error Limits

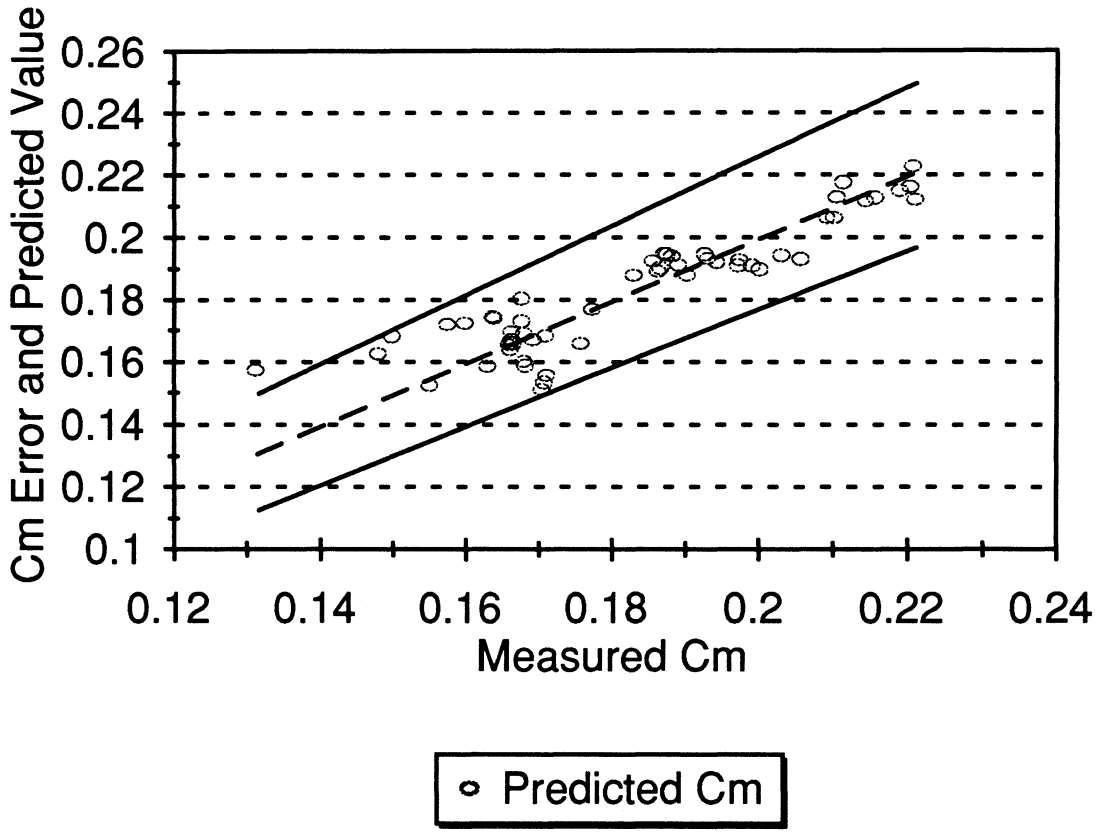

C_m Correlation: $C_m = 0.1352 + 1.0502 * x_i - 0.0101\left\{\frac{1}{^\circ F}\right\} * T_{subcooling}$

$R^2 = 0.834, \sigma = 0.0086$

Figure 29 - Metastability Parameter Correlation with Error Limits

To re-size the nozzle throat diameter for R-134a, the following parameters were used from the current experimental results with R-12:

1. average nozzle inlet pressure; 120.2 psia (828.75 kPa), and
2. maximum quality recorded in the data; 0.0985.

Since the procedure for calculating the nozzle throat diameter for R-134a was conceived for this work, the choice of parameters to use from the current experiment were arbitrary. Therefore the choice of inlet quality was chosen based wholly on the expected results of the smallest nozzle throat.

From the above properties, an HEM critical mass flow rate of 0.663 lb_m/min (0.3 kg/min) was calculated using R-12 as the refrigerant.

Using an HEM analysis, the critical mass flux, G_C, for R-134a was calculated. The nozzle properties assumed for this analysis were the following:

1. nozzle inlet pressure of 120.2 psia (828.75 kPa), and
2. a nozzle inlet quality of 0, which will yield the smallest possible throat diameter.

The HEM analysis was based on isentropic expansion through the nozzle. An iteration was used to determine the maximum mass flux for R-134a using the identical procedure as in Sec. 4.4.1.

The critical mass flux obtained was 775.57 lb_m/(min in.^{2}) (0.545 kg/(min mm^2)).

Nozzle throat area can then be determined from the following equation:

$$G_c)_{R-134a} = \frac{\dot{m}_{HEM,R-12}}{A_{throat,R-134a}}. \tag{29}$$

From this analysis, a diameter of 0.033 in. (0.8382 mm) was obtained. The nozzle throat diameter used for this experimentation with R-12 was 0.036 in. (0.9144 mm).

Chapter 6
Conclusions and Recommendations

Conclusions concerning the experimental results were difficult to make. The dependence of the nozzle efficiency and metastability parameter on the subcooling could not be explained at the time of this writing. Though other conclusions regarding the basis for this experiment could be made.

During this work, the following items were accomplished:

- The entire experimental apparatus was designed and built.
- Successful operation of the experimental apparatus was achieved.
- The theory behind the measurement of the nozzle efficiency developed for this experiment was tested and proven to be valid.
- A metastability parameter was defined and it was shown that the efficiency decreased with increased metastability.
- A re-design of the nozzle throat using R-134a refrigerant yielded a diameter of 0.033 in. (0.8382 mm), corresponding to a 16% reduction in the throat area of the present nozzle using R-12 refrigerant.

The original objective was to gain a better understanding of the two-phase flow through the converging-diverging nozzle by measuring its efficiency. Instead, the experiment testing illustrated short comings in the apparatus. These short comings were the basis for additional work and experimentation.

The recommendations for further work include the following:

1. Addition of a heat exchanger upstream of the bubbly flow valve to control the subcooled temperature leaving the receiver. The temperature of the subcooled liquid leaving the heat exchanger could be controlled with a PID strategy similar to the evaporator and condenser control schemes. Controlling the condenser subcooling between all the data would aid in understanding the results reliance on the subcooling.
2. Relocation of the pressure transducer measuring the nozzle exit pressure. This transducer was located too far downstream creating substantial pressure loss in the refrigerant line. Though this effect was compensated for in the efficiency calculation, moving the pressure transducer will eliminate the need to adjust the

data outside of the data acquisition program and make the nozzle efficiency calculation more accurate.

3. After the above modifications have been completed, nozzles of differing geometries could be tested, as well as different bubbly flow tube inner diameters and lengths.
4. Because of the convenience of the window port into the pressure vessel, some quantitative analysis of the nozzle exit flow can be performed. High speed photography combined with proper lighting techniques will provide information concerning the flow pattern (i.e., droplet size, flow configuration, etc.).
5. Determination of the single-phase efficiency of the nozzle using an ideal gas. By re-defining the metastability parameter as Eq. 30,

$$C_m = \frac{\left(\frac{\dot{m}}{C_{d(1-\phi)}} - \dot{m}_{HEM} \right)}{\dot{m}_{FROZ} - \dot{m}_{HEM}}, \tag{30}$$

the frictional effects can be removed yielding a parameter which represents only the non-equilibrium and not a combination of non-equilibrium and friction as the C_m does in this work.

APPENDIX A
DERIVATION OF THRUST AS A FUNCTION OF STRAIN

This appendix contains the derivation of Eq. 7 given in the Sec. 1.3.1.3 for the thrust as a function of strain. Three equations from statics will form the basis for the derivation.

1. Definition of a bending moment at the base of the inlet tube,

$$M = FL_g. \tag{31}$$

2. Definition of the moment of inertia for a hollow tube,

$$I = \frac{\pi}{64}\left(OD^4 - ID^4\right). \tag{32}$$

3. Relation for the maximum surface strain of a cylinder,

$$\varepsilon = \frac{M(OD)}{2EI}. \tag{33}$$

Substitution of both Eq. 31 and 32 into Eq. 33, and after simplification, yields

$$\varepsilon = \frac{16FL_g(OD)}{\pi\left(OD^4 - ID^4\right)E}. \tag{34}$$

From the definition of output voltage for a full Wheatstone bridge,

$$V_o = \varepsilon C_g V_i. \tag{35}$$

where V_O is the full Wheatstone bridge voltage output, C_g is the gage factor for the strain gages, and V_i is the excitation voltage.

Substitution of Eq. 34 into Eq. 35 gives

$$V_o = \frac{16FL_g(OD)}{\pi(OD^4 - ID^4)E} C_g V_i. \tag{36}$$

Equation 36 is the verification for the usage of strain gages configured in a Wheatstone bridge to measure thrust.

APPENDIX B
INSTRUMENTATION CALIBRATION

This appendix contains the procedure for calibration of the following instrumentation:

1. test stand for nozzle thrust measurement,
2. gage and differential pressure transducers, and
3. differential pressure transmitter for flow meter.

A FORTRAN computer program listed in Sec. A.4 was used to collect the calibration data from the above instrumentation. These calibrations were performed with the instrument in-situ.

B.1 Calibration of the Test Stand

To calibrate the test stand, the routine below was followed:

1. The pressure vessel was dismantled and the entire test stand was situated in the horizontal plane.
2. A level was carefully used to verify that the axis of the nozzle was as vertical as possible.
3. The nozzle weight was balanced out using the amplifier balancing bridge.
4. Precision masses were placed on a small table that was constructed to securely fit over the nozzle.
5. A computer calibration program was used to collect the data for later analysis with spreadsheet software.

Mass was placed on the nozzle in an increasing sequence. After the maximum mass was tested, the calibration proceeded in the opposite manner; decreasing the incremental masses placed on the nozzle. This procedure allowed inspection of the hysteresis, exposing possible improper strain gage mounting. For this work, all calibration curves yielded acceptable hysteresis results.

This calibration procedure was performed several times before operating the experiment. The repeatability of the calibration data was acceptable and as a result, all the data was used to construct a correlation.

To prove the strain gage calibration curve after running the apparatus several times, the test stand was re-calibrated with good results.

Figure 30 shows the comparison of the two calibration curves, obtained six months apart. The standard deviation ratio between these calibrations was 1.25%.

The following curve fit was obtained from calibration:

$$F = A + B*V_{SG} + C*V_{SG}^{2} + D*V_{SG}^{3}. \tag{37}$$

Where F was the nozzle thrust (lb_f), and V_{SG} was the output voltage from the strain gage Wheatstone bridge. The calibration range and constants for Eq. 37 are shown in Table 12.

Table 12a - Strain Gages Calibration Range and Calibration Constants

Instrument Type	Calibration Range	A (lb_f)	B (lb_f/V)	C (lb_f/V^2)	D (lb_f/V^3)
SG	0-0.154 lb_f	4.9668E-4	6.6898E-2	-4.4886E-3	1.1382E-3

Table 12b - Strain Gages Calibration Range and Calibration Constants

Instrument Type	Calibration Range	A (N)	B (N/V)	C (N/V^2)	D (N/V^3)
SG	0-0.686 N	2.2093E-3	2.9758E-1	-1.9966E-2	5.0628E-3

In the data acquisition program, the thrust was calculated in Newtons, then converted to pound-force units.

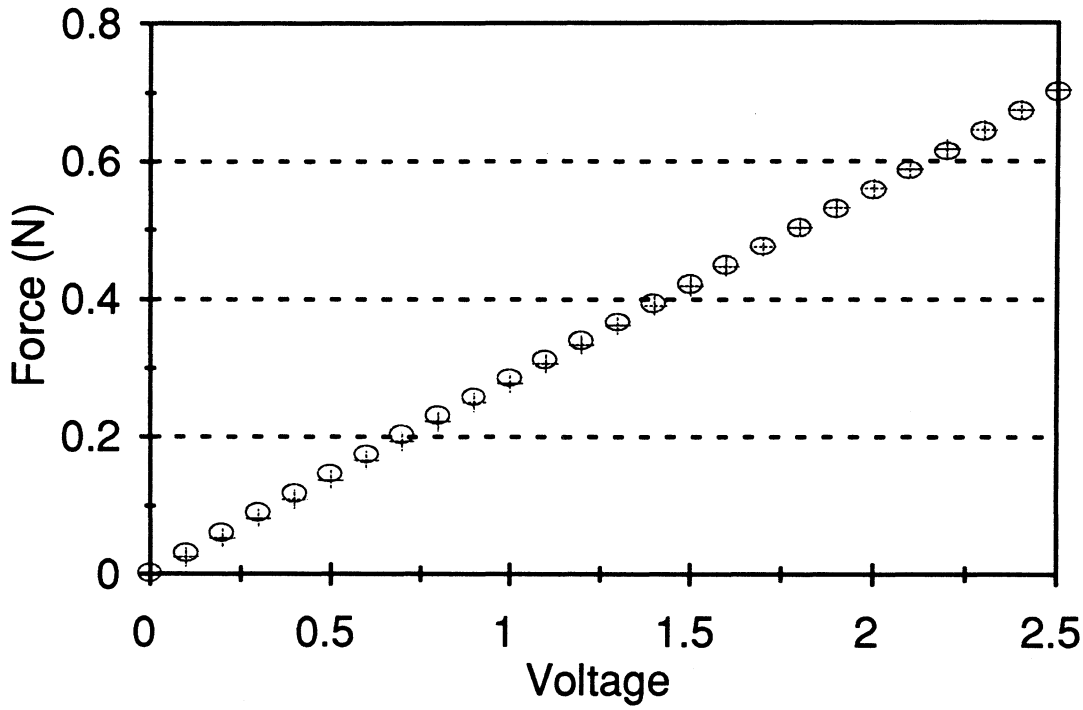

Figure 30 - Comparison of Strain Gage Calibration Curves After Experimental Operation

B.2 Calibration of Gage and Differential Pressure Transducers

For the transducers, or voltage output type pressure cells, a dead weight tester was used for calibration. Calibration of the transducers was performed in-situ. As done for the strain gages, the pressure cells were checked for hysteresis by increasing the incremental applied pressure to the desired maximum, then decreasing.

The following equation was used in the data acquisition program to calculate the measured pressure as a function of the transducer output voltage:

$$P = A + B*V_{PT} + C*V_{PT}^{2} + D*V_{PT}^{3}, \tag{38}$$

where P was the pressure, V_{PT} was the pressure transducer voltage output, and A,B,C, and D were the appropriate calibration constants listed in Table 13 along with each instruments calibration range.

Table 13a - All Pressure Transducers Calibration Range and Calibration Constants

Instrument Type	Calibration Range	A (psig)	B (psig/V)	C (psig/V^2)	D (psig/V^3)
P1	0-240 psig	-1.7389E-2	9.7780E1	-1.0113E0	2.2601E-1
P2	0-235 psig	1.6736E-1	9.5413E1	-4.1651E-1	-3.6295E-3
P3	0-95 psig	1.7771E-1	3.8480E1	-1.1549E0	4.2103E-1
DP2	0-50 psid	1.1105E-2	1.0218E1	-2.2586E-2	-
DP3	0-50 psid	3.5152E-2	1.0284E1	-3.8416E-2	-

Table 13b - All Pressure Transducers Calibration Range and Calibration Constants

Instrument Type	Calibration Range	A (kPag)	B (kPag/V)	C (kPag/V^2)	D (kPag/V^3)
P1	0-1654.7 kPag	-1.1989E0	6.7417E2	-6.9726E0	1.5583E0
P2	0-1620.3 kPag	1.1539E0	6.5785E2	-2.8717E0	-2.5024E-2
P3	0-655.0 kPag	1.2253E0	2.6531E2	-7.9627E0	2.9029E0
DP2	0-344.7 kPad	7.6566E-2	7.0450E1	-1.5572E-1	-
DP3	0-344.7 kPad	2.4236E-1	7.0905E1	-2.6487E-1	-

In the data acquisition program, these calculations were done in the English units, psig and psid. All gage pressure measurements were converted to absolute by adding the ambient pressure to the measurement. The ambient pressure was recorded and inputted into the program at the same time the transducers were balanced.

B.3 Calibration of Differential Pressure Transmitter for Mass Flow Measurement

The mass flow differential pressure unit produced a 4-20 mA output. This had to be converted to voltage for use with the data acquisition system. A parallel circuit with two 500Ω precision resistors was fabricated to simulate one 250Ω resistor. Signal wires entering the computer were soldered to each node of the parallel resistor circuit as shown in Fig. 31. This allowed measurement of a voltage proportional to the current output of the transmitter by Ohm's Law.

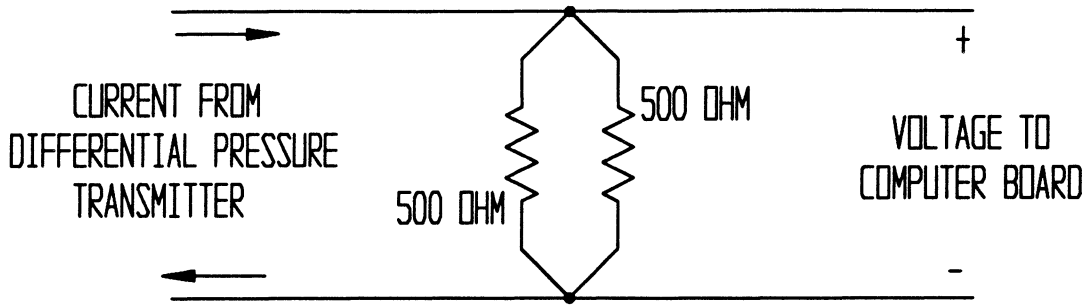

Figure 31 - Resistor Circuit for Conversion of Transmitter Current Output to Voltage

Once the wiring was established, the transmitter was calibrated. A 60 in. (1524 mm) Merium manometer served as the calibration tool to provide the low pressure sensitivity that the dead weight tester was incapable of. The manometer contained merium oil with a specific gravity of 0.826. An air line provided the pressure to one side of the manometer while the transmitter was fixed to the other.

The following equation was used in the data acquisition program to calculate the measured differential pressure as a function of the converted output voltage:

$$DP = \mathrm{A} + \mathrm{B} * V_{DPT} + \mathrm{C} * V_{DPT}^{\ 2} + \mathrm{D} * V_{DPT}^{\ 3}, \tag{39}$$

where DP was the pressure, V_{PT} was the differential pressure transmitter converted voltage output, and A,B,C, and D were the calibration constants listed in Table 14 along with the instruments calibration range.

Table 14a - Differential Pressure Transmitter Calibration Range and Calibration Constants

Instrument Type	Calibration Range	A (psid)	B (psid/V)	C (psid/V^2)	D (psid/V^3)
DP1	0-1.498 psid	-5.1756E-1	5.2475E-1	-9.2768E-3	1.3785E-3

Table 14b - Differential Pressure Transmitter Calibration Range and Calibration Constants

Instrument Type	Calibration Range	A (kPad)	B (kPad/V)	C (kPad/V^2)	D (kPad/V^3)
DP1	0-10.328 kPad	-3.5684E0	3.6180E0	-6.3961E-2	9.5044E-3

In the data acquisition program, this differential pressure was calculated in psid.

B.4 Calibration Computer Program

This program was used for the calibration of all pressure cells and the strain gage bridge. The results were written to an external file to be analyzed on spreadsheet software.

```
C$NOEX
C$NOWA
C
C     PROGRAM CALINST
C
C THIS PROGRAM WAS USED FOR THE CALIBRATION OF THE SIX PRESSURE
C TRANSDUCERS; GAGE AND DIFFERENTIAL. THE OUTPUT WHICH CONSISTED
C OF THE PRESSURE AND VOLTAGE SIGNAL WAS WRITTEN TO AN EXTERNAL FILE.
C A DEAD WEIGHT TESTER WAS USED FOR CALIBRATION OF ALL BUT DP1 WHICH WAS
C USED WITH THE FLOWMETER. FOR THE VERY SMALL PRESSURE DROP ACROSS THE
C ORIFICE METER, A MANOMETER WITH MERIUM OIL (S.G. = 0.826) WAS USED
C FOR CALIBRATION. THIS PROGRAM IS ALSO USED TO CALIBRATE THE STRAIN
C GAGES.
C
C VARIABLE DECLARATIONS
      DOUBLE PRECISION ADVR,TVOLTS,NOC,PFS,MFS,AVEV,PSOH,TSOH
      DOUBLE PRECISION ROW,G,WHEIGHT,SG,FORCE
      INTEGER*2 LPINIT,LPSB,LPAV,LPTERM,LPDSC,LPESC,ADV(100)
      INTEGER*2 LPSCF,LPADS,I,GAIN,BOARD,A,CHAN
      REAL FREQ,MASS
C CONSTANTS
      NOC=4096.0D0
      ROW=1.599962D0
      G=386.04D0
      SG=0.826D0
C INPUTS FOR SELECTION OF INSTRUMENT TO BE CALIBRATED
3     PRINT*, 'ENTER THE BOARD'
      READ(*,*) BOARD
      PRINT*, 'ENTER THE CHANNEL TO CALIBRATE'
      READ(*,*) CHAN
C
C DATA ACQUISITION VARIABLE ASSIGNMENTS
      IF (BOARD .EQ. 1) THEN
      FREQ=5000.0D0
      PFS=5.0D0
      MFS=-5.0D0
      GAIN=1
C
C STATEMENT TO OPEN EXTERNAL FILES FOR DATA STORAGE
       IF (CHAN .EQ. 0) THEN
        OPEN(UNIT=1,FILE='CALDP1.FOR')
       ELSE IF (CHAN .EQ. 1) THEN
        OPEN(UNIT=1,FILE='CALDP2.FOR')
       ELSE
        OPEN(UNIT=1,FILE='CALDP3.FOR')
       ENDIF
      ELSE
```

```
      FREQ=2000.0D0
      PFS=2.5D0
      MFS=-2.5D0
      GAIN=100
       IF (CHAN .EQ. 0) THEN
        OPEN(UNIT=1,FILE='CALP1.FOR')
       ELSE IF (CHAN .EQ. 1) THEN
        OPEN(UNIT=1,FILE='CALP2.FOR')
       ELSE IF (CHAN .EQ. 2) THEN
        OPEN(UNIT=1,FILE='CALP3.FOR')
       ELSE
        OPEN(UNIT=1,FILE='CALSG.FOR')
       ENDIF
     ENDIF
C
C
C PROMPTS FOR CALIBRATION PRESSURE INPUTS
5     IF ((BOARD .EQ. 1) .AND. (CHAN .EQ. 0)) THEN
       PRINT*, 'ENTER THE PRESSURE SIDE OIL HEIGHT (in)'
       READ(*,*) PSOH
       PRINT*, 'ENTER THE TRANSDUCER SIDE OIL HEIGHT (in)'
       READ(*,*) TSOH
       PRESS=ROW*G/20736.0D0*(TSOH-PSOH)
       WHEIGHT=SG*(TSOH-PSOH)
      ELSE IF ((BOARD .EQ. 2) .AND. (CHAN .EQ. 3)) THEN
       PRINT*, 'ENTER THE MASS ON THE NOZZLE (g)'
       READ(*,*) MASS
       FORCE=9.807E-3*MASS
      ELSE
       PRINT*, 'ENTER THE PRESSURE FOR THIS RUN'
       READ(*,*) PRESS
      ENDIF
C
      PAUSE 'PRESS ENTER TO BEGIN DATA ACQUISITION'
C
C DATA ACQUISITION STATEMENTS FOR SIGNAL SAMPLING
      C=LPTERM()
      C=LPINIT()
      C=LPSB(BOARD)
      C=LPSETA(0,CHAN,CHAN,GAIN)
      C=LPSCF(FREQ)
      C=LPDSC()
      C=LPADS(100,ADV(1))
      C=LPESC()
C
      TVOLTS=0.0D0
C
C CONVERSION OF ANALOG DATA VALUE TO VOLTAGE
      DO 10 I=1,100,1
      ADVR=ADV(I)
      TVOLTS=(ADVR/NOC)*(PFS-MFS)-PFS+TVOLTS
10    CONTINUE
C
      AVEV=TVOLTS/100
C
C OUTPUT STATEMENTS AND EXTERNAL FILE ASSIGNMENTS
```

```
      IF ((BOARD .EQ. 1) .AND. (CHAN .EQ. 0)) THEN
      PRINT*, PRESS,WHEIGHT,AVEV
      WRITE(1,*) PRESS,AVEV
      ELSE IF ((BOARD .EQ. 2) .AND. (CHAN .EQ. 3)) THEN
      PRINT*, FORCE,AVEV
      WRITE(1,*) FORCE,AVEV
      ELSE
      PRINT*, PRESS,AVEV
      WRITE(1,*) PRESS,AVEV
      ENDIF
C
      PRINT*,' '
C
C STATEMENT TO ALLOW EXIT FROM PROGRAM
      PRINT*, 'ENTER 1 TO REPEAT PROCEDURE, 2 TO RESTART, 3 TO QUIT'
      READ(*,*) A
      PRINT*,' '
C
      IF (A .EQ. 3) THEN
      CLOSE(UNIT=1)
      GOTO 500
      ELSE IF (A .EQ. 2) THEN
      CLOSE(UNIT=1)
      GOTO 3
      ELSE
      GOTO 5
      ENDIF
C
C
500   END
```

APPENDIX C
COMPUTER PROGRAM FOR TEST STAND TUBING DESIGN

The following FORTRAN program was used to calculate the optimum thrust tubing material, and size. This program is based on Eq. 36 given for the calculation of output voltage based on all the relevant parameters including the thrust estimation which is also calculated in the program.

Clearly, this program was written well before the apparatus was built, therefore many of the parameters used were based on previous work by Menegay [1].

```
C$NOEX
C$NOWA
C
C PROGRAM HEMNOZZL.FOR
C
C PROGRAM TO CALCULATE THRUST, STRAIN, AND OUTPUT
C VOLTAGE FROM STRAIN GAGES,
C
C VARIABLE DECLARATIONS
      REAL MDOT,K,NMN,L,I,PSAT,PCOND,PEVAP,TSUB,PLOSS,TC,HCOND,HINMN
      REAL PINMN,TINMN,HF,T,ID,LL,MASS
      INTEGER D,H,N,G,B
      CHARACTER*4 REF
      PI=3.141592654
C
C INPUT OF NECESSARY PARAMETERS
500   WRITE(*,*) 'CONDENSER PRESSURE (psi)'
      READ(*,*) PCOND
      WRITE(*,*) 'EVAPORATOR PRESSURE (psi)'
      READ(*,*) PEVAP
      WRITE(*,*) 'AMOUNT OF SUBCOOLING OF CONDENSED FLUID (F)'
      READ(*,*) TSUB
      WRITE(*,*) 'PRESSURE LOSS OF BUBBLY FLOW TUBE (psi)'
      READ(*,*) PLOSS
      WRITE(*,*) 'EFFICIENCY OF MOTIVE NOZZLE (%)'
      READ(*,*) NMN
      NMN=NMN/100.0
C MASS FLOW RATE BASED ON PREVIOUS WORK
      MDOT=-1.56406667E-5*PCOND+1.01116E-2
C THIS ANALYSIS WAS WRITTEN FOR R-12 REFRIGERANT ONLY
      PRINT *, 'THE REFRIGERANT IS R12'
      REF='RR12'
C CALL FOR REFRIGERANT SUBROUTINES
```

```
      CALL RINIT(REF,IERR)
C TEMPERATURE AT INPUTTED CONDENSER PRESSURE
      TSAT=T2OFP(REF,PCOND)
C SUBCOOLED TEMPERATURE
      TC=TSAT-TSUB
      PSAT=P2OFT(REF,TC)
      HCOND=HFOFT(REF,TC)+VFOFT(REF,TC)*(PCOND-PSAT)
      HINMN=HCOND
C
C THE FOLLOWING PROPERTIES WERE CALCULATED
C AT NOZZLE INLET PRESSURE:
C PRESSURE, TEMPERATURE, QUALITY, ENTROPY, AND
C SPECIFIC VOLUME.
C
         PINMN=PCOND-PLOSS
         TINMN=T2OFP(REF,PINMN)
         HF=HFOFT(REF,TINMN)
         SF=SFOFT(REF,TINMN)
         SFG=SFGOFT(REF,TINMN)
         HF=HFOFT(REF,TINMN)
         HFG=HFGOFT(REF,TINMN)
         VF=VFOFT(REF,TINMN)
         VFG=VFGOFT(REF,TINMN)
         XINMN=(HCOND-HF)/HFG
         SINMN=SF+XINMN*SFG
C
C THE FOLLOWING PROPERTIES WERE CALCULATED
C AT NOZZLE EXIT PRESSURE AS DEFINED BY THE INPUT
C OF THE EVAPORATOR PRESSURE;
C
C ENTROPY DEFINITION; ISENTROPIC
         SIMN=SINMN
         VINMN=VF+XINMN*VFG
         TEVAP=T2OFP(REF,PEVAP)
         SFEV=SFOFT(REF,TEVAP)
         SFGEV=SFGOFT(REF,TEVAP)
         XIMN=(SIMN-SFEV)/SFGEV
         HFEV=HFOFT(REF,TEVAP)
         HFGEV=HFGOFT(REF,TEVAP)
         HIMN=HFEV+XIMN*HFGEV
      ENDIF
C
C   VELOCITY OF FLUID OUT OF MOTIVE NOZZLE
      HINMN=HINMN*2.324444E3
      HIMN=HIMN*2.324444E3
      UMN=SQRT(2.0E0*NMN*(HINMN-HIMN))
      WRITE(*,*) 'MOTIVE NOZZLE VELOCITY=',UMN
      PAUSE 'HIT ENTER TO CONTINUE'
C   THRUST OUT OF NOZZLE
      F=UMN*MDOT
C
      WRITE(*,*)'THRUST OF NOZZLE (N)',F
C
C INPUT OF LOAD BEAM CHARACTERISTICS
C
      WRITE(*,*)'DISTANCE BETWEEN STRAIN GAGES AND NOZZLE OUTLET (IN)'
```

```
      READ(*,*) L
      L=L/12.0*0.3048
C
C   DETERMINATION OF MATERIAL PROPERTIES FOR LOAD BEAM
20     PRINT *, 'TYPE OF METAL TUBING FOR STRAIN APPARATUS'
C
      WRITE(*,*)'TYPE A  1. FOR STAINLESS STEEL'
      WRITE(*,*)'       2. FOR ALUMINUM'
      WRITE(*,*)'       3. FOR COPPER'
      WRITE(*,*)'       4. FOR CARBON STEEL'
      WRITE(*,*)'       5. TO INPUT MODULUS OF ELAS AND DEN'
      READ(*,*) J
C
C ABOVE CHOICE DEFINITION FOR MATERIAL PROPERTIES
      IF (J .EQ. 1) THEN
        E=1.903E11
        DEN=7840.79
      ELSEIF (J .EQ. 2) THEN
        E=7.101575E10
        DEN=2705.62
      ELSEIF (J .EQ. 3) THEN
        E=1.068684E10
        DEN=8954.77
      ELSEIF (J .EQ. 4) THEN
        E=2.06842E11
        DEN=7844.1
      ELSEIF (J .EQ. 5) THEN
        WRITE(*,*) 'ENTER THE MODULUS OF ELASTICITY'
        READ(*,*) E
        WRITE(*,*) 'ENTER THE DENSITY'
        READ(*,*) DEN
      ELSE
        PRINT *, 'INPUT IS OUT OF RANGE'
        GO TO 20
      ENDIF
C
C STATEMENT ALLOWING THE TRIAL OF DIFFERENT TUBING SIZES
      WRITE(*,*)'ENTER THE OUTER DIAMETER OF THE DESIRED TUBING (in)'
      READ(*,*) OD
      OD=OD/12.0*0.3048
100   WRITE(*,*)'CHOOSE EITHER GAUGE OR IN. FOR WALL THICKNESS INPUT'
      WRITE(*,*)'TYPE A 1. FOR GAUGE'
      WRITE(*,*)'       2. FOR INCHES'
      READ(*,*) D
C
      IF (D .EQ. 1) THEN
C
          WRITE(*,*)'ENTER THE GAUGE RATING'
          READ(*,*) G
C
       ELSE
C
          WRITE(*,*)'ENTER THE THICKNESS IN INCHES'
          READ(*,*) T
C
       ENDIF
```

```
C
C     GAUGE RATING CONVERSION TO INCHES
C
      IF (D .EQ. 1) THEN
        IF (G .EQ. 0) THEN
           T=0.340
        ELSE IF (G .EQ. 1) THEN
           T=0.300
        ELSE IF (G .EQ. 2) THEN
           T=0.284
        ELSE IF (G .EQ. 3) THEN
           T=0.259
        ELSE IF (G .EQ. 4) THEN
           T=0.238
        ELSE IF (G .EQ. 5) THEN
           T=0.220
        ELSE IF (G .EQ. 6) THEN
           T=0.203
        ELSE IF (G .EQ. 7) THEN
           T=0.180
        ELSE IF (G .EQ. 8) THEN
           T=0.165
        ELSE IF (G .EQ. 9) THEN
           T=0.148
        ELSE IF (G .EQ. 10) THEN
           T=0.134
        ELSE IF (G .EQ. 11) THEN
           T=0.120
        ELSE IF (G .EQ. 12) THEN
           T=0.109
        ELSE IF (G .EQ. 13) THEN
           T=0.095
        ELSE IF (G .EQ. 14) THEN
           T=0.083
        ELSE IF (G .EQ. 15) THEN
           T=0.072
        ELSE IF (G .EQ. 16) THEN
           T=0.065
        ELSE IF (G .EQ. 17) THEN
           T=0.058
        ELSE IF (G .EQ. 18) THEN
           T=0.049
        ELSE IF (G .EQ. 19) THEN
           T=0.042
        ELSE IF (G .EQ. 20) THEN
           T=0.035
        ELSE IF (G .EQ. 21) THEN
           T=0.032
        ELSE IF (G .EQ. 22) THEN
           T=0.028
        ELSE IF (G .EQ. 23) THEN
           T=0.025
        ELSE IF (G .EQ. 24) THEN
           T=0.022
        ELSE IF (G .EQ. 25) THEN
           T=0.020
```

```
        ELSE IF (G .EQ. 26) THEN
           T=0.018
        ELSE IF (G .EQ. 27) THEN
           T=0.016
        ELSE IF (G .EQ. 28) THEN
           T=0.014
        ELSE IF (G .EQ. 29) THEN
           T=0.013
        ELSE IF (G .EQ. 30) THEN
           T=0.012
        ELSE IF (G .EQ. 31) THEN
           T=0.010
        ELSE IF (G .EQ. 32) THEN
           T=0.009
        ELSE IF (G .EQ. 33) THEN
           T=0.008
        ELSE IF (G .EQ. 34) THEN
           T=0.007
        ELSE IF (G .EQ. 35) THEN
           T=0.005
        ELSE IF (G .EQ. 36) THEN
           T=0.004
        ELSE
           WRITE(*,*)'CANNOT FIND ENTERED GAUGE'
           WRITE(*,*)'PLEASE RECHECK INFORMATION'
           GO TO 100
        ENDIF
      ENDIF
C
      T=T/12.0*0.3048
      ID=OD-2.0*T
C
C EXCITATION VOLTAGE, STRAIN GAGE FACTOR, AND DESIGN
C CHOICE INPUT
C
      WRITE(*,*)'EXCITATION VOLTAGE (V)'
      READ(*,*) VIN
      WRITE(*,*)'NOMINAL STRAIN GAGE FACTOR'
      READ(*,*) CG
      I=PI/64.0*(OD**4-ID**4)
      WRITE(*,*)'ENTER A 1. FOR A ONE TUBE SYSTEM'
      WRITE(*,*)'       2. FOR A TWO TUBE SYSTEM'
      READ(*,*) N
C STRAIN CALCULATION
      IF (N .EQ. 1) THEN
      STRAIN=F*L*OD/E/2.0/I
      ELSE
      STRAIN=F*L*OD/E/4.0/I
      ENDIF
C
      STRAIN1=STRAIN*1.0E6
      WRITE(*,*)'STRAIN (MICRO IN/IN) = ',STRAIN1
C
C CONVERSION OF STRAIN TO VOLTAGE
      VOUT=STRAIN*CG*VIN
C
```

```
      IF (VOUT .LT. 0.010) THEN
        VOUT1=VOUT*1000.0
        WRITE(*,*)'VOLTAGE OUTPUT (mV) = ',VOUT1
      ELSE
        WRITE(*,*)'VOLTAGE OUTPUT (V) = ',VOUT
      ENDIF
C
      WRITE(*,*)'ENTER 1. TO REPEAT PROGRAM'
      WRITE(*,*)'     2. TO QUIT'
      READ(*,*) N
      IF (N .EQ. 1) THEN
      GO TO 500
      ENDIF
      END
```

APPENDIX D
FLOW METER ELEMENTS SIZING PROCEDURE

The sizing of the flow meter was relatively simple. Equation 10, repeated below, for the mass flow rate calculation which was also used for sizing of the flow meter elements;

$$W = 359.1\left\{\frac{\text{lb}_\text{m}}{\text{in}^2\,\text{hr}}\left[(\text{in.H}_2\text{O})\frac{\text{lb}_\text{m}}{\text{ft}^3}\right]^{\frac{1}{2}}\right\} d^2 K\sqrt{h_w \rho}\,, \tag{10}$$

where W was the mass flow rate (lb_m/hr), d was the orifice diameter (in.), K was the flow coefficient, h_w was the pressure drop across the orifice (in. H2O), and the constant serves to correct for the units (this constant cannot be used with SI units).

The disadvantage of using this equation to size the elements was that the mass flow and fluid density must be known. For this experiment, these were estimated with Menegay's previous work [2].

Given an average mass flow rate, a guess for the orifice diameter, and the resulting flow coefficient calculated from Eq. 40 [17] , the differential pressure across the orifice can be calculated.

$$\begin{aligned} K = [0.5991 + \frac{0.0044}{D} + \left(0.3155 + \frac{0.0175}{D}\right)(\beta^4 + 2\beta^{16})] \\ + [\frac{0.00052}{D} - 0.000192 + \left(0.01648 - \frac{0.00116}{D}\right)(\beta^4 + 4\beta^{16})]\lambda \end{aligned} \tag{40}$$

where:

D	=	the inner diameter of the upstream and downstream piping, (in.),
β	=	the ratio of the orifice diameter to the piping inner diameter,
λ	=	$1000/\sqrt{\text{Re}_D}$,
Re_D	=	pipe Reynolds number.

This equation was valid when: 0.5 in. (12.7 mm) $\leq D \leq 1.5$ in. (38.1 mm),
$0.1 < \beta < 0.8$, and
$Re_D > 1000$.

Solving Eq. 10 for the differential pressure,

$$h_w = \left(\frac{W}{359.1 d^2 K} \right)^2 \frac{1}{\rho}. \tag{41}$$

With this equation, the orifice diameter was iterated until an acceptable differential pressure was obtained. Orifice sizes were only limited by specification to 64ths of an inch. Trial parameters consisted of the following:

- $W = 78.31$ lbm/hr (27.95 kg/hr),
- $d = 13/64$ in. (4.98 mm),
- $D = 0.556$ in. (14.1 mm),
- $K = 0.617$, and
- $\rho = 2.73$ lbm/ft^3 (43.73 kg/m^3).

Equation 41 with the above parameters yielded a differential pressure of 26.9 in. H_2O (422.9 mm H_2O). The inexpensive, readily available differential pressure cells capable of measuring in this range were configured to a standard of 0-50 in. H_2O (0-1270 mm H_2O). This was acceptable for this estimation of the differential pressure.

APPENDIX E
PULSE DAMPING MODEL FOR FLOW METER

Damping of the pressure pulsations emanating from the compressor was required to ensure accurate mass flow rate measurement with the orifice meter. This appendix contains the following two sections:

1. theory behind pulse damping system, and
2. computer program model for the design of the system.

E.1 Pulse Damping Model Theory

The prime mover used in this work was a single piston, single acting reciprocating compressor. This type of compressor caused the exiting fluid to experience extreme velocity changes, and hence, mass flow rate variations. This created a problem for the measurement of the mass flow rate with an orifice meter.

The solution for this problem came from an electrical analogy. In electrical terms, the compressor was represented by a current source. A low pass filter then became the fluid mechanic analogy of the desired pulse damping system. Figure 32 shows the two analogies. A capacitors analogy in fluid mechanics was a volume while a resistors was a flow restriction. The result was a volume and valve directly downstream of the compressor.

To model the system, three mass flow equations were needed:

1. An accurate model for the compressor outlet mass flow. Being a single piston, single acting compressor, the mass flow actually shuts off for half the cycle of the compressor crank. Therefore, a half-sine wave model which forced the mass flow equal to zero during the compressor intake mode was developed,

$$\dot{m}_{inlet,volume} = \dot{m}_{avg,comp}\pi\sin(\omega t),$$
$$\dot{m}_{inlet,volume} = 0 \text{ when } \sin(\omega t) = 0. \tag{42}$$

This equation assumed that the suction side mass flow fluctuation did not affect the discharge side. This was a reasonable assumption since the pressure vessels large volume of compressible vapor probably damped out much of the suction side variations.

2. An equation for the conservation of mass for the large volume,

$$\frac{dm}{dt} = (\dot{m}_{inlet} - \dot{m}_{exit})_{volume}. \tag{43}$$

3. Valve mass flow equation,

$$\dot{m}_{exit,valve} = AC_d\sqrt{2\rho(P_{inlet} - P_{exit})_{valve}}. \tag{44}$$

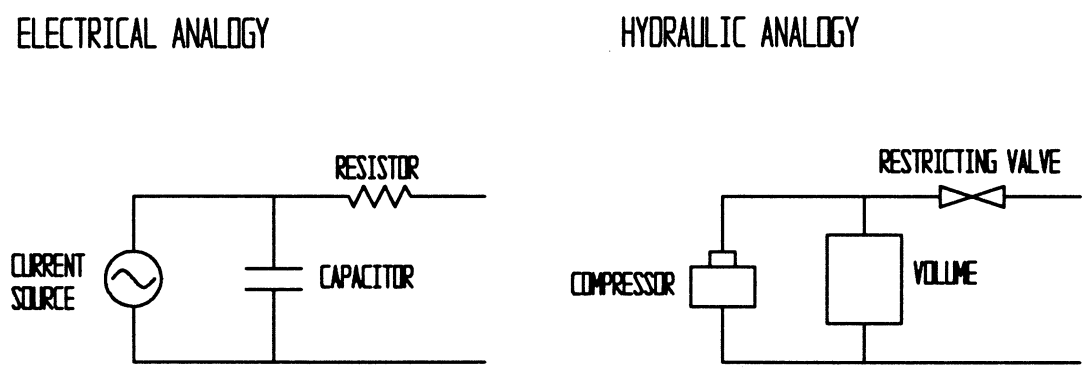

Figure 32 - Electrical and Hydraulic Pulse Damping Analogies

By setting the equation for the conservation of mass in the volume equal to the compressor mass flow minus the valve mass flow, and using the isothermal relation of the perfect gas law as in Eq. 45,

$$\frac{dm}{dt}\left(\frac{RT}{V}\right)=\frac{dP}{dt}, \tag{45}$$

the following relation for the pressure variation with time was derived:

$$\frac{dP}{dt}=\frac{RT}{V}\dot{m}_{avg,comp}\pi\sin(\omega t)-\frac{AC_d}{V}\sqrt{2RTP(P-P_{exit})}. \tag{46}$$

The following parameters of Eq. 46 were fixed by previous results:

1. Individual gas constant, R, was (68.76 J/kgK).
2. Absolute temperature, T, was 554.67 R (308.15 K).
3. Volume, V, of oil separator (used as volume) was 140 in^3 (2.3E6 mm^3).
4. Average mass flow rate from compressor, $\dot{m}_{avg,comp}$, was 1.31 lb_m/min (0.59 kg/min).
5. Exit pressure, P_{exit}, from the valve which was equal to the controlled condenser pressure was chosen to be 180 psia (1241.1 kPa).

A value for the area multiplied by the discharge coefficient, ACd, was calculated from the average mass flow rate, fluid density, and valve pressure drop with the following equation:

$$AC_d=\frac{\dot{m}_{avg,comp}}{\sqrt{2\rho(\Delta P)_{valve}}}. \tag{47}$$

The time step had to be less than the time for one full revolution of the compressor crank. Since the compressor runs at 3550 RPM, the time per revolution was 16.9E-3 sec. A time step was chosen to allow almost 17 points per cycle.

The program iterated the pressure, P, in Eq. 46 to determine the pressure variations in the flow downstream of the valve. Once this was value was obtained, the mass flow rate was determined from Eq. 47, solved for the mass flow rate. The results are shown graphically in Fig. 33. For this work, a valve pressure drop of 12.0 psid was chosen; this yielded a predicted mass flow variation of ±0.37%.

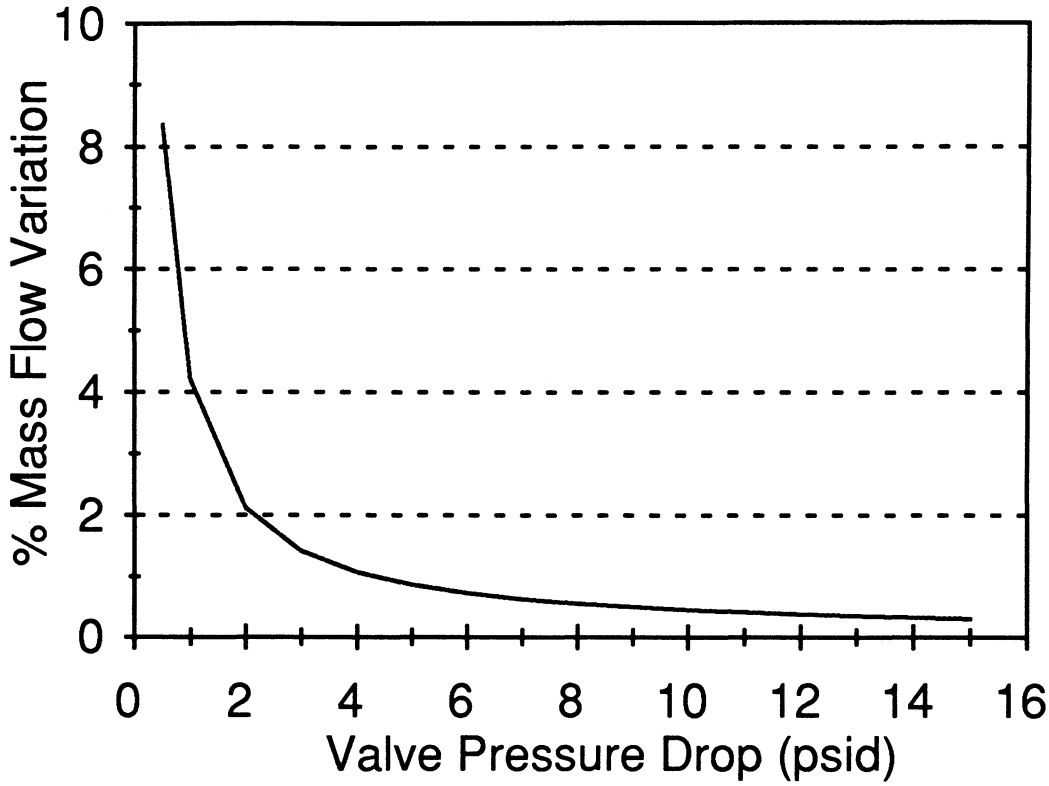

Figure 33 - Results of Pulse Damping Model

E.2 Computer Program for Pulse Damping System

```
C$NOEX
C$NOWARN
C     PROGRAM PRFLUCT
C
C     THIS PROGRAM CALCULATES THE THEORETICAL PRESSURE FLUCTUATIONS
C     IN THE SYSTEM DUE TO THE SIMPLEX COMPRESSOR.  THE FLUCTUATIONS
C     ARE TO BE ATTENUATED THROUGH USE OF A PULSE DAMPING DRUM AND
C     A FLUID RESTRICTION VALVE.
C
C
C VARIABLE DECLARATION
      IMPLICIT DOUBLE PRECISION (A-H,P-Z)
      DOUBLE PRECISION DELTAT,MAVG,N,MDOT
      INTEGER I,J,K,L,II
      DIMENSION P(40000)
C
C ASSIGNMENT OF INDIVIDUAL GAS CONSTANT, TEMPERATURE OF FLUID, AVERAGE
C MASS FLOW RATE, ANGULAR SPEED, AND DENSITY, RESPECTIVELY
      R=68.76
      T=380.15
      MAVG=1.19673E-2
      W=371.75513
      ROW=52.65
C CONVERSION UNITS FROM AND TO PSI, KPA
      U=14.696/101325.0
      X=101325.0/14.696
      I=0
      J=0
      L=0
      Q=0.0
      II=0
      PI=3.141592654
C
C OPEN EXTERNAL FILES FOR STORAGE OF DATA FOR VARYING
C VALVE PRESSURE DROPS.  THE NUMBER AFTER 'OUTPUT' SPECIFIES
C THE PRESSURE DROP.
10    II=II+1
      IF (II .EQ. 1) THEN
      A=0.5D0
      OPEN(UNIT=1,FILE='OUTPUT-5.FOR')
      ELSE IF (II .EQ. 2) THEN
      A=1.0D0
      OPEN(UNIT=1,FILE='OUTPUT1.FOR')
      ELSE IF (II .EQ. 3) THEN
      A=2.0D0
      OPEN(UNIT=1,FILE='OUTPUT2.FOR')
      ELSE IF (II .EQ. 4) THEN
      A=3.0D0
      OPEN(UNIT=1,FILE='OUTPUT3.FOR')
```

```
      ELSE IF (II .EQ. 5) THEN
      A=4.0D0
      OPEN(UNIT=1,FILE='OUTPUT4.FOR')
      ELSE IF (II .EQ. 6) THEN
      A=5.0D0
      OPEN(UNIT=1,FILE='OUTPUT5.FOR')
      ELSE IF (II .EQ. 7) THEN
      A=6.0D0
      OPEN(UNIT=1,FILE='OUTPUT6.FOR')
      ELSE IF (II .EQ. 8) THEN
      A=7.0D0
      OPEN(UNIT=1,FILE='OUTPUT7.FOR')
      ELSE IF (II .EQ. 9) THEN
      A=8.0D0
      OPEN(UNIT=1,FILE='OUTPUT8.FOR')
      ELSE IF (II .EQ. 10) THEN
      A=9.0D0
      OPEN(UNIT=1,FILE='OUTPUT9.FOR')
      ELSE IF (II .EQ. 11) THEN
      A=10.0D0
      OPEN(UNIT=1,FILE='OUTPUT10.FOR')
      ELSE IF (II .EQ. 12) THEN
      A=12.0D0
      OPEN(UNIT=1,FILE='OUTPUT12.FOR')
      ELSE IF (II .EQ. 13) THEN
      A=14.0D0
      OPEN(UNIT=1,FILE='OUTPUT14.FOR')
      ELSE IF (II .EQ. 14) THEN
      A=15.0D0
      OPEN(UNIT=1,FILE='OUTPUT15.FOR')
      ELSE IF (II .EQ. 15) THEN
      GOTO 500
      ENDIF
C
C ASSIGNMENT OF VALVE EXIT PRESSURE
      Pe=180
C ADDITION OF VALVE PRESSURE DROP TO EXIT PRESSURE TO
C DETERMINE THE INLET PRESSURE.
      P(1)=X*(Pe+A)
      Pe=X*(Pe)
      A=A*X
C AREA MULTIPLIED BY DISCHARGE COEFFICIENT
      ACD=MAVG/SQRT(2*ROW*A)
C
C ASSIGNMENT OF VOLUME OF DAMPING DRUM (OIL SEPARATOR FOR SYSTEM)
      Y=140.0D0
C CONVERSION OF UNITS
      V=Y*1.6387064D-5
C
C TIME STEP FOR ITERATIONS
      DELTAT=0.001D0
C
C OUTER LOOP FOR ITERATION OF TIME STEP (COMPRESSOR ROTATION)
C
      DO I=1,12000
      PPSI=P(I)
```

```
C QUALIFICATION FOR SETTING COMPRESSOR MASS FLOW TO ZERO
          IF (SIN(W*I*DELTAT) .GT. 0.0) THEN
            L=1
          ELSE
            L=0
          ENDIF
C CONSTANT DEFINITION
     E=R*T/V
C COMPRESSOR MASS FLOW
     Q=E*L*MAVG*PI*(SIN(W*I*DELTAT))
C
C INNER ITERATION FOR DETERMINATION OF PRESSURE FOR SINGLE TIME STEP
C
       LOOP
C VALVE MASS FLOW
     G=ACD/V*SQRT(2*R*T*PPSI*(PPSI-Pe))
     P(I+1)=(Q-G)*DELTAT+P(I)
C STATEMENTS FOR INCREMENTING GUESSED PRESSURE
       IF (PPSI .GT. P(I+1)) THEN
       PPSI=PPSI-(PPSI-P(I+1))/10
       ELSE
       PPSI=PPSI+(P(I+1)-PPSI)/10
       ENDIF
C
C EXIT QUALIFICATION OF INNER LOOP
C
        UNTIL (ABS(PPSI-P(I+1)) .LT. 1.0)
C      PRINT*, PPSI*U,(I*DELTAT)
     IF (I .GT. 9999) THEN
C OUTPUT COMMANDS
     MDOT=ACD*SQRT(2*ROW*(P(I)-Pe))
     WRITE(1,*) PPSI*U,(I*DELTAT),MDOT
     ENDIF
C
C END OF OUTER LOOP
C
     END DO
C CLOSING OF EXTERNAL FILES
     CLOSE(UNIT=1)
C
     GOTO 10
C
500    END
```

APPENDIX F
GAGE PRESSURE TRANSDUCER BALANCING PROGRAM

This program was used only for the balancing of the gage pressure transducers; a procedure which was performed before operating the experimental apparatus. A constant iteration within the program allowed it to be run while the transducers were being balanced.

```
C$NOEX
C$NOWA
C PROGRAM BALPRT
C
C THIS PROGRAM IS USED TO BALANCE THE SIGNAL FROM THE THREE PRESSURE
C TRANSDUCERS: P1, P2, & P3.  THESE PRESSURE TRANSDUCERS ARE CONNECTED
C TO BALANCING CIRCUITRY.
C
C VARIALBLE DECLARATIONS
      DOUBLE PRECISION ADVR,NOC,PFS,MFS,AVEV1,AVEV2,AVEV3,TVOLTS
      INTEGER*2 LPINIT,LPSB,LPAV,LPTERM,LPDSC,LPESC,ADV(300)
      INTEGER*2 LPSCF,LPADS,I,GAIN,BOARD,CHAN
      REAL FREQ
C ASSIGNMENT OF DATA ACQUISITION PARAMETERS
      NOC=4096.0D0
      BOARD=2
      FREQ=2000.0D0
      PFS=2.5D0
      MFS=-2.5D0
      GAIN=100
C
C DATA ACQUISITION COMMANDS
5     C=LPTERM()
      C=LPINIT()
      C=LPSB(BOARD)
      C=LPSETA(0,0,2,GAIN)
      C=LPSCF(FREQ)
      C=LPDSC()
      C=LPADS(300,ADV(1))
      C=LPESC()
C
      TVOLTS=0.0D0
C
C CONVERSION OF ANALOG DATA VALUE RETRIEVED BY DATA ACQUISITION
C TO VOLTAGE
      DO 10 I=1,300,3
      ADVR=ADV(I)
```

```
      TVOLTS=(ADVR/NOC)*(PFS-MFS)-PFS+TVOLTS
10     CONTINUE
      AVEV1=TVOLTS/100
C
      TVOLTS=0.0D0
C
      DO 20 I=2,300,3
      ADVR=ADV(I)
      TVOLTS=(ADVR/NOC)*(PFS-MFS)-PFS+TVOLTS
20     CONTINUE
      AVEV2=TVOLTS/100
C
      TVOLTS=0.0D0
C
      DO 30 I=3,300,3
      ADVR=ADV(I)
      TVOLTS=(ADVR/NOC)*(PFS-MFS)-PFS+TVOLTS
30     CONTINUE
      AVEV3=TVOLTS/100
C
C OUTPUT TO SCREEN FOR BALANCING WITH THE BALANCING BRIDGE
      PRINT*, AVEV1,AVEV2,AVEV3
C
C
C
      GOTO 5
C
500    END
```

APPENDIX G
PROCEDURE FOR THERMOCOUPLE TEMPERATURE MEASUREMENT

Three type-T thermocouples were used on the experimental apparatus for this work. Each of these were wired to a reference block to obtain an accurate temperature measurement. The block was equipped with an RTD to measure the junctions' temperature.

Thermocouple temperature was calculated using the following procedure called software compensation:

1. The RTD temperature from the reference junction was converted to temperature using Eq. 47,

$$T_{\text{Ref}} = V_{\text{RTD}} * 10.0, \tag{47}$$

where V_{RTD} was the voltage from the RTD on the reference block, and T_{Ref} was the resulting reference temperature (degrees C).

2. This reference temperature was then converted into a type-T thermocouple voltage using the appropriate relation, Eq. 48 or Eq. 49 [29].

$$(\text{For } T_{\text{Ref}} = 0 - 400^{\circ}\text{C}) \quad V_{type-T} = A1 * T_{\text{Ref}} + A2 * T_{\text{Ref}}{}^{2} + \ldots + A8 * T_{\text{Ref}}{}^{8}, \tag{48}$$

where V_{type-T} was the corresponding type-T voltage (μV), and

A1=3.874077384E+1
A2=3.3190198092E-2
A3=2.0714183645E-4
A4=-2.1945834823E-6
A5=1.103190055E-8
A6=-3.0927581898E-11
A7=4.5653337165E-14
A8=-2.761687804E-17.

$$(\text{For } T_{\text{Ref}} = -270 - 0^{\circ}\text{C})\ V_{type-T} = B1 * T_{\text{Ref}} + B2 * T_{\text{Ref}}{}^{2} + \ldots + B14 * T_{\text{Ref}}{}^{14}, \qquad (49)$$

where V_{type-T} was the corresponding type-T voltage (μV), and

B1=3.874077384D+1
B2=4.4123932482D-2
B3=1.1405238498D-4
B4=1.9974406568D-5
B5=9.0445401187D-7
B6=2.2766018504D-8
B7=3.624740938D-10
B8=3.8648924201D-12
B9=2.8298678519D-14
B10=1.4281383349D-16
B11=4.8833254364D-19
B12=1.0803474683D-21
B13=1.3949291026D-24
B14=7.9795893156D-28.

3. Adding the above voltage to the measured thermocouple voltage,

$$V_T = V_{TC} + V_{type-T}, \qquad (50)$$

where V_{TC} was the voltage from the thermocouple alone (V), and V_{type-T} was given above.

4. Equation 51 with the constants below was used to calculate the resulting temperature,

$$T = \text{C0} + \text{C1} * V_{\text{T}} + \text{C2} * V_{\text{T}}{}^{2} + \ldots + \text{C7} * V_{\text{T}}{}^{7}, \qquad (51)$$

where T was the actual temperature of the process fluid (degrees C), and

C0=0.10086091D0
C1=25727.94369D0
C2=-767345.8295D0

C3=78025595.81D0

C4=-9247486589.0D0

C5=6.97688D+11

C6=-2.66192D+13

C7=3.94078D+14.

APPENDIX H
DATA ACQUISITION COMPUTER PROGRAM

This appendix contains the FORTRAN computer program used for the acquiring and storage of all data during experimental operation. Since the program used for the calibration of the thermocouple and the data acquisition program are essentially identical, only the full data acquisition program will be shown. The differences between the two is limited to the data sent to the screen and external files. This is pointed out in the comment lines of the program.

```
C$NOEX
C$NOWA
C
C DAQPROG.FOR
C THIS PROGRAM IS USED TO READ AND CONVERT ALL INSTRUMENTATION
C VOLTAGES TO THEIR CORRESPONDING PRESSURE, DIFFERENTIAL PRESSURE,
C OR TEMPERATURE.
C
C DESCRIPTION OF INSTRUMENTATION AND PROGRAM VARIABLES:
C DP1  DIFFERENTIAL PRESSURE ACROSS THE ORIFICE METER
C DP2  DIFFERENTIAL PRESSURE ACROSS THE BUBBLY FLOW VALVE AND TUBE
C DP3  DIFFERENTIAL PRESSURE ACROSS THE BUBBLY FLOW TUBE ONLY
C CRJT  COLD REFERENCE JUNCTION TEMPERATURE FOR THERMOCOUPLE CORRECTION
C P1   GAGE PRESSURE OF CONDENSER
C P2   GAGE PRESSURE UPSTREAM OF PRESSURE VESSEL
C P3   GAGE PRESSURE OF EVAPORATOR
C SGT  STRAIN GAGE DERIVED THRUST OF NOZZLE
C T1   TEMPERATURE OF INLET TO CONDENSER (SUPERHEAT)
C T2   TEMPERATURE OF INLET TO PRESSURE VESSEL (SUBCOOLING OF CONDENSER)
C T3   TEMPERATURE OF OUTLET OF EVAPORATOR (SUPERHEAT OF EVAPORATOR)
C
C LPCLAB SUBROUTINES AND VARIABLES DEFINITION STATEMENT
C
      INTEGER*2 NREAD,BOARD,MODE,SCHAN,ECHAN,NOCHAN,GAIN,OUT(2)
      INTEGER*2 TNREAD,ADV(300),LPTERM,LPINIT,LPSB,LPSETA,LPSCF
      INTEGER*2 LPDCS,LPADS,LPESC,LPGV,DACNO,HR,MIN,SEC,HSEC,TREAD
      INTEGER NOHSEC
C
      INTEGER KOUNT,BOARDINC,J,K,L,I
C
      REAL VFANCI,VFANEI,SUMERC,PROPC,INTC,DERVIC,SUMERE,PROPE
      REAL INTE,DERIVE,PATM,P1CON,P3CON,KPC,KIC,KDC,KPE,KIE,KDE
      REAL PCOND,PEVAP,PEOLD,PCOLD,T1R,P2R,T2R,PINN,T2A,H,S2,S1
      REAL VFANCP,VFANEP,FREQ,X,DEN,S,HE,TE,TSUB,P3R,P1,P2,P3
```

```
      REAL TSUPER,P1N
C
      DOUBLE PRECISION DP1A,DP1B,DP1C,DP1D,DP2A,DP2B,DP2C
      DOUBLE PRECISION DP3A,DP3B,DP3C,P1A,P1B,P1C,P1D
      DOUBLE PRECISION P2A,P2B,P2C,P2D,P3A,P3B,P3C,P3D
      DOUBLE PRECISION SGA,SGB,SGC,SGD,A1,A2,A3,A4,A5,A6,A7,A8
      DOUBLE PRECISION B1,B2,B3,B4,B5,B6,B7,B8,B9,B10,B11,B12
      DOUBLE PRECISION B13,B14,C0,C1,C2,C3,C4,C5,C6,C7,PFS,MFS
      DOUBLE PRECISION NOC,TVOLTS,ADVR,NREADR,AVEV(11)
      DOUBLE PRECISION DP1,DP2,DP3,CRJT,CRJV,SGT,SGTP
      DOUBLE PRECISION AVEVT1,AVEVT2,AVEVT3,T1,T2,T3,W,WINI,DUM
      DOUBLE PRECISION EFF
C
      CHARACTER*4 REF
C
5     FORMAT(6F11.6)
7     FORMAT(7F10.3)
8     FORMAT(5F11.3)
9     FORMAT(5F10.5)
10    FORMAT(1X,I6,7F10.3)
C
C ROSEMOUNT MODEL 2024
C DIFFERENTIAL PRESSURE CELL 1 (DP1) CALIBRATION RANGE (0-1.498 PSID)
      DP1A=-0.5175592D0
      DP1B=0.52475236D0
      DP1C=-0.0092768D0
      DP1D=0.00137849D0
C STATHAM LABORATORIES MODEL P80fTC-50D-350
C DIFFERENTIAL PRESSURE CELL 2 (DP2) CALIBRATION RANGE (0-50 PSID)
      DP2A=0.01110451D0
      DP2B=10.2183336D0
      DP2C=-0.0225858D0
C STATHAM LABORATORIES MODEL P80fTC-50D-350
C DIFFERENTIAL PRESSURE CELL 3 (DP3) CALIBRATION RANGE (0-50 PSID)
      DP3A=0.03515162D0
      DP3B=10.2836911D0
      DP3C=-0.0384164D0
C TELEDYNE MODEL 226-SA  0-300 PSIG
C GAGE PRESSURE CELL 1 (P1) CALIBRATION RANGE (0-240 PSIG)
      P1A=-0.01738892D0
      P1B=97.780473243D0
      P1C=-1.011336467D0
      P1D=0.2260125702D0
C STATHAM LABORATORIES MODEL P24a-300a-350
C GAGE PRESSURE CELL 2 (P2) CALIBRATION RANGE (0-235 PSIG)
      P2A=0.16735785D0
      P2B=95.4135469D0
      P2C=-0.416509D0
      P2D=-0.0036295D0
C FREDERICK FLADER TYPE PSH S  0-100PSIA
C GAGE PRESSURE CELL 3 (P3) CALIBRATION RANGE (0-95 PSIG)
      P3A=0.17771059D0
      P3B=38.4801399D0
      P3C=-1.1548537D0
      P3D=0.42103019D0
C MEASUREMENTS GROUP STRAIN GAGES MODEL WK-09-125AD-350
```

```
C FULL WHEATSTONE BRIDGE CALIBRATION RANGE (0-3.3045 MICRO-STRAIN)(0-0.686N)
      SGA=0.00220934D0
      SGB=0.29757868D0
      SGC=-0.0199661D0
      SGD=0.00506281D0
C TYPE-T THERMOCOUPLE CALIBRATION FOR 0-400C  (NBS MONOGRAPH 125)
      A1=3.874077384D+1
      A2=3.3190198092D-2
      A3=2.0714183645D-4
      A4=-2.1945834823D-6
      A5=1.103190055D-8
      A6=-3.0927581898D-11
      A7=4.5653337165D-14
      A8=-2.761687804D-17
C TYPE-T THERMOCOUPLE CALIBRATION FOR -270-0C  (NBS MONOGRAPH 125)
      B1=3.874077384D+1
      B2=4.4123932482D-2
      B3=1.1405238498D-4
      B4=1.9974406568D-5
      B5=9.0445401187D-7
      B6=2.2766018504D-8
      B7=3.624740938D-10
      B8=3.8648924201D-12
      B9=2.8298678519D-14
      B10=1.4281383349D-16
      B11=4.8833254364D-19
      B12=1.0803474683D-21
      B13=1.3949291026D-24
      B14=7.9795893156D-28
C TYPE-T THERMOCOUPLE CALIBRATION CONSTANTS (OMEGA TEMP HANDBOOK)
      C0=0.10086091D0
      C1=25727.94369D0
      C2=-767345.8295D0
      C3=78025595.81D0
      C4=-9247486589.0D0
      C5=6.97688D+11
      C6=-2.66192D+13
      C7=3.94078D+14
C INITIALIZE FAN VOLTAGES FOR CONTROL
      VFANCI=4.98E0
      VFANEI=4.98E0
C INITIALIZE ERROR SUM FOR CONTROL
      SUMERC=0.0E0
      PROPC=0.0E0
      INTC=0.0E0
      DERIVC=0.0E0
      SUMERE=0.0E0
      PROPE=0.0E0
      INTE=0.0E0
      DERIVE=0.0E0
C INITIALIZE COUNTER FOR CONTROL LOOP
      KOUNT=0
C INPUT OF AMBIENT AND CONTROL PARAMETERS
      WRITE(*,*) 'ENTER ATMOSPHERIC PRESSURE (PSIA)'
      READ(*,*) PATM
      WRITE(*,*) 'ENTER CONTROL CONDENSER PRESSURE (PSIA)'
```

```
      READ(*,*) P1CON
      WRITE(*,*) 'ENTER CONTROL EVAPORATOR PRESSURE (PSIA)'
      READ(*,*) P3CON
C
C OPEN FILES FOR DATA OUTPUT
      IF (P1CON .EQ. 150.0E0) THEN
      OPEN(UNIT=2,FILE='DAQ150.FOR')
      OPEN(UNIT=3,FILE='DAQ2150.FOR')
      OPEN(UNIT=4,FILE='DAQ3150.FOR')
      ELSE IF (P1CON .EQ. 155.0E0) THEN
      OPEN(UNIT=2,FILE='DAQ155.FOR')
      OPEN(UNIT=3,FILE='DAQ2155.FOR')
      OPEN(UNIT=4,FILE='DAQ3155.FOR')
      ELSE IF (P1CON .EQ. 160.0E0) THEN
      OPEN(UNIT=2,FILE='DAQ160.FOR')
      OPEN(UNIT=3,FILE='DAQ2160.FOR')
      OPEN(UNIT=4,FILE='DAQ3160.FOR')
      ELSE IF (P1CON .EQ. 165.0E0) THEN
      OPEN(UNIT=2,FILE='DAQ165.FOR')
      OPEN(UNIT=3,FILE='DAQ2165.FOR')
      OPEN(UNIT=4,FILE='DAQ3165.FOR')
      ELSE IF (P1CON .EQ. 170.0E0) THEN
      OPEN(UNIT=2,FILE='DAQ170.FOR')
      OPEN(UNIT=3,FILE='DAQ2170.FOR')
      OPEN(UNIT=4,FILE='DAQ3170.FOR')
      ELSE IF (P1CON .EQ. 175.0E0) THEN
      OPEN(UNIT=2,FILE='DAQ175.FOR')
      OPEN(UNIT=3,FILE='DAQ2175.FOR')
      OPEN(UNIT=4,FILE='DAQ3175.FOR')
      ELSE IF (P1CON .EQ. 180.0E0) THEN
      OPEN(UNIT=2,FILE='DAQ180.FOR')
      OPEN(UNIT=3,FILE='DAQ2180.FOR')
      OPEN(UNIT=4,FILE='DAQ3180.FOR')
      ELSE
      OPEN(UNIT=2,FILE='DAQDAT.FOR')
      OPEN(UNIT=3,FILE='DAQ2DAT.FOR')
      OPEN(UNIT=4,FILE='DAQ3DAT.FOR')
      END IF
C
C DEFINITION OF PID CONTROL CONSTANTS
      KPC=1.25E0
      KIC=0.184E0
      KDC=8.5E0
      KPE=1.875E0
      KIE=0.225E0
      KDE=3.92E0
C INITIALIZE EVAP AND COND PRESSURE FOR DERIVATIVE CONTROL
      PCOND=P1CON
      PEVAP=P3CON
C INITIALIZE TIME
      CALL SETTIME(0,0,0,0)
C
C DATA ACQUISITION ROUTINE PARAMETER DEFINITIONS
C BOARD IS THE DATA ACQUISITION CARD TO BE USED FOR SIGNAL MEASUREMENT;
C MODE IS THE TIMING FUNCTION FOR TRIGGERING; CHAN IS THE CHANNEL FOR
C STARTING AND ENDING DATA ACQUISITION; NOCHAN IS THE NUMBER OF CHANNELS;
```

```
C GAIN IS THE AMPLIFICATION PROVIDED BY THE BOARD;FREQ IS THE FREQUENCY
C OF DATA ACQUISITION; NOC IS THE NUMBER OF CODES FOR ASSIGNMENT ON BOARD.
C
C BOARD INCREMENT STATEMENT; BOARD 1 IS FOR HIGH LEVEL INPUTS, BOARD 2
C IS FOR LOW LEVEL INPUTS; BOARDINC EQUAL TO 1 IS FOR THE BOARD 1 INPUTS,
C BOARDINC EQUAL TO 2 IS FOR THE BOARD 2 INPUTS WITH A GAIN OF 100, AND
C BOARDINC EQUAL TO 3 IS FOR THE BOARD 2 INPUTS WITH A GAIN OF 500.
C
      NOC=4096.0D0
C NUMBER OF READINGS PER CHANNEL
      NREAD=25
      NREADR=NREAD
C
C SUBROUTINE CALL FOR QUALITY CALCULATION
      REF='RR12'
      CALL RINIT(REF,IERR)
C
18    BOARDINC=1
      KOUNT=KOUNT+1
      J=1
      WINI=1.0D0
      W=0.0D0
      PEOLD=PEVAP
      PCOLD=PCOND
C
C ASSIGNMENT OF CONSTANTS FOR BOARD
20    IF (BOARDINC .EQ. 1) THEN
       BOARD=1
       MODE=0
       SCHAN=0
       ECHAN=3
       NOCHAN=ECHAN-SCHAN+1
       GAIN=1
       FREQ=5000.0E0
       PFS=5.0D0
       MFS=-5.0D0
       TNREAD=NOCHAN*NREAD
      ELSE IF (BOARDINC .EQ. 2) THEN
       BOARD=2
       MODE=0
       SCHAN=0
       ECHAN=3
       NOCHAN=ECHAN-SCHAN+1
       GAIN=100
       FREQ=2000.0E0
       PFS=2.5D0
       MFS=-2.5D0
       TNREAD=NOCHAN*NREAD
      ELSE IF (BOARDINC .EQ. 3) THEN
       BOARD=2
       MODE=0
       SCHAN=4
       ECHAN=6
       NOCHAN=ECHAN-SCHAN+1
       GAIN=500
       FREQ=2000.0E0
```

```
       PFS=2.5D0
       MFS=-2.5D0
       TNREAD=NOCHAN*NREAD
      ELSE IF (BOARDINC .EQ. 4) THEN
C DATA ACQUISITION ROUTINES TO ALLOW EXTERNAL FILE WRITING
      C=LPTERM()
      C=LPINIT()
      BOARD=1
      C=LPSB(BOARD)
      MODE=0
      SCHAN=4
      ECHAN=4
      GAIN=1
      C=LPSETA(MODE,SCHAN,ECHAN,GAIN)
      FREQ=5000.0E0
      C=LPSCF(FREQ)
      C=LPDSC()
      TREAD=1
      C=LPADS(TREAD,OUT(1))
      C=LPESC()
C END OF EXTERNAL ROUTINES
       GOTO 50
      ENDIF
C
C START OF DATA ACQUISITION ROUTINES
      C=LPTERM()
      C=LPINIT()
      C=LPSB(BOARD)
      C=LPSETA(MODE,SCHAN,ECHAN,GAIN)
      C=LPSCF(FREQ)
      C=LPDSC()
      C=LPADS(TNREAD,ADV(1))
      C=LPESC()
C END OF DATA ACQUISITION ROUTINES
C
C ADD AND AVERAGE DATA FROM ARRAY, THEN ASSIGN AVERAGES TO ARRAY
      DO 40 K=1,NOCHAN,1
      TVOLTS=0.0D0
      DO 30 I=K,TNREAD,NOCHAN
       ADVR=ADV(I)
       TVOLTS=(ADVR/NOC)*(PFS-MFS)-PFS+TVOLTS
30    CONTINUE
       AVEV(J)=TVOLTS/NREADR
       J=J+1
40    CONTINUE
C
      BOARDINC=BOARDINC+1
      GOTO 20
50     CONTINUE
C
C TIME
      CALL GETTIM(HR,MIN,SEC,HSEC)
      NOHSEC=HR*360000+MIN*6000+SEC*100+HSEC
C
C DIFFERENTIAL PRESSURE CALCULATION OF DP1 IN PSID
      DP1=DP1A+DP1B*AVEV(1)+DP1C*AVEV(1)**2+DP1D*AVEV(1)**3
```

```
C DIFFERENTIAL PRESSURE CALCULATION OF DP2 IN PSID
      DP2=DP2A+DP2B*AVEV(2)+DP2C*AVEV(2)**2
C DIFFERENTIAL PRESSURE CALCULATION OF DP3 IN PSID
      DP3=DP3A+DP3B*AVEV(3)+DP3C*AVEV(3)**2
C COLD REFERENCE JUNCTION TEMPERATURE CALCULATION IN DEGREES C
      CRJT=AVEV(4)*10.0D0
C
      IF (CRJT .GT. 0.0) THEN
C CALCULATION OF TYPE-T REFERENCE VOLTAGE FOR COLD REFERENCE JUNCTION
C TEMPERATURE RANGE (0-400 C), CRJV IN MICROVOLTS
        CRJV=A1*CRJT+A2*CRJT**2+A3*CRJT**3
        CRJV=CRJV+A4*CRJT**4+A5*CRJT**5+A6*CRJT**6
        CRJV=CRJV+A7*CRJT**7+A8*CRJT**8
C CONVERSION OF CRJV TO VOLTS
        CRJV=CRJV/1.0D6
      ELSE IF (CRJT .LT. 0.0) THEN
C CALCULATION OF TYPE-T REFERENCE VOLTAGE FOR COLD REFERENCE JUNCTION
C TEMPERATURE RANGE (-270-0 C), CRJV IN MICROVOLTS
        CRJV=B1*CRJT+B2*CRJT**2+B3*CRJT**3
        CRJV=CRJV+B4*CRJT**4+B5*CRJT**5+B6*CRJT**6
        CRJV=CRJV+B7*CRJT**7+B8*CRJT**8+B9*CRJT**9
        CRJV=CRJV+B10*CRJT**10+B11*CRJT**11+B12*CRJT**12
        CRJV=CRJV+B13*CRJT**13+B14*CRJT**14
C CONVERSION OF CRJV TO VOLTS
        CRJV=CRJV/1.0D6
      ELSE
        CRJV=0.0D0
      ENDIF
C
C GAGE PRESSURE CALCULATION OF P1 IN PSIG
      P1=P1A+P1B*AVEV(5)+P1C*AVEV(5)**2+P1D*AVEV(5)**3
C GAGE PRESSURE CALCULATION OF P2 IN PSIG
      P2=P2A+P2B*AVEV(6)+P2C*AVEV(6)**2+P2D*AVEV(6)**3
C GAGE PRESSURE CALCULATION OF P3 IN PSIG
      P3=P3A+P3B*AVEV(7)+P3C*AVEV(7)**2+P3D*AVEV(7)**3
C STRAIN GAGE THRUST CALCULATION IN NEWTONS
      SGT=SGA+SGB*AVEV(8)+SGC*AVEV(8)**2+SGD*AVEV(8)**3
C CONVERSION OF THRUST FROM NEWTONS TO POUNDS-FORCE
      SGTP=SGT*0.224809D0
C
C TEMPERATURE CALCULATIONS IN DEGREES C
C CONVERSION OF THERMOCOUPLE VOLTAGE SIGNALS FROM AMPLIFIED SIGNALS AND
C ADDITION OF COLD JUNCTION REFERENCE VOLTAGE
      AVEVT1=AVEV(9)/500.0D0+CRJV
      AVEVT2=AVEV(10)/500.0D0+CRJV
      AVEVT3=AVEV(11)/500.0D0+CRJV
C CALCULATION OF THERMOCOUPLE TEMPERATURES FROM TYPE-T POLYNOMIAL (C)
C AND CONVERSION TO (F)
      T1=C0+C1*AVEVT1+C2*AVEVT1**2+C3*AVEVT1**3
      T1=T1+C4*AVEVT1**4+C5*AVEVT1**5+C6*AVEVT1**6
      T1=T1+C7*AVEVT1**7
      T1=1.8D0*(273.15D0+T1)-459.67D0
      T1R=T1+459.67D0
      T2=C0+C1*AVEVT2+C2*AVEVT2**2+C3*AVEVT2**3
      T2=T2+C4*AVEVT2**4+C5*AVEVT2**5+C6*AVEVT2**6
      T2=T2+C7*AVEVT2**7
```

```
      T2=1.8D0*(273.15D0+T2)-459.67D0
C ***********************************************************************
C THERMOCOUPLE CORRECTION
      T2=T2+(0.11369E0*T2-10.7334E0)
C ***********************************************************************
      T3=C0+C1*AVEVT3+C2*AVEVT3**2+C3*AVEVT3**3
      T3=T3+C4*AVEVT3**4+C5*AVEVT3**5+C6*AVEVT3**6
      T3=T3+C7*AVEVT3**7
      T3=1.8D0*(273.15D0+T3)-459.67D0
C
C CONVERSION OF GAGE PRESSURES TO ABSOLUTE PRESSURES
      P1=P1+PATM
      P2=P2+PATM
      TSUB=T2OFP(REF,P2)-459.67E0-T2
      P3=P3+PATM
      P3R=P3
      PCOND=P1
      PEVAP=P3
      P1N=P1+DP1
C
C PROPERTIES ENTERING NOZZLE
      P2R=P2
      T2R=T2+459.67D0
      PINN=P2R-DP2
      H=HLOFPT(REF,P2R,T2R)
      T2A=T2OFP(REF,PINN)
      X=XTH(REF,T2A,H)
      S=S2OFTH(REF,T2A,H)
C
C SUBROUTINE CALL FOR MASS FLOW RATE PARAMETER; DENSITY
      DEN=1/(VSOFPT(REF,P1N,T1R))
C
C ITERATION ROUTINE FOR MASS FLOW RATE
      WINI=1.0D0
      DO 63 L=1,50
       DUM=(5.16553D-7*T1R-3.61185D-5)**0.41D0
       W=0.7966604D0*SQRT(DP1*DEN)
       W=W+0.1677255D0*SQRT(DP1*DEN/WINI)*DUM
C EXIT QUALIFICATION
      IF (ABS(WINI-W) .LT. 1.0D-6) THEN
       GOTO 65
      ENDIF
       WINI=W
63    CONTINUE
65    CONTINUE
C ISENTROPIC ENTHALPY LEAVING NOZZLE
      TE=T2OFP(REF,P3R)
      HE=H2OFTS(REF,TE,S)
C NOZZLE EFFICIENCY (END CONSTANT FOR UNITS)
      EFF=(SGTP**2)/2/(W**2)/(H-HE)*148.82628D0
C SUPERHEAT LEAVING THE EVAPORATOR
      TSUPER=T3-(TE-459.67E0)
C
C CONTROL ROUTINE FOR EVAPORATOR AND CONDENSER PRESSURE
C DAC0=CONDENSER FAN, DAC1=EVAPORATOR FAN
      IF (KOUNT .GE. 2) THEN
```

```
        S2=SUMERC
        SUMERC=SUMERC+(PCOND-P1CON)
        S1=SUMERE
        SUMERE=SUMERE+(P3CON-PEVAP)
        PROPC=KPC*(PCOND-P1CON)
        INTC=KIC*SUMERC
        DERIVC=KDC*(PCOND-PCOLD)
        PROPE=KPE*(P3CON-PEVAP)
        INTE=KIE*SUMERE
        DERIVE=KDE*(PEOLD-PEVAP)
        VFANCP=VFANCI+PROPC+INTC+DERIVC
        VFANEP=VFANEI+PROPE+INTE+DERIVE
         IF (VFANCP .GT. 4.98E0) THEN
          VFANCP=4.98E0
          SUMERC=S2
          INTC=KIC*SUMERC
         ENDIF
         IF (VFANCP .LT. -4.98E0) THEN
          VFANCP=-4.98E0
          SUMERC=S2
          INTC=KIC*SUMERC
         ENDIF
         IF (VFANEP .GT. 4.98E0) THEN
          VFANEP=4.98E0
          SUMERE=S1
          INTE=KIE*SUMERE
         ENDIF
         IF (VFANEP .LT. -4.98E0) THEN
          VFANEP=-4.98E0
          SUMERE=S1
          INTE=KIE*SUMERE
         ENDIF
C GENERATE VOLTAGE TO FANS FOR CONTROL
      BOARD=1
      D=LPSB(BOARD)
      DACNO=0
      D=LPGV(DACNO,VFANCP)
      DACNO=1
      D=LPGV(DACNO,VFANEP)
      BOARD=2
      D=LPSB(BOARD)
      D=LPDV(1,3276)
C OUTPUT TO SCREEN AND FILE COMMANDS
      WRITE(*,10) NOHSEC,TSUB,P1,P3,EFF,PINN,DP2,DP3
      WRITE(*,7) TSUPER,W,P2,T1,T2,T3,X
      IF (OUT(1) .GT. 3150) THEN
       WRITE(2,10) NOHSEC,TSUB,P1,P3,PINN,DP2,DP3
       WRITE(3,8) T1,T2,T3,P2,TSUPER
       WRITE(4,9) EFF,DP1,X,SGTP,W
C
C*******************************************************************************************
C ADDITIONAL STATMENTS FOR T2 THERMOCOUPLE CALIBRATION
C CALCULATED TEMPERATURE AT MEASURED PRESSURE (P2)
      TCALC=TSUB+T2
```

```
C OUTPUT STATEMENTS
      WRITE(*,9) P1,P3,T2,TCALC,P2
      WRITE(3,*) T2,P2,TCALC
C END OF ADDITIONAL STATEMENTS
C*********************************************************************************************
      ENDIF
      WRITE(*,*) ' '
C
      ENDIF
C
C RESET TIME
      IF (NOHSEC .GT. 999500) THEN
      CALL SETTIME(0,0,0,0)
      ENDIF
C
      GOTO 18
      END
```

APPENDIX I
RAW EXPERIMENTAL DATA

This appendix contains all the averaged data for each run. It is arranged in order of increasing condenser pressures.

PROPERTY	RUN 1	RUN 2	RUN 3	RUN 4	RUN 5	RUN 6	RUN 7
Pcond (psia)	149.96	149.99	150.01	150.05	154.96	154.98	154.98
Pevap (psia)	54.99	54.98	54.93	55.01	55.01	55.00	55.00
Tsuperheat (F)	25.01	3.30	29.20	0.00	0.00	26.14	25.55
Tsubcool (F)	3.84	3.70	3.96	3.18	3.42	4.87	4.21
P in nozzle (psia)	111.55	111.45	111.04	112.59	113.92	112.48	113.31
Quality in nozzle	0.066	0.067	0.067	0.067	0.073	0.069	0.071
DP1 (psid)	0.917	0.913	0.889	0.922	0.869	0.832	0.854
DP2 (psid)	35.59	35.66	36.03	34.51	38.05	39.02	38.75
DP3 (psid)	10.27	10.36	10.03	10.65	10.58	10.41	10.06
T1 (F)	142.83	137.04	140.87	140.91	139.58	141.34	143.13
T2 (F)	104.21	104.33	104.05	104.84	107.03	105.35	106.29
T3 (F)	68.60	46.88	72.73	41.92	42.31	69.74	69.15
P2 (psia)	147.14	147.11	147.07	147.10	151.97	151.50	152.06
Efficiency	0.290	0.292	0.284	0.305	0.298	0.294	0.293
S.D.	0.0109	0.0102	0.0104	0.0104	0.0104	0.0081	0.013
S.D./AVE	0.0388	0.0362	0.0378	0.0351	0.036	0.0336	0.0458
Thrust (lbf)	0.079	0.080	0.077	0.082	0.083	0.079	0.080
S.D.	0.0015	0.0013	0.0013	0.0014	0.0014	0.0012	0.0017
S.D./AVE	0.0184	0.0163	0.017	0.0139	0.0166	0.0157	0.0215
W (lbm/min)	1.399	1.408	1.382	1.407	1.396	1.363	1.377
S.D.	0.0054	0.006	0.005	0.0067	0.006	0.0053	0.006
S.D./AVE	0.0038	0.0043	0.0036	0.0047	0.0043	0.0039	0.0044
Uex,act (ft/sec)	108.92	109.35	107.52	112.77	114.88	111.45	112.69
Pth,HEM (psia)	83.95	83.65	83.84	84.39	84.72	84.08	84.91
Pe,HEM (psia)	9.75	9.65	9.64	9.79	9.72	9.68	9.51
HEM W (lbm/min)	0.665	0.664	0.662	0.670	0.668	0.666	0.667
HEM THRUST (lbf)	0.167	0.167	0.166	0.168	0.170	0.169	0.170
HEM Ue (ft/sec)	476.79	477.94	477.26	478.30	488.65	479.61	490.35
W/HEMW (Cd)	2.10	2.12	2.09	2.10	2.09	2.05	2.06
Pth,froz (psia)	60.75	60.85	60.64	61.39	62.73	61.48	62.11
FROZW	5.08	5.02	5.00	5.06	4.78	4.94	4.86
Cm	0.166	0.171	0.166	0.168	0.177	0.163	0.169

PROPERTY	RUN 8	RUN 9	RUN 10	RUN 11	RUN 12	RUN 13	RUN 14
Pcond (psia)	154.99	155.00	159.94	159.95	159.98	159.99	160.03
Pevap (psia)	55.00	54.87	55.01	55.00	55.05	55.02	54.92
Tsuperheat (F)	14.36	29.20	0.40	16.04	31.74	0.37	29.70
Tsubcool (F)	4.44	4.09	4.83	4.68	0.88	1.33	4.60
P in nozzle (psia)	112.78	113.41	114.50	115.06	118.38	118.85	115.50
Quality in nozzle	0.070	0.072	0.076	0.074	0.082	0.081	0.075
DP1 (psid)	0.840	0.840	0.796	0.795	0.967	0.968	0.791
DP2 (psid)	38.65	38.78	42.46	41.42	38.06	38.24	41.64
DP3 (psid)	10.55	9.93	10.35	10.38	11.48	12.08	9.90
T1 (F)	141.71	144.47	138.54	143.90	149.14	144.11	145.07
T2 (F)	105.75	106.47	108.05	107.97	111.75	111.61	108.37
T3 (F)	57.97	72.67	44.01	59.64	75.39	43.99	73.22
P2 (psia)	151.43	152.19	156.96	156.49	156.44	157.09	157.14
Efficiency	0.297	0.286	0.299	0.295	0.216	0.223	0.289
S.D.	0.0087	0.0151	0.0131	0.0095	0.0076	0.0081	0.0157
S.D./AVE	0.0359	0.0545	0.0449	0.0393	0.0371	0.0379	0.0556
Thrust (lbf)	0.080	0.079	0.082	0.081	0.080	0.082	0.081
S.D.	0.0013	0.0021	0.0017	0.0015	0.0014	0.0015	0.0021
S.D./AVE	0.0169	0.0262	0.0207	0.0181	0.0171	0.0185	0.0266
W (lbm/min)	1.369	1.363	1.365	1.353	1.480	1.492	1.348
S.D.	0.0056	0.006	0.0083	0.0056	0.005	0.0046	0.0061
S.D./AVE	0.0041	0.0044	0.0061	0.0041	0.0034	0.0031	0.0045
Uex,act (ft/sec)	112.54	111.89	116.59	116.10	104.33	106.26	115.61
Pth,HEM (psia)	84.18	84.61	85.10	86.46	87.38	87.85	85.90
Pe,HEM (psia)	9.78	9.61	9.70	9.66	9.78	9.85	9.70
HEM W (lbm/min)	0.666	0.667	0.666	0.671	0.676	0.680	0.673
HEM THRUST (lbf)	0.169	0.170	0.171	0.172	0.177	0.177	0.173
HEM Ue (ft/sec)	478.81	489.22	490.13	491.64	503.03	503.02	491.98
W/HEMW (Cd)	2.06	2.04	2.05	2.02	2.19	2.19	2.00
Pth,froz (psia)	61.78	62.21	63.30	63.26	65.78	65.85	63.70
FROZW	4.90	4.81	4.64	4.77	4.50	4.56	4.73
Cm	0.166	0.168	0.176	0.166	0.210	0.209	0.166

PROPERTY	RUN 15	RUN 16	RUN 17	RUN 18	RUN 19	RUN 20	RUN 21
Pcond (psia)	164.61	164.93	164.94	164.94	164.98	165.02	165.05
Pevap (psia)	55.12	54.85	55.03	54.99	55.04	55.03	55.02
Tsuperheat (F)	29.70	28.53	0.00	19.53	29.12	0.00	0.30
Tsubcool (F)	6.19	4.65	3.75	5.91	1.28	4.39	3.42
P in nozzle (psia)	115.66	118.91	119.29	117.05	120.37	118.92	117.86
Quality in nozzle	0.076	0.076	0.079	0.074	0.086	0.077	0.083
DP1 (psid)	0.702	0.716	0.773	0.811	0.928	0.737	0.764
DP2 (psid)	45.59	42.98	42.61	44.40	40.94	42.93	43.61
DP3 (psid)	9.86	10.56	10.47	10.87	11.52	11.03	9.90
T1 (F)	143.82	146.15	147.39	144.67	147.80	144.67	139.84
T2 (F)	108.74	110.57	111.45	109.11	113.67	110.81	111.61
T3 (F)	73.42	71.97	42.26	63.12	72.77	43.28	43.92
P2 (psia)	161.25	161.89	161.83	161.45	161.31	161.85	161.47
Efficiency	0.302	0.333	0.316	0.305	0.219	0.347	0.276
S.D.	0.019	0.0177	0.0228	0.0097	0.0079	0.0127	0.0121
S.D./AVE	0.0767	0.0539	0.0732	0.0389	0.0377	0.0372	0.0462
Thrust (lbf)	0.079	0.087	0.089	0.087	0.083	0.090	0.083
S.D.	0.0022	0.0022	0.0027	0.0015	0.0015	0.0015	0.0018
S.D./AVE	0.0278	0.0251	0.0306	0.0168	0.0183	0.017	0.0214
W (lbm/min)	1.294	1.304	1.353	1.392	1.481	1.326	1.361
S.D.	0.0239	0.0096	0.0268	0.0072	0.0041	0.0092	0.0092
S.D./AVE	0.0185	0.0074	0.0198	0.0052	0.0028	0.0069	0.0067
Uex,act (ft/sec)	118.45	128.82	126.48	120.32	108.01	131.36	117.78
Pth,HEM (psia)	86.46	88.51	88.29	87.45	88.77	88.52	86.86
Pe,HEM (psia)	9.86	10.11	10.09	9.85	9.97	10.12	9.66
HEM W (lbm/min)	0.671	0.686	0.684	0.680	0.680	0.685	0.672
HEM THRUST (lbf)	0.173	0.178	0.178	0.175	0.180	0.178	0.176
HEM Ue (ft/sec)	490.17	492.92	493.88	492.86	504.19	492.84	503.64
W/HEMW (Cd)	1.93	1.90	1.98	2.05	2.18	1.94	2.02
Pth,froz (psia)	63.86	65.51	65.89	64.25	67.17	65.52	65.46
FROZW	4.69	4.81	4.67	4.84	4.39	4.76	4.43
Cm	0.155	0.150	0.168	0.171	0.216	0.157	0.183

PROPERTY	RUN 22	RUN 23	RUN 24	RUN 25	RUN 26	RUN 27	RUN 28
Pcond (psia)	165.06	165.98	167.03	167.93	168.94	169.80	169.81
Pevap (psia)	55.03	55.04	55.06	55.04	55.03	55.02	55.08
Tsuperheat (F)	0.52	0.00	0.00	1.32	2.80	1.05	26.03
Tsubcool (F)	1.72	3.39	3.06	3.44	3.46	3.38	6.19
P in nozzle (psia)	121.00	118.81	119.78	119.43	119.89	120.88	118.81
Quality in nozzle	0.084	0.083	0.084	0.085	0.085	0.086	0.079
DP1 (psid)	0.929	0.803	0.779	0.764	0.825	0.818	0.751
DP2 (psid)	41.14	43.62	43.55	44.65	45.12	45.27	47.56
DP3 (psid)	11.95	10.28	10.27	10.47	10.57	10.61	10.73
T1 (F)	145.60	140.75	141.49	141.82	142.90	143.84	145.52
T2 (F)	113.62	112.08	112.84	112.81	113.22	113.83	111.12
T3 (F)	44.15	41.34	41.21	44.96	46.44	44.68	69.71
P2 (psia)	162.13	162.43	163.33	164.08	165.01	166.15	166.36
Efficiency	0.224	0.273	0.283	0.294	0.268	0.278	0.305
S.D.	0.0079	0.01	0.0109	0.0109	0.0106	0.0106	0.0108
S.D./AVE	0.0368	0.0385	0.0405	0.0391	0.0414	0.0401	0.0434
Thrust (lbf)	0.084	0.086	0.087	0.088	0.088	0.090	0.087
S.D.	0.0014	0.0016	0.0015	0.0015	0.0016	0.0016	0.0016
S.D./AVE	0.0169	0.0183	0.0167	0.0107	0.0177	0.0175	0.0187
W (lbm/min)	1.487	1.399	1.382	1.372	1.427	1.425	1.362
S.D.	0.0084	0.0083	0.0083	0.0098	0.0108	0.0107	0.01
S.D./AVE	0.0057	0.0059	0.006	0.0072	0.0076	0.0075	0.0074
Uex,act (ft/sec)	109.47	118.14	121.48	123.63	118.81	122.21	123.64
Pth,HEM (psia)	89.20	87.61	88.58	88.23	88.49	89.68	88.21
Pe,HEM (psia)	10.00	9.81	9.98	9.83	9.89	10.08	10.01
HEM W (lbm/min)	0.685	0.677	0.680	0.678	0.679	0.683	0.682
HEM THRUST (lbf)	0.181	0.178	0.179	0.179	0.179	0.180	0.178
HEM Ue (ft/sec)	504.97	503.46	502.98	504.28	504.37	503.69	494.07
W/HEMW (Cd)	2.17	2.07	2.03	2.02	2.10	2.09	2.00
Pth,froz (psia)	67.20	66.21	66.58	66.63	66.69	67.28	65.61
FROZW	4.50	4.47	4.46	4.40	4.42	4.41	4.65
Cm	0.210	0.190	0.186	0.186	0.200	0.199	0.171

PROPERTY	RUN 29	RUN 30	RUN 31	RUN 32	RUN 33	RUN 34	RUN 35
Pcond (psia)	169.91	169.98	169.98	170.00	170.06	170.95	171.92
Pevap (psia)	54.99	55.07	55.01	55.04	55.04	55.03	55.05
Tsuperheat (F)	26.06	0.22	18.04	26.83	0.62	1.30	1.16
Tsubcool (F)	6.07	4.72	6.49	1.55	1.76	3.34	3.17
P in nozzle (psia)	118.34	121.10	118.84	122.22	122.94	121.47	122.35
Quality in nozzle	0.081	0.081	0.078	0.091	0.090	0.086	0.087
DP1 (psid)	0.719	0.704	0.758	0.881	0.876	0.806	0.798
DP2 (psid)	48.16	45.69	47.63	44.10	44.15	45.67	45.81
DP3 (psid)	10.36	10.81	10.75	11.41	11.64	10.68	10.72
T1 (F)	147.91	144.02	145.22	150.56	148.54	147.20	147.95
T2 (F)	111.30	112.78	110.86	115.73	115.88	114.32	114.96
T3 (F)	69.64	43.89	61.65	70.47	44.26	44.93	44.81
P2 (psia)	166.50	166.79	166.47	166.31	167.10	167.15	168.16
Efficiency	0.307	0.333	0.310	0.225	0.225	0.279	0.281
S.D.	0.0101	0.019	0.01	0.0083	0.0077	0.0113	0.0125
S.D./AVE	0.0403	0.0577	0.0394	0.0385	0.0359	0.0425	0.0467
Thrust (lbf)	0.085	0.091	0.088	0.085	0.086	0.090	0.091
S.D.	0.0016	0.0022	0.0015	0.0015	0.0014	0.0016	0.0018
S.D./AVE	0.0184	0.0248	0.0168	0.0179	0.0164	0.0179	0.0203
W (lbm/min)	1.328	1.323	1.370	1.464	1.465	1.413	1.406
S.D.	0.0089	0.0112	0.0086	0.0073	0.0067	0.0086	0.0093
S.D./AVE	0.0067	0.0084	0.0063	0.005	0.0045	0.0061	0.0066
Uex,act (ft/sec)	124.18	132.27	124.28	112.49	112.69	123.13	124.75
Pth,HEM (psia)	87.35	90.30	88.24	89.82	90.14	89.28	90.35
Pe,HEM (psia)	9.75	10.10	10.04	9.82	10.14	10.08	10.15
HEM W (lbm/min)	0.677	0.690	0.684	0.683	0.687	0.685	0.688
HEM THRUST (lbf)	0.177	0.180	0.178	0.183	0.184	0.181	0.183
HEM Ue (ft/sec)	503.46	503.79	493.71	516.15	506.55	504.79	505.35
W/HEMW (Cd)	1.96	1.92	2.00	2.14	2.13	2.06	2.05
Pth,froz (psia)	65.55	67.10	65.64	68.42	68.74	67.68	68.15
FROZW	4.54	4.64	4.71	4.25	4.31	4.43	4.42
Cm	0.168	0.160	0.171	0.219	0.214	0.194	0.193

PROPERTY	RUN 36	RUN 37	RUN 38	RUN 39	RUN 40	RUN 41	RUN 42
Pcond (psia)	171.97	173.00	173.96	174.79	174.84	174.84	174.88
Pevap (psia)	55.02	55.04	55.07	55.00	55.03	55.03	55.00
Tsuperheat (F)	17.41	0.51	0.00	12.05	28.90	28.88	19.21
Tsubcool (F)	3.22	3.19	3.02	6.19	5.51	5.51	5.21
P in nozzle (psia)	123.95	124.68	125.40	121.20	121.94	121.94	121.82
Quality in nozzle	0.083	0.084	0.085	0.083	0.086	0.086	0.087
DP1 (psid)	0.831	0.833	0.824	0.701	0.669	0.669	0.657
DP2 (psid)	44.23	44.53	44.80	50.22	50.08	50.08	50.25
DP3 (psid)	11.49	11.56	11.61	10.50	10.06	10.06	9.99
T1 (F)	148.34	147.95	149.01	146.94	144.07	144.06	148.03
T2 (F)	114.92	115.42	116.01	113.42	114.37	114.37	114.69
T3 (F)	61.03	44.16	43.54	55.65	72.53	72.51	62.82
P2 (psia)	168.18	169.22	170.15	171.42	172.02	172.02	172.06
Efficiency	0.289	0.290	0.294	0.305	0.282	0.282	0.279
S.D.	0.011	0.0101	0.0106	0.0111	0.0294	0.0293	0.0417
S.D./AVE	0.0399	0.0366	0.038	0.0447	0.1047	0.1047	0.1499
Thrust (lbf)	0.095	0.096	0.097	0.088	0.084	0.084	0.083
S.D.	0.0017	0.0016	0.0015	0.0018	0.0044	0.0044	0.0062
S.D./AVE	0.0178	0.0168	0.0155	0.0203	0.0518	0.0518	0.0742
W (lbm/min)	1.437	1.446	1.440	1.337	1.313	1.313	1.293
S.D.	0.0058	0.012	0.0107	0.0104	0.0131	0.0131	0.0078
S.D./AVE	0.004	0.0083	0.0074	0.0078	0.01	0.01	0.006
Uex,act (ft/sec)	127.17	128.23	130.04	127.64	124.15	124.13	123.92
Pth,HEM (psia)	92.15	92.28	92.60	89.40	90.34	90.14	89.82
Pe,HEM (psia)	10.15	10.28	10.40	10.00	10.14	10.14	10.02
HEM W (lbm/min)	0.700	0.703	0.705	0.687	0.688	0.688	0.685
HEM THRUST (lbf)	0.186	0.186	0.187	0.181	0.182	0.182	0.182
HEM Ue (ft/sec)	508.27	507.85	507.67	505.33	504.78	504.77	506.16
W/HEMW (Cd)	2.05	2.06	2.04	1.95	1.91	1.91	1.89
Pth,froz (psia)	68.75	69.28	69.60	67.20	67.94	67.94	67.82
FROZW	4.65	4.63	4.61	4.55	4.45	4.45	4.40
Cm	0.187	0.189	0.188	0.168	0.166	0.166	0.164

PROPERTY	RUN 43	RUN 44	RUN 45	RUN 46	RUN 47	RUN 48	RUN 49
Pcond (psia)	174.91	174.91	174.96	175.00	175.04	175.93	176.97
Pevap (psia)	55.02	55.09	55.01	55.03	55.03	55.10	55.03
Tsuperheat (F)	31.50	0.21	19.36	0.23	11.77	1.08	0.60
Tsubcool (F)	6.29	3.02	5.24	1.49	2.23	3.12	3.42
P in nozzle (psia)	122.23	125.80	121.79	126.58	123.79	126.31	125.81
Quality in nozzle	0.082	0.086	0.087	0.093	0.094	0.087	0.088
DP1 (psid)	0.580	0.810	0.657	0.846	0.845	0.804	0.849
DP2 (psid)	49.67	45.34	50.30	45.50	47.61	45.84	47.27
DP3 (psid)	10.19	11.73	9.99	12.08	11.25	11.87	11.36
T1 (F)	149.45	149.72	148.05	148.93	151.13	150.59	147.04
T2 (F)	113.54	116.44	114.67	118.42	117.37	116.82	116.93
T3 (F)	75.12	43.90	62.97	43.87	55.40	44.78	44.23
P2 (psia)	171.90	171.09	172.09	172.08	171.40	172.15	173.09
Efficiency	0.313	0.301	0.281	0.239	0.226	0.303	0.268
S.D.	0.0265	0.0111	0.042	0.0333	0.0088	0.011	0.0106
S.D./AVE	0.0853	0.0386	0.1501	0.0333	0.041	0.0379	0.0413
Thrust (lbf)	0.082	0.098	0.083	0.091	0.087	0.099	0.096
S.D.	0.0033	0.0016	0.0062	0.0014	0.0016	0.0018	0.0017
S.D./AVE	0.0409	0.0166	0.0747	0.015	0.0182	0.0186	0.0177
W (lbm/min)	1.212	1.431	1.293	1.465	1.459	1.429	1.482
S.D.	0.0098	0.0106	0.0067	0.0059	0.0069	0.0142	0.0103
S.D./AVE	0.0081	0.0074	0.0052	0.004	0.0048	0.01	0.007
Uex,act (ft/sec)	129.92	132.23	124.15	120.43	115.05	133.50	125.56
Pth,HEM (psia)	90.63	92.60	90.39	92.78	90.99	92.91	93.21
Pe,HEM (psia)	10.03	10.40	9.99	10.18	9.99	10.51	10.41
HEM W (lbm/min)	0.695	0.705	0.685	0.700	0.685	0.707	0.703
HEM THRUST (lbf)	0.183	0.188	0.182	0.189	0.185	0.188	0.188
HEM Ue (ft/sec)	506.76	508.33	506.52	519.08	516.66	507.86	508.19
W/HEMW (Cd)	1.74	2.03	1.89	2.09	2.13	2.02	2.11
Pth,froz (psia)	67.83	70.00	67.99	70.98	69.59	70.31	70.21
FROZW	4.64	4.58	4.40	4.32	4.19	4.55	4.49
Cm	0.131	0.187	0.164	0.211	0.221	0.188	0.206

PROPERTY	RUN 50	RUN 51	RUN 52	RUN 53	RUN 54	RUN 55	RUN 56
Pcond (psia)	177.92	178.83	179.89	179.95	179.97	180.00	180.02
Pevap (psia)	55.05	55.05	55.29	55.05	55.02	55.95	55.03
Tsuperheat (F)	0.00	0.92	21.02	0.57	0.11	0.00	32.68
Tsubcool (F)	3.40	3.53	2.24	3.55	5.91	1.48	3.93
P in nozzle (psia)	126.35	126.87	127.05	127.55	126.44	128.84	126.25
Quality in nozzle	0.089	0.089	0.098	0.089	0.083	0.097	0.091
DP1 (psid)	0.830	0.810	0.817	0.794	0.652	0.844	0.785
DP2 (psid)	47.73	48.10	50.14	48.54	50.35	48.17	49.94
DP3 (psid)	11.47	11.55	11.23	11.65	11.00	12.06	11.08
T1 (F)	148.10	149.24	153.47	149.82	149.33	151.32	153.11
T2 (F)	117.40	117.66	119.94	118.14	116.09	120.62	117.81
T3 (F)	43.06	44.58	64.93	44.22	43.73	42.72	76.31
P2 (psia)	174.07	174.97	177.19	176.10	176.79	177.01	176.19
Efficiency	0.273	0.282	0.224	0.290	0.271	0.224	0.341
S.D.	0.0092	0.0111	0.0089	0.0112	0.0174	0.0082	0.0108
S.D./AVE	0.0352	0.0412	0.0416	0.0404	0.0512	0.0384	0.0419
Thrust (lbf)	0.097	0.098	0.089	0.099	0.095	0.091	0.094
S.D.	0.0015	0.0016	0.0017	0.0017	0.0022	0.0017	0.0017
S.D./AVE	0.0157	0.0107	0.0195	0.0167	0.0229	0.0181	0.0175
W (lbm/min)	1.469	1.453	1.455	1.443	1.308	1.484	1.427
S.D.	0.0076	0.0118	0.0076	0.0104	0.0146	0.0056	0.0096
S.D./AVE	0.0052	0.0081	0.0054	0.0082	0.0111	0.0038	0.0067
Uex,act (ft/sec)	127.46	129.96	118.17	132.81	140.84	118.42	127.38
Pth,HEM (psia)	92.95	93.27	92.85	93.55	93.24	94.04	92.65
Pe,HEM (psia)	10.35	10.47	10.25	10.55	10.44	10.44	10.25
HEM W (lbm/min)	0.704	0.706	0.695	0.709	0.712	0.704	0.701
HEM THRUST (lbf)	0.189	0.190	0.190	0.190	0.189	0.192	0.188
HEM Ue (ft/sec)	509.94	509.35	518.96	509.48	508.93	519.70	517.64
W/HEMW (Cd)	2.09	2.06	2.09	2.04	1.84	2.11	2.04
Pth,froz (psia)	70.55	70.67	71.65	71.15	70.04	72.44	70.65
FROZW	4.47	4.49	4.14	4.51	4.74	4.24	4.38
Cm	0.203	0.197	0.220	0.193	0.148	0.221	0.197

APPENDIX J
ERROR ANALYSIS COMPUTER PROGRAM

The program used for determination of the error for the thrust, mass flow rate, efficiency, and metastability parameter is located in this appendix.

```
C$NOEX
C$NOWA
C
C PROGRAM ERROR.FOR
C
C PROGRAM TO CALCULATE THE ERROR IN THE THRUST, MASS FLOW RATE, EFFICIENCY,
C AND METASTABILITY PARAMETER FROM THE APPROPRIATE SOURCES OF ERROR.
C
C VARIABLE DECLARATION
      DOUBLE PRECISION ATH,P1,P3,DP1,DP2,T1,T2,P2,THR
      REAL THRPOS,THRNEG,P2POS,P2NEG,T2POS,T2NEG,DP2POS
      REAL DP2NEG,PINNPOS,PINNNEG,HPOS,HNEG,T2APOS,T2ANEG,XPOS,XNEG
      REAL SPOS,SNEG,P1POS,P1NEG,T1POS,T1NEG,DP1POS,DP1NEG
      REAL P3POS,P3NEG,DENPOS,DENNEG,MUPOS,MUNEG,WINI,WPOS,W,WNEG
      REAL TEPOS,TENEG,HEPOS,HENEG,EFFPOS,EFFNEG,TIN,XINMN,HINMN,STH
      REAL MDOTL,PTH,TTH,HTH,XTHR,VTH,UTH,MDOT,HEMWPOS,HEMWNEG
      REAL FROZWPOS,FROZWNEG,P1R,CMPOS,CMNEG
      INTEGER L
      CHARACTER*4 REF
C
      REF='RR12'
      ATH=7.068583471D-6
C
C CALL TO REFRIGERANT SUBROUTINES
      CALL RINIT(REF,IERR)
C
C OPEN FILE STATEMENTS FOR INPUT AND OUTPUT USING EXTERNAL FILES
      OPEN(UNIT=2,FILE='OUTPUT.PRN')
      OPEN(UNIT=3,FILE='OUTPUT2.PRN')
      OPEN(UNIT=11,FILE='THRW.PRN')
      OPEN(UNIT=12,FILE='EFF.PRN')
      OPEN(UNIT=13,FILE='HEMFROZ.PRN')
C
15    FORMAT(4F12.6)
20    FORMAT(5F12.6)
C
      LOOP
C
C INPUT STATEMENT
      READ(UNIT=2,END=25,FMT=15) P1,P3,DP1,DP2
25    READ(UNIT=3,END=100,FMT=15) T1,T2,P2,THR
```

```
C
C THRUST ERROR:*************************************************************************
C
      THRPOS=THR+0.003046D0
      THRNEG=THR-0.003046D0
C
C END OF THRUST ERROR*******************************************************************
C
C MASS FLOW RATE ERROR:
C
C INSTRUMENTATION WITH THEIR APPROPRIATE ERROR
C SYMBOLS ARE THE SAME AS USED THROUGHOUT THIS PAPER
C NEG: MEASUREMENT MINUS ERROR,
C POS: MEASUREMENT PLUS ERROR.
      P2POS=P2+0.01668D0
      P2NEG=P2-0.01668D0
      T2POS=T2+459.67D0+1.8D0+0.09D0
      T2NEG=T2+459.67D0-1.8D0-0.09D0
      DP2POS=DP2+0.00053D0
      DP2NEG=DP2-0.00053D0
      PINNPOS=P2POS-DP2NEG
      PINNNEG=P2NEG-DP2POS
      HPOS=HLOFPT(REF,P2POS,T2POS)
      HNEG=HLOFPT(REF,P2NEG,T2NEG)
      T2APOS=T2OFP(REF,PINNPOS)
      T2ANEG=T2OFP(REF,PINNNEG)
      P1POS=P1+0.006314D0
      P1NEG=P1-0.006314D0
      T1POS=T1+459.67D0+1.8D0+0.09D0
      T1NEG=T1+459.67D0-1.8D0-0.09D0
      DP1POS=DP1+0.001198D0
      DP1NEG=DP1-0.001198D0
      P3POS=P3+0.020517D0+1.66D0
      P3NEG=P3-0.020517D0+1.66D0
C
C SUBROUTINE CALL FOR MASS FLOW RATE PARAMETER; DENSITY
      DENPOS=1/(VSOFPT(REF,P1POS,T1NEG))
      DENNEG=1/(VSOFPT(REF,P1NEG,T1POS))
C
C ITERATION ROUTINE FOR MASS FLOW RATE**************************************
C THIS STATEMENT BLOCK WAS LIFTED UNCHANGED FROM THE DATA
C ACQUISITION PROGRAM
C
      WINI=1.0D0
      DO 63 L=1,50
       DUMPOS=(5.16553D-7*T1POS-3.61185D-5)**0.41D0
       WPOS=0.7966604D0*SQRT(DP1POS*DENPOS)
       WPOS=WPOS+0.1677255D0*SQRT(DP1POS*DENPOS/WINI)*MUNEG
      IF (ABS(WINI-WPOS) .LT. 1.0D-6) THEN
       GOTO 65
      ENDIF
       WINI=WPOS
63    CONTINUE
65    CONTINUE
C ADDITION OF 3/4% ERROR IN FLOW METER
      WPOS=WPOS+0.0075D0*WPOS
```

```
      WINI=1.0D0
       DUMNEG=(5.16553D-7*T1NEG-3.61185D-5)**0.41D0
       WNEG=0.7966604D0*SQRT(DP1NEG*DENNEG)
       WNEG=WNEG+0.1677255D0*SQRT(DP1NEG*DENNEG/WINI)*MUPOS
      IF (ABS(WINI-WNEG) .LT. 1.0D-6) THEN
       GOTO 69
      ENDIF
       WINI=WNEG
67    CONTINUE
69    CONTINUE
C SUBTRACTION OF 3/4% ERROR IN FLOW METER
      WNEG=WNEG-0.0075D0*WNEG
C
C END OF MASS FLOW ERROR*************************************************************
C
C EFFICIENCY ERROR:******************************************************************
C
C ISENTROPIC ENTHALPY LEAVING NOZZLE
      SPOS=S2OFTH(REF,T2ANEG,HNEG)
      SNEG=S2OFTH(REF,T2APOS,HPOS)
      TEPOS=T2OFP(REF,P3POS)
      TENEG=T2OFP(REF,P3NEG)
      HEPOS=H2OFTS(REF,TEPOS,SPOS)
      HENEG=H2OFTS(REF,TENEG,SNEG)
C NOZZLE EFFICIENCY (END CONSTANT FOR UNITS)
     EFFPOS=(THRPOS**2)/2/(WNEG**2)/(HNEG-HEPOS)*148.82628D0
     EFFNEG=(THRNEG**2)/2/(WPOS**2)/(HPOS-HENEG)*148.82628D0
C
CEND OF EFFICIENCY ERROR*************************************************************
C
C METASTABILITY PARAMETER ERROR:*****************************************************
C
C THIS PART OF THE PROGRAM CALCULATES THE MAXIMUM AND MINIMUM
C HOMOGENEOUS, EQUILIBRIUM MASS FLOW RATE (ISENTROPIC CASE)
C
C ASSIGNMENT OF VARIABLES TO YIELD THE MAXIMUM FLOW RATE VALUE
C ALL OF THESE CAN BE OBTAINED FROM THE NOZZLE INLET PRESSURE AND QUALITY
      TIN=T2ANEG
      XNEG=XTH(REF,T2ANEG,HNEG)
      XINMN=XNEG
      HINMN=HFOFT(REF,TIN)+XINMN*HFGOFT(REF,TIN)
      STH=S2OFTH(REF,TIN,HINMN)
C
      MDOTL=0.0E0
      PTH=PINNNEG-1.0E0
C
C ITERATION FOR CHOKING MASS FLOW RATE
      LOOP
C
C TEMPERATURE, ENTHALPY, QUALITY, AND SPECIFIC VOLUME
C AT THE GUESSED PRESSURE
      TTH=T2OFP(REF,PTH)
      HTH=H2OFTS(REF,TTH,STH)
      XTHR=XTH(REF,TTH,HTH)
      VTH=VFOFT(REF,TTH)+XTHR*VFGOFT(REF,TTH)
C VELOCITY AT GUESSED PRESSURE
```

```
      UTH=SQRT(2*(HINMN-HTH)*25033.69673D0)
C MASS FLOW RATE USING ABOVE PARAMETERS
      MDOT=ATH*UTH/VTH*60
C THROAT PRESSURE ITERATION
      PTH=PTH-0.1E0
C
C EXIT QUALIFICATION
      IF (MDOT .LT. MDOTL) THEN
      HEMWPOS=MDOTL
      GOTO 160
      ENDIF
C
      MDOTL=MDOT
      ENDLOOP
C
160   CONTINUE
C
C ASSIGNMENT OF VARIABLES TO YIELD THE MINIMUM FLOW RATE VALUE
C ALL OF THESE CAN BE OBTAINED FROM THE NOZZLE INLET PRESSURE AND QUALITY
      TIN=T2APOS
      XPOS=XTH(REF,T2APOS,HPOS)
      XINMN=XPOS
      HINMN=HFOFT(REF,TIN)+XINMN*HFGOFT(REF,TIN)
      STH=S2OFTH(REF,TIN,HINMN)
C
      MDOTL=0.0E0
      PTH=PINNPOS-1.0E0
C
C ITERATION FOR CHOKING MASS FLOW RATE
      LOOP
C TEMPERATURE, ENTHALPY, QUALITY, AND SPECIFIC VOLUME
C AT THE GUESSED PRESSURE
      TTH=T2OFP(REF,PTH)
      HTH=H2OFTS(REF,TTH,STH)
      XTHR=XTH(REF,TTH,HTH)
      VTH=VFOFT(REF,TTH)+XTHR*VFGOFT(REF,TTH)
C VELOCITY AT GUESSED PRESSURE
      UTH=SQRT(2*(HINMN-HTH)*25033.69673D0)
C MASS FLOW RATE USING ABOVE PARAMETERS
      MDOT=ATH*UTH/VTH*60
C THROAT PRESSURE ITERATION
      PTH=PTH-0.1E0
C
C EXIT QUALIFICATION
      IF (MDOT .LT. MDOTL) THEN
      HEMWNEG=MDOTL
      GOTO 170
      ENDIF
C
      MDOTL=MDOT
      ENDLOOP
C
170   CONTINUE
C
C THIS PART OF THE PROGRAM CALCULATES THE MINIMUM AND MAXIMUM
C FROZEN MASS FLOW RATE (CONSTANT QUALITY CASE)
```

```
C
C ASSIGNMENT OF VARIABLES TO YIELD THE MAXIMUM FLOW RATE VALUE
C ALL OF THESE CAN BE OBTAINED FROM THE NOZZLE INLET PRESSURE AND QUALITY
      TIN=T2ANEG
      XINMN=XNEG
      HINMN=HFOFT(REF,TIN)+XINMN*HFGOFT(REF,TIN)
C
      MDOTL=0.0E0
      PTH=PINNNEG-1.0E0
C
C ITERATION FOR CHOKING MASS FLOW RATE
      LOOP
C
C TEMPERATURE, QUALITY, ENTROPY, ENTHALPY, AND SPECIFIC VOLUME
C AT THE GUESSED PRESSURE
      TTH=T2OFP(REF,PTH)
      XTHR=XINMN
      STH=SFOFT(REF,TTH)+XTHR*SFGOFT(REF,TTH)
      HTH=H2OFTS(REF,TTH,STH)
      VTH=VFOFT(REF,TTH)+XTHR*VFGOFT(REF,TTH)
C VELOCITY AT GUESSED PRESSURE
      UTH=SQRT(2*(HINMN-HTH)*25033.69673D0)
C MASS FLOW RATE USING ABOVE PARAMETERS
      FROZW=ATH*UTH/VTH*60
C
C THROAT PRESSURE ITERATION
      PTH=PTH-0.1E0
C
C EXIT QUALIFICATION
      IF (FROZW .LT. MDOTL) THEN
      FROZWPOS=MDOTL
      GOTO 200
      ENDIF
C
      MDOTL=FROZW
      ENDLOOP
C
200   CONTINUE
C
C ASSIGNMENT OF VARIABLES TO YIELD THE MINIMUM FLOW RATE VALUE
C ALL OF THESE CAN BE OBTAINED FROM THE NOZZLE INLET PRESSURE AND QUALITY
C
      TIN=T2APOS
      XINMN=XPOS
      HINMN=HFOFT(REF,TIN)+XINMN*HFGOFT(REF,TIN)
C
      MDOTL=0.0E0
      PTH=PINNPOS-1.0E0
C
C ITERATION FOR CRITICAL MASS FLOW RATE
      LOOP
C
C TEMPERATURE, QUALITY, ENTROPY, ENTHALPY, AND SPECIFIC VOLUME
C AT THE GUESSED PRESSURE
      TTH=T2OFP(REF,PTH)
      XTHR=XINMN
```

```
      STH=SFOFT(REF,TTH)+XTHR*SFGOFT(REF,TTH)
      HTH=H2OFTS(REF,TTH,STH)
      VTH=VFOFT(REF,TTH)+XTHR*VFGOFT(REF,TTH)
C
C VELOCITY AT GUESSED PRESSURE
      UTH=SQRT(2*(HINMN-HTH)*25033.69673D0)
C MASS FLOW RATE USING ABOVE PARAMETERS
      FROZW=ATH*UTH/VTH*60
C
C THROAT PRESSURE ITERATION
      PTH=PTH-0.1E0
C
C EXIT QUALIFICATION
      IF (FROZW .LT. MDOTL) THEN
      FROZWNEG=MDOTL
      GOTO 210
      ENDIF
C
      MDOTL=FROZW
      ENDLOOP
C
210   CONTINUE
C
C METASTABILITY PARAMETER CALCULATION
      CMPOS=(WPOS-HEMWNEG)/(FROZWNEG-HEMWNEG)
      CMNEG=(WNEG-HEMWPOS)/(FROZWPOS-HEMWPOS)
C
      P1R=P1
C WRITE STATEMENTS FOR OUTPUT AND DATA STORAGE
C
      WRITE(*,20) P1R,THRPOS,THRNEG,WPOS,WNEG
      WRITE(*,*) P1R,EFFPOS,EFFNEG
      WRITE(*,*) P1R,CMPOS,CMNEG
      WRITE(*,*) ' '
C
      WRITE(11,20) P1R,THRPOS,THRNEG,WPOS,WNEG
      WRITE(12,*) P1R,EFFPOS,EFFNEG
      WRITE(13,*) P1R,CMPOS,CMNEG
C
      ENDLOOP
C
100   CONTINUE
C
C CLOSE FILE STATEMENTS
      CLOSE(UNIT=2)
      CLOSE(UNIT=3)
      CLOSE(UNIT=10)
      CLOSE(UNIT=11)
      CLOSE(UNIT=12)
      CLOSE(UNIT=13)
      CLOSE(UNIT=14)
C
      END
```

APPENDIX K
ERROR RAW DATA

The results of the program listed in Appendix K are given here. Raw error for the following four measurements is presented below:

1. thrust,
2. mass flow rate,
3. nozzle efficiency, and
4. the metastability parameter.

Also given with the error is the average percent error, the standard deviation, and the standard deviation ratio.

K.1 Thrust Raw Error Data

The thrust data is contained in one section since the error was equal in the high the low calculations, therefore the error was the same for both.

RUN	Low Thrust	Thrust (lbf)	High Thrust	Error	Error %	Error %,ave
1	0.0853	0.0822	0.0792	0.00305	0.0371	0.0351
2	0.0800	0.0770	0.0739	0.00305	0.0396	
3	0.0828	0.0798	0.0767	0.00305	0.0382	Std. Dev.
4	0.0820	0.0790	0.0759	0.00305	0.0386	0.0024
5	0.0861	0.0831	0.0800	0.00305	0.0367	
6	0.0817	0.0787	0.0756	0.00305	0.0387	Std. Dev. ratio
7	0.0834	0.0804	0.0773	0.00305	0.0379	0.0674
8	0.0829	0.0798	0.0768	0.00305	0.0382	
9	0.0821	0.0790	0.0760	0.00305	0.0385	
10	0.0855	0.0825	0.0794	0.00305	0.0369	
11	0.0844	0.0814	0.0783	0.00305	0.0374	
12	0.0825	0.0794	0.0764	0.00305	0.0384	
13	0.0903	0.0872	0.0842	0.00305	0.0349	
14	0.0901	0.0871	0.0840	0.00305	0.0350	
15	0.0933	0.0903	0.0872	0.00305	0.0337	
16	0.0885	0.0854	0.0824	0.00305	0.0357	
17	0.0917	0.0887	0.0856	0.00305	0.0344	
18	0.0972	0.0942	0.0911	0.00305	0.0323	
19	0.1000	0.0970	0.0939	0.00305	0.0314	
20	0.1023	0.0993	0.0962	0.00305	0.0307	
21	0.1009	0.0978	0.0948	0.00305	0.0311	
22	0.0932	0.0901	0.0871	0.00305	0.0338	

23	0.0909	0.0879	0.0848	0.00305	0.0347
24	0.0932	0.0902	0.0872	0.00305	0.0338
25	0.0861	0.0830	0.0800	0.00305	0.0367
26	0.0909	0.0879	0.0848	0.00305	0.0347
27	0.0921	0.0891	0.0860	0.00305	0.0342
28	0.0846	0.0816	0.0785	0.00305	0.0373
29	0.0900	0.0870	0.0839	0.00305	0.0350
30	0.0859	0.0829	0.0798	0.00305	0.0367
31	0.0941	0.0910	0.0880	0.00305	0.0335
32	0.0944	0.0914	0.0883	0.00305	0.0333
33	0.0886	0.0855	0.0825	0.00305	0.0356
34	0.0887	0.0856	0.0826	0.00305	0.0356
35	0.0939	0.0909	0.0879	0.00305	0.0335
36	0.0978	0.0947	0.0917	0.00305	0.0322
37	0.0991	0.0960	0.0930	0.00305	0.0317
38	0.1001	0.0970	0.0940	0.00305	0.0314
39	0.1011	0.0980	0.0950	0.00305	0.0311
40	0.0985	0.0954	0.0924	0.00305	0.0319
41	0.0860	0.0830	0.0799	0.00305	0.0367
42	0.0862	0.0832	0.0801	0.00305	0.0366
43	0.0875	0.0844	0.0814	0.00305	0.0361
44	0.0875	0.0844	0.0814	0.00305	0.0361
45	0.0937	0.0906	0.0876	0.00305	0.0336
46	0.0898	0.0867	0.0837	0.00305	0.0351
47	0.0915	0.0884	0.0854	0.00305	0.0345
48	0.1019	0.0988	0.0958	0.00305	0.0308
49	0.0852	0.0822	0.0791	0.00305	0.0371
50	0.0831	0.0800	0.0770	0.00305	0.0381
51	0.0912	0.0882	0.0851	0.00305	0.0345
52	0.0995	0.0964	0.0934	0.00305	0.0316
53	0.0874	0.0843	0.0813	0.00305	0.0361
54	0.0884	0.0853	0.0823	0.00305	0.0357
55	0.0838	0.0807	0.0777	0.00305	0.0377
56	0.0900	0.0870	0.0839	0.00305	0.0350

K.2 Raw Data for Mass Flow Rate Error

The data for mass flow rate is divided into two sections; a high error analysis, and a low error analysis. Each section contains both the high and low error calculation for the mass flow rate, but each contains the analysis for the respective data.

K.2.1 High Mass Flow Rate Error Analysis

RUN	High $\dot{m}$	$\dot{m}$ (lbm/min)	Low $\dot{m}$	High error	High error %	High error %,ave
1	1.423	1.407	1.392	0.01548	0.01100	0.0113
2	1.397	1.382	1.367	0.01524	0.01103	
3	1.424	1.408	1.393	0.01560	0.01108	High Std. Dev.
4	1.415	1.399	1.384	0.01535	0.01097	0.0003
5	1.412	1.396	1.381	0.01555	0.01114	
6	1.378	1.363	1.348	0.01518	0.01114	High Std. Dev. ratio
7	1.392	1.377	1.362	0.01527	0.01109	0.0280
8	1.384	1.369	1.354	0.01515	0.01107	
9	1.378	1.363	1.348	0.01510	0.01108	
10	1.381	1.365	1.350	0.01545	0.01132	
11	1.368	1.353	1.338	0.01515	0.01120	
12	1.309	1.294	1.280	0.01512	0.01169	
13	1.377	1.362	1.347	0.01551	0.01139	
14	1.319	1.304	1.290	0.01479	0.01133	
15	1.341	1.326	1.312	0.01504	0.01134	
16	1.343	1.328	1.313	0.01509	0.01136	
17	1.368	1.353	1.338	0.01496	0.01106	
18	1.443	1.427	1.411	0.01618	0.01134	
19	1.485	1.469	1.452	0.01668	0.01136	
20	1.459	1.443	1.427	0.01645	0.01140	
21	1.469	1.453	1.436	0.01654	0.01139	
22	1.428	1.413	1.397	0.01592	0.01127	
23	1.444	1.427	1.412	0.01689	0.01183	
24	1.441	1.425	1.409	0.01630	0.01144	
25	1.376	1.361	1.346	0.01552	0.01141	
26	1.388	1.372	1.356	0.01565	0.01141	
27	1.471	1.455	1.438	0.01642	0.01129	
28	1.226	1.212	1.198	0.01409	0.01162	
29	1.475	1.459	1.443	0.01639	0.01123	
30	1.497	1.481	1.465	0.01641	0.01108	
31	1.500	1.484	1.467	0.01676	0.01129	
32	1.481	1.465	1.448	0.01651	0.01127	
33	1.481	1.465	1.449	0.01638	0.01118	
34	1.415	1.399	1.383	0.01588	0.01135	
35	1.425	1.406	1.393	0.01859	0.01322	
36	1.454	1.437	1.421	0.01614	0.01123	
37	1.462	1.446	1.430	0.01623	0.01123	

38	1.457	1.440	1.424	0.01629	0.01131
39	1.447	1.431	1.415	0.01615	0.01129
40	1.323	1.308	1.293	0.01523	0.01165
41	1.308	1.293	1.278	0.01488	0.01151
42	1.308	1.293	1.279	0.01488	0.01150
43	1.328	1.313	1.298	0.01527	0.01164
44	1.328	1.313	1.298	0.01528	0.01164
45	1.338	1.323	1.308	0.01518	0.01148
46	1.407	1.392	1.376	0.01566	0.01125
47	1.352	1.337	1.322	0.01537	0.01150
48	1.445	1.429	1.413	0.01616	0.01131
49	1.509	1.492	1.476	0.01650	0.01106
50	1.497	1.480	1.464	0.01623	0.01096
51	1.385	1.370	1.354	0.01558	0.01138
52	1.499	1.482	1.465	0.01684	0.01136
53	1.504	1.487	1.471	0.01656	0.01114
54	1.480	1.464	1.448	0.01647	0.01125
55	1.363	1.348	1.333	0.01507	0.01118
56	1.397	1.382	1.366	0.01573	0.01138

K.2.2 Low Mass Flow Rate Error Analysis

RUN	High $\dot{m}$	$\dot{m}$ (lbm/min)	Low $\dot{m}$	Low error	Low error %	Low error %,ave
1	1.423	1.407	1.392	-0.01532	-0.01089	-0.0111
2	1.397	1.382	1.367	-0.01508	-0.01091	
3	1.424	1.408	1.393	-0.01543	-0.01096	Low Std. Dev.
4	1.415	1.399	1.384	-0.01520	-0.01086	0.0003
5	1.412	1.396	1.381	-0.01538	-0.01102	
6	1.378	1.363	1.348	-0.01501	-0.01102	Low Std. Dev. ratio
7	1.392	1.377	1.362	-0.01510	-0.01096	-0.0257
8	1.384	1.369	1.354	-0.01514	-0.01106	
9	1.378	1.363	1.348	-0.01493	-0.01095	
10	1.381	1.365	1.350	-0.01523	-0.01115	
11	1.368	1.353	1.338	-0.01498	-0.01107	
12	1.309	1.294	1.280	-0.01413	-0.01092	
13	1.377	1.362	1.347	-0.01524	-0.01119	
14	1.319	1.304	1.290	-0.01455	-0.01115	
15	1.341	1.326	1.312	-0.01480	-0.01116	
16	1.343	1.328	1.313	-0.01486	-0.01119	
17	1.368	1.353	1.338	-0.01523	-0.01125	
18	1.443	1.427	1.411	-0.01592	-0.01116	
19	1.485	1.469	1.452	-0.01646	-0.01121	
20	1.459	1.443	1.427	-0.01618	-0.01121	
21	1.469	1.453	1.436	-0.01626	-0.01119	
22	1.428	1.413	1.397	-0.01577	-0.01117	
23	1.444	1.427	1.412	-0.01527	-0.01070	
24	1.441	1.425	1.409	-0.01578	-0.01108	
25	1.376	1.361	1.346	-0.01529	-0.01123	
26	1.388	1.372	1.356	-0.01542	-0.01124	

27	1.471	1.455	1.438	-0.01619	-0.01113
28	1.226	1.212	1.198	-0.01383	-0.01141
29	1.475	1.459	1.443	-0.01619	-0.01109
30	1.497	1.481	1.465	-0.01624	-0.01097
31	1.500	1.484	1.467	-0.01657	-0.01117
32	1.481	1.465	1.448	-0.01632	-0.01114
33	1.481	1.465	1.449	-0.01619	-0.01105
34	1.415	1.399	1.383	-0.01567	-0.01120
35	1.425	1.406	1.393	-0.01304	-0.00927
36	1.454	1.437	1.421	-0.01602	-0.01114
37	1.462	1.446	1.430	-0.01617	-0.01119
38	1.457	1.440	1.424	-0.01599	-0.01110
39	1.447	1.431	1.415	-0.01596	-0.01115
40	1.323	1.308	1.293	-0.01481	-0.01132
41	1.308	1.293	1.278	-0.01466	-0.01134
42	1.308	1.293	1.279	-0.01468	-0.01135
43	1.328	1.313	1.298	-0.01490	-0.01135
44	1.328	1.313	1.298	-0.01490	-0.01135
45	1.338	1.323	1.308	-0.01491	-0.01127
46	1.407	1.392	1.376	-0.01544	-0.01110
47	1.352	1.337	1.322	-0.01508	-0.01128
48	1.445	1.429	1.413	-0.01591	-0.01113
49	1.509	1.492	1.476	-0.01632	-0.01094
50	1.497	1.480	1.464	-0.01606	-0.01085
51	1.385	1.370	1.354	-0.01534	-0.01120
52	1.499	1.482	1.465	-0.01658	-0.01119
53	1.504	1.487	1.471	-0.01635	-0.01099
54	1.480	1.464	1.448	-0.01596	-0.01090
55	1.363	1.348	1.333	-0.01490	-0.01105
56	1.397	1.382	1.366	-0.01550	-0.01122

K.3 Raw Data for Efficiency Error

The data for efficiency is divided into two sections; a high error analysis, and a low error analysis. Each section contains both the high and low error calculation for the efficiency, but each contains the analysis for the respective data.

K.3.1 High Efficiency Error Analysis

RUN	High Efficiency	Efficiency	Low Efficiency	High error	High error %	High error %,ave
1	0.329	0.284	0.246	0.04419	0.15537	0.1404
2	0.335	0.290	0.251	0.04442	0.15299	
3	0.350	0.305	0.265	0.04549	0.14932	High Std. Dev.
4	0.336	0.292	0.253	0.04444	0.15221	0.0073
5	0.341	0.297	0.257	0.04484	0.15123	
6	0.339	0.294	0.255	0.04489	0.15266	High Std. Dev. ratio
7	0.329	0.286	0.248	0.04321	0.15115	0.0521
8	0.342	0.298	0.259	0.04373	0.14680	
9	0.336	0.293	0.254	0.04388	0.14996	
10	0.339	0.295	0.257	0.04368	0.14789	
11	0.343	0.299	0.260	0.04390	0.14702	
12	0.332	0.289	0.251	0.04281	0.14826	
13	0.348	0.305	0.266	0.04337	0.14216	
14	0.347	0.302	0.262	0.04502	0.14903	
15	0.380	0.333	0.292	0.04740	0.14232	
16	0.395	0.347	0.304	0.04834	0.13951	
17	0.361	0.316	0.278	0.04465	0.14117	
18	0.349	0.305	0.268	0.04335	0.14190	
19	0.353	0.310	0.271	0.04374	0.14127	
20	0.351	0.307	0.269	0.04397	0.14320	
21	0.379	0.333	0.293	0.04563	0.13705	
22	0.347	0.305	0.268	0.04220	0.13838	
23	0.322	0.282	0.247	0.03989	0.14147	
24	0.322	0.282	0.247	0.03990	0.14142	
25	0.320	0.281	0.245	0.03994	0.14238	
26	0.319	0.279	0.244	0.03979	0.14251	
27	0.306	0.271	0.241	0.03573	0.13201	
28	0.386	0.341	0.299	0.04471	0.13095	
29	0.327	0.290	0.257	0.03701	0.12747	
30	0.318	0.282	0.249	0.03625	0.12865	
31	0.309	0.273	0.242	0.03535	0.12941	
32	0.303	0.268	0.237	0.03488	0.13007	
33	0.343	0.303	0.269	0.03936	0.12981	
34	0.340	0.301	0.266	0.03894	0.12938	
35	0.332	0.294	0.260	0.03843	0.13075	
36	0.328	0.290	0.256	0.03849	0.13281	
37	0.328	0.289	0.255	0.03832	0.13242	

38	0.318	0.281	0.247	0.03674	0.13069
39	0.317	0.279	0.245	0.03791	0.13599
40	0.316	0.278	0.245	0.03791	0.13620
41	0.305	0.268	0.235	0.03688	0.13753
42	0.335	0.294	0.258	0.04080	0.13892
43	0.323	0.283	0.248	0.03955	0.13976
44	0.312	0.273	0.239	0.03861	0.14122
45	0.316	0.276	0.241	0.04008	0.14525
46	0.256	0.223	0.195	0.03255	0.14578
47	0.256	0.224	0.196	0.03168	0.14122
48	0.256	0.225	0.197	0.03117	0.13882
49	0.271	0.239	0.211	0.03172	0.13278
50	0.254	0.224	0.198	0.02970	0.13231
51	0.250	0.219	0.192	0.03121	0.14244
52	0.257	0.225	0.198	0.03126	0.13870
53	0.257	0.226	0.199	0.03089	0.13668
54	0.254	0.224	0.198	0.03004	0.13385
55	0.247	0.216	0.188	0.03179	0.14749
56	0.359	0.313	0.273	0.04546	0.14506

K.3.2 Low Efficiency Error Analysis

RUN	High Efficiency	Efficiency	Low Efficiency	Low Error	Low error %	Low error %,ave
1	0.329	0.284	0.246	-0.03859	-0.13567	-0.1240
2	0.335	0.290	0.251	-0.03884	-0.13377	
3	0.350	0.305	0.265	-0.03985	-0.13081	Low Std. Dev.
4	0.336	0.292	0.253	-0.03888	-0.13318	0.0061
5	0.341	0.297	0.257	-0.03922	-0.13227	
6	0.339	0.294	0.255	-0.03929	-0.13362	Low Std. Dev. ratio
7	0.329	0.286	0.248	-0.03789	-0.13253	-0.0490
8	0.342	0.298	0.259	-0.03842	-0.12898	
9	0.336	0.293	0.254	-0.03848	-0.13152	
10	0.339	0.295	0.257	-0.03840	-0.13000	
11	0.343	0.299	0.260	-0.03853	-0.12902	
12	0.332	0.289	0.251	-0.03789	-0.13122	
13	0.348	0.305	0.266	-0.03858	-0.12647	
14	0.347	0.302	0.262	-0.04019	-0.13304	
15	0.380	0.333	0.292	-0.04154	-0.12473	
16	0.395	0.347	0.304	-0.04240	-0.12236	
17	0.361	0.316	0.278	-0.03865	-0.12220	
18	0.349	0.305	0.268	-0.03799	-0.12436	
19	0.353	0.310	0.271	-0.03832	-0.12378	
20	0.351	0.307	0.269	-0.03852	-0.12544	
21	0.379	0.333	0.293	-0.04043	-0.12144	
22	0.347	0.305	0.268	-0.03739	-0.12261	
23	0.322	0.282	0.247	-0.03536	-0.12539	
24	0.322	0.282	0.247	-0.03538	-0.12541	
25	0.320	0.281	0.245	-0.03533	-0.12594	
26	0.319	0.279	0.244	-0.03521	-0.12611	

27	0.306	0.271	0.241	-0.02934	-0.10838
28	0.386	0.341	0.299	-0.04236	-0.12405
29	0.327	0.290	0.257	-0.03305	-0.11383
30	0.318	0.282	0.249	-0.03235	-0.11481
31	0.309	0.273	0.242	-0.03151	-0.11534
32	0.303	0.268	0.237	-0.03106	-0.11583
33	0.343	0.303	0.269	-0.03438	-0.11339
34	0.340	0.301	0.266	-0.03456	-0.11483
35	0.332	0.294	0.260	-0.03387	-0.11525
36	0.328	0.290	0.256	-0.03341	-0.11529
37	0.328	0.289	0.255	-0.03402	-0.11755
38	0.318	0.281	0.247	-0.03465	-0.12325
39	0.317	0.279	0.245	-0.03363	-0.12063
40	0.316	0.278	0.245	-0.03364	-0.12087
41	0.305	0.268	0.235	-0.03312	-0.12354
42	0.335	0.294	0.258	-0.03613	-0.12302
43	0.323	0.283	0.248	-0.03500	-0.12369
44	0.312	0.273	0.239	-0.03417	-0.12497
45	0.316	0.276	0.241	-0.03508	-0.12714
46	0.256	0.223	0.195	-0.02846	-0.12745
47	0.256	0.224	0.196	-0.02803	-0.12496
48	0.256	0.225	0.197	-0.02765	-0.12313
49	0.271	0.239	0.211	-0.02824	-0.11822
50	0.254	0.224	0.198	-0.02646	-0.11788
51	0.250	0.219	0.192	-0.02759	-0.12591
52	0.257	0.225	0.198	-0.02780	-0.12334
53	0.257	0.226	0.199	-0.02744	-0.12142
54	0.254	0.224	0.198	-0.02673	-0.11910
55	0.247	0.216	0.188	-0.02779	-0.12895
56	0.359	0.313	0.273	-0.04018	-0.12821

K.4 Raw Data for Metastability Parameter Error

The data for metastability parameter is divided into two sections; a high error analysis, and a low error analysis. Each section contains both the high and low error calculation for the metastability parameter, but each contains the analysis for the respective data.

K.4.1 High Metastability Parameter Error Analysis

RUN	Cm+	Cm	Cm-	High error	High error %	High % error,ave
1	0.190	0.166	0.143	0.02426	0.14620	0.1348
2	0.192	0.166	0.144	0.02546	0.15322	
3	0.191	0.168	0.144	0.02332	0.13902	High Std. Dev.
4	0.196	0.171	0.148	0.02531	0.14800	0.0076
5	0.190	0.166	0.144	0.02383	0.14337	
6	0.187	0.163	0.141	0.02385	0.14627	High Std. Dev. ratio
7	0.191	0.168	0.145	0.02265	0.13471	0.0565
8	0.201	0.177	0.153	0.02379	0.13418	
9	0.193	0.169	0.147	0.02400	0.14176	
10	0.190	0.166	0.145	0.02342	0.14067	
11	0.199	0.176	0.152	0.02347	0.13351	
12	0.189	0.166	0.144	0.02303	0.13845	
13	0.196	0.171	0.149	0.02503	0.14649	
14	0.178	0.155	0.135	0.02258	0.14559	
15	0.172	0.150	0.130	0.02199	0.14669	
16	0.180	0.157	0.137	0.02274	0.14440	
17	0.192	0.168	0.146	0.02381	0.14197	
18	0.195	0.171	0.149	0.02346	0.13709	
19	0.194	0.171	0.148	0.02315	0.13578	
20	0.191	0.168	0.146	0.02263	0.13449	
21	0.182	0.160	0.139	0.02168	0.13554	
22	0.192	0.168	0.148	0.02370	0.14107	
23	0.188	0.166	0.145	0.02206	0.13268	
24	0.188	0.166	0.145	0.02210	0.13290	
25	0.187	0.164	0.144	0.02292	0.13988	
26	0.187	0.164	0.144	0.02299	0.14046	
27	0.169	0.148	0.129	0.02107	0.14234	
28	0.222	0.197	0.174	0.02500	0.12679	
29	0.219	0.193	0.171	0.02599	0.13456	
30	0.223	0.197	0.174	0.02507	0.12696	
31	0.229	0.203	0.179	0.02563	0.12625	
32	0.232	0.206	0.181	0.02633	0.12807	
33	0.211	0.188	0.164	0.02307	0.12298	
34	0.212	0.187	0.164	0.02465	0.13165	
35	0.213	0.188	0.165	0.02488	0.13211	
36	0.214	0.189	0.166	0.02471	0.13069	
37	0.212	0.187	0.164	0.02560	0.13719	

38	0.219	0.193	0.171	0.02625	0.13625
39	0.221	0.194	0.172	0.02634	0.13556
40	0.224	0.199	0.174	0.02504	0.12578
41	0.227	0.200	0.177	0.02688	0.13425
42	0.210	0.186	0.163	0.02360	0.12662
43	0.210	0.186	0.163	0.02427	0.13068
44	0.215	0.190	0.167	0.02488	0.13069
45	0.208	0.183	0.160	0.02446	0.13364
46	0.235	0.209	0.182	0.02610	0.12475
47	0.238	0.210	0.186	0.02787	0.13261
48	0.241	0.214	0.189	0.02621	0.12225
49	0.237	0.211	0.186	0.02553	0.12074
50	0.249	0.221	0.197	0.02784	0.12616
51	0.243	0.216	0.190	0.02726	0.12633
52	0.246	0.219	0.193	0.02650	0.12100
53	0.249	0.221	0.197	0.02816	0.12736
54	0.248	0.220	0.196	0.02784	0.12638
55	0.238	0.210	0.185	0.02776	0.13188
56	0.150	0.131	0.113	0.01843	0.14040

K.4.2 Low Metastability Parameter Error Analysis

RUN	Cm+	Cm	Cm-	Low error	Low error %	Low error %,ave
1	0.190	0.166	0.143	-0.02261	-0.13629	-0.1256
2	0.192	0.166	0.144	-0.02169	-0.13051	
3	0.191	0.168	0.144	-0.02379	-0.14185	Low Std. Dev.
4	0.196	0.171	0.148	-0.02285	-0.13363	0.0078
5	0.190	0.166	0.144	-0.02230	-0.13421	
6	0.187	0.163	0.141	-0.02183	-0.13388	Low Std. Dev. ratio
7	0.191	0.168	0.145	-0.02324	-0.13825	-0.0620
8	0.201	0.177	0.153	-0.02395	-0.13513	
9	0.193	0.169	0.147	-0.02254	-0.13318	
10	0.190	0.166	0.145	-0.02193	-0.13174	
11	0.199	0.176	0.152	-0.02333	-0.13275	
12	0.189	0.166	0.144	-0.02251	-0.13533	
13	0.196	0.171	0.149	-0.02192	-0.12832	
14	0.178	0.155	0.135	-0.02049	-0.13210	
15	0.172	0.150	0.130	-0.01993	-0.13298	
16	0.180	0.157	0.137	-0.02058	-0.13066	
17	0.192	0.168	0.146	-0.02129	-0.12698	
18	0.195	0.171	0.149	-0.02238	-0.13081	
19	0.194	0.171	0.148	-0.02280	-0.13371	
20	0.191	0.168	0.146	-0.02217	-0.13174	
21	0.182	0.160	0.139	-0.02109	-0.13187	
22	0.192	0.168	0.148	-0.02041	-0.12145	
23	0.188	0.166	0.145	-0.02120	-0.12752	
24	0.188	0.166	0.145	-0.02114	-0.12710	
25	0.187	0.164	0.144	-0.01970	-0.12020	
26	0.187	0.164	0.144	-0.01971	-0.12043	

27	0.169	0.148	0.129	-0.01904	-0.12862
28	0.222	0.197	0.174	-0.02347	-0.11902
29	0.219	0.193	0.171	-0.02224	-0.11517
30	0.223	0.197	0.174	-0.02385	-0.12078
31	0.229	0.203	0.179	-0.02437	-0.12004
32	0.232	0.206	0.181	-0.02442	-0.11877
33	0.211	0.188	0.164	-0.02404	-0.12814
34	0.212	0.187	0.164	-0.02284	-0.12197
35	0.213	0.188	0.165	-0.02289	-0.12152
36	0.214	0.189	0.166	-0.02347	-0.12413
37	0.212	0.187	0.164	-0.02232	-0.11960
38	0.219	0.193	0.171	-0.02216	-0.11498
39	0.221	0.194	0.172	-0.02250	-0.11580
40	0.224	0.199	0.174	-0.02468	-0.12399
41	0.227	0.200	0.177	-0.02330	-0.11641
42	0.210	0.186	0.163	-0.02363	-0.12678
43	0.210	0.186	0.163	-0.02306	-0.12420
44	0.215	0.190	0.167	-0.02368	-0.12438
45	0.208	0.183	0.160	-0.02313	-0.12635
46	0.235	0.209	0.182	-0.02695	-0.12878
47	0.238	0.210	0.186	-0.02445	-0.11634
48	0.241	0.214	0.189	-0.02557	-0.11925
49	0.237	0.211	0.186	-0.02516	-0.11899
50	0.249	0.221	0.197	-0.02416	-0.10948
51	0.243	0.216	0.190	-0.02556	-0.11845
52	0.246	0.219	0.193	-0.02588	-0.11814
53	0.249	0.221	0.197	-0.02432	-0.11002
54	0.248	0.220	0.196	-0.02391	-0.10854
55	0.238	0.210	0.185	-0.02553	-0.12130
56	0.150	0.131	0.113	-0.01822	-0.13880

APPENDIX L
SHOCK ANALYSIS COMPUTER PROGRAMS

L.1 Computer Program for Isentropic Expansion Pressure Determination

The following FORTRAN program was used to calculate the isentropic, subsonic and supersonic expansion nozzle exit pressures. The procedure for this method is fully outlined in Sec. 3.7.2.

```
C$NOEX
C$NOWA
C
C PROGRAM CRITHEM.FOR
C
C THIS PROGRAM CALCULATES THE CRITICAL MASS FLOW RATE, AND REQUIRED BACK
C PRESSURE OF THE NOZZLE FOR ISENTROPIC SUB- OR SUPERSONIC EXPANSION.
C
C VARIABLE DECLARATIONS
      REAL PINMN,XINMN,TINMN,SGINMN,SFINMN,SINMN,HINMN,TTH
      REAL XTHR,VGTH,VFTH,VTH,UTH,MDOT,MDOTL,PE,SE,TE,HE,XE,VGE,VFE
      REAL VE,UE,AE,F,HTH,STH,FROZW
      DOUBLE PRECISION ATH,AESET
      INTEGER I,K
      CHARACTER*4 REF
      REF='RR12'
      I=1
C NOZZLE AREA ASSIGNMENTS
      ATH=7.068583472D-6
      AESET=3.233767855D-5
C SUBROUTINE CALL STATEMENT FOR REFRIGERANT PROPERTIES
      CALL RINIT(REF,IERR)
C INPUT OF AVERAGE NOZZLE INLET PRESSURE USED FOR ANALYSIS
      PINMN=120.0E0
C
C INPUT OF AVERAGE NOZZLE INLET QUALITY
       XINMN=0.081936
C TEMPERATURE AT INLET OF NOZZLE;
      TINMN=T2OFP(REF,PINMN)
C ENTROPY AT NOZZLE INLET
      SINMN=SFOFT(REF,TINMN)+XINMN*SFGOFT(REF,TINMN)
C ENTHALPY AT NOZZLE INLET
      HINMN=H2OFTS(REF,TINMN,SINMN)
```

```
C
      MDOTL=0.0E0
C GUESSED PRESSURE FOR ITERATION
      PTH=PINMN-1.0E0
C LOOP FOR CRITICAL MASS FLOW RATE DETERMINATION
      LOOP
C STATEMENT FOR ISENTROPIC PROCESS
      STH=SINMN
C
C TEMPERATURE, ENTHALPY, QUALITY, AND SPECIFIC VOLUME
C AT GUESSED THROAT PRESSURE
      TTH=T2OFP(REF,PTH)
      HTH=H2OFTS(REF,TTH,STH)
      XTHR=XTH(REF,TTH,HTH)
      VTH=VFOFT(REF,TTH)+XTHR*VFGOFT(REF,TTH)
C
C VELOCITY; END CONSTANT FOR CONVERSION
C OF UNITS TO ft/sec.
      UTH=SQRT(2*(HINMN-HTH)*25033.69673D0)
C
C MASS FLOW
      MDOT=ATH*UTH/VTH*60
C OUTPUT TO SCREEN STATEMENT
      WRITE(*,*) PTH,MDOT
C
C EXIT QUALIFICATION FOR LOOP
      IF (MDOT .LT. MDOTL) THEN
      WRITE(*,*) PINMN,PTH,MDOTL
      GOTO 30
      ENDIF
C
C INCREMENT FOR THROAT PRESSURE GUESS
      PTH=PTH-0.2E0
C RE-ASSIGNMENT OF LAST MASS FLOW CALCULATION TO
C DETERMINE EXIT QUALIFICATION
      MDOTL=MDOT
C END LOOP FOR CRITICAL MASS FLOW RATE CALCULATION
      END LOOP
C
30    CONTINUE
C
C FIRST GUESS FOR ISENTROPIC EXPANSION BACK PRESSURE;
C IF THE SUBSONIC CASE WAS DESIRED, THE EXIT PRESSURE WAS
C EXPECTED TO BE HIGHER THAN THE THROAT PRESSURE FOR CHOKING
C THE ADDITION OF 1 PSI TO THE THROAT PRESSURE CALCULATED ABOVE
C SERVES ONLY TO BEGIN THE CALCULATION
      PE=PTH+1.0E0
C STATEMENT FOR ISENTROPIC PROCESS
      SE=SINMN
C
C BEGINNING OF LOOP FOR ISENTROPIC NOZZLE EXIT PRESSURE
      LOOP
C
C TEMPERATURE, ENTHALPY, QUALITY, AND SPECIFIC VOLUME
C AT GUESSED EXIT PRESSURE
      TE=T2OFP(REF,PE)
```

```
      HE=H2OFTS(REF,TE,SE)
      XE=XTH(REF,TE,HE)
      VE=VFOFT(REF,TE)+XE*VFGOFT(REF,TE)
C
C EXIT VELOCITY
      UE=SQRT(2*(HINMN-HE)*25033.69673D0)
C
C FROM CRITICAL MASS FLOW RATE CALCULATED ABOVE
C THE EXIT AREA CAN BE CALCULATED AND COMPARED TO THE
C ACTUAL NOZZLE EXIT AREA
      AE=MDOTL*VE/UE/60
C
C EXIT QUALIFICATION FOR CALCULATED AND ACTUAL NOZZLE AREAS
      IF (AE .GT. AESET) THEN
      WRITE(*,*) PE,AE,AESET
      GOTO 60
      END IF
C
C INCREMENT FOR EXIT PRESSURE GUESS:
C ADDITION FOR SUBSONIC EXIT PRESSURE
      PE=PE+0.01E0
C
C SUBTRACTION FOR SUPERSONIC EXIT PRESSURE
      PE=PE-0.01E0
      END LOOP
C
50    CONTINUE
C
60    CONTINUE
      END
```

L.2 Computer Program for Back Pressure Nozzle Exit Shock Wave

The following computer program was used to determine the back pressure required for a standing normal shock wave at the nozzle exit plane. A full discussion of this procedure was given in Sec. 3.7.2.

```
C$NOWA
C$NOEX
C
C PROGRAM NOZEX.FOR
C
C VARIABLE DECLARATION
      REAL P2,U2,H2,T2,X2,V2,ROW2,U22,ROW1,U1,H1,P1,S1,T1
      CHARACTER*4 REF
C
      REF='RR12'
C CALL TO REFRIGERANT SUBROUTINES
      CALL RINIT(REF,IERR)
```

```
C
C INPUT OF RESULTS FROM PROGRAM CRITHEM.FOR ABOVE
C ISENTROPIC, SUPERSONIC EXPANSION EXIT PRESSURE
C PRESSURE (psia):
      P1=10.0D0
C VELOCITY (ft/sec):
      U1=500.9D0
C DENSITY (slugs/ft^3):
      ROW1=0.0216543D0
C TEMPERATURE AND ENTHALPY AT ISENTROPIC EXPANSION
C BACK PRESSURE
      T1=T2OFP(REF,P1)
      H1=H2OFTS(REF,T1,S1)
C
C THIS PROGRAM IS A MANUAL ITERATION WITH REQUIRED INPUT
C OF GUESSED PRESSURE
5     WRITE(*,*) 'ENTER THE DOWNSTREAM PRESSURE'
      READ(*,*) P2
C
C VELOCITY OF FLUID AT GUESSED NOZZLE BACK PRESSURE
      U2=((P1-P2)*144+ROW1*U1**2)/ROW1/U1
C
C ENTHALPY AT GUESSED BACK PRESSURE
      H2=0.5D0*(U1**2-U2**2)/25033.69673D0+H1
C
C TEMPERATURE, QUALITY, AND SPECIFIC VOLUME
C AT GUESSED BACK PRESSURE
      T2=T2OFP(REF,P2)
      X2=(H2-HFOFT(REF,T2))/HFGOFT(REF,T2)
      V2=VFOFT(REF,T2)+X2*VFGOFT(REF,T2)
C
C DENSITY AND CONVERSION OF UNITS TO (slugs/ft^3)
      ROW2=1/V2/32.17D0
C
C VELOCITY FROM CONTINUITY EQUATION
      U22=ROW1*U1/ROW2
C OUTPUT OF BOTH VELOCITY CALCULATIONS FOR COMPARISON
      WRITE(*,*)U2,U22
C
      GOTO 5
      END
```

APPENDIX M
ISENTROPIC AND FROZEN ANALYSIS COMPUTER PROGRAM

This appendix contains two FORTRAN computer programs to calculate the following nozzle properties assuming either HEM or frozen conditions:

1. HEM critical mass flow rate,
2. frozen critical mass flow rate,
3. nozzle thrust resulting from isentropic, supersonic expansion,
4. fluid velocity out of nozzle resulting from isentropic, supersonic expansion,
5. nozzle exit pressure resulting from isentropic, supersonic expansion, and
6. nozzle exit pressure resulting from frozen expansion.

The above factors were shown in Appendix I with all the raw data.

M.1 Program for HEM Critical Mass Flow Calculation

```
C$NOEX
C$NOWA
C
C PROGRAM CRITHEM.FOR
C
C THIS PROGRAM CALCULATES THE HEM CRITICAL MASS FLOW RATE, THRUST, AND OUTLET
C PRESSURE OF THE NOZZLE FOR A GIVEN INLET PRESSURE AND QUALITY.
C
C VARIABLE DECLARATIONS
      REAL PINMN(100),XINMN(100),TINMN,SGINMN,SFINMN,SINMN,HINMN,TTH
      REAL XTHR,VGTH,VFTH,VTH,UTH,MDOT,MDOTL,PE,SE,TE,HE,XE,VGE,VFE
      REAL VE,UE,AE,F,HTH,STH,FROZW
      DOUBLE PRECISION ATH,AESET
      INTEGER I,K
      CHARACTER*4 REF
      REF='RR12'
      I=1
C NOZZLE AREA ASSIGNMENTS
      ATH=7.068583472D-6
      AESET=3.233767855D-5
C OPEN EXTERNAL FILE FOR OUTPUT DATA
      OPEN(UNIT=1,FILE='CRITDATA.PRN')
15    FORMAT(2F10.4)
```

```
C
      K=1
C CALL FOR REFRIGERANT SUBROUTINES
      CALL RINIT(REF,IERR)
     OPEN(UNIT=2,FILE='OUTPUT.PRN')
C
     LOOP
C
C INPUT OF DATA
     READ(UNIT=2,END=5,FMT=15) PINMN(I),XINMN(I)
     WRITE(*,*) PINMN(I),XINMN(I)
     I=I+1
     ENDLOOP
5    ENDFILE(UNIT=2)
6     CONTINUE
C
C NOZZLE INLET TEMPERATURE, ENTROPY, AND ENTHALPY
C
      TINMN=T2OFP(REF,PINMN(K))
      SINMN=SFOFT(REF,TINMN)+XINMN(K)*SFGOFT(REF,TINMN)
      HINMN=H2OFTS(REF,TINMN,SINMN)
C
      MDOTL=0.0E0
      PTH=PINMN(K)-1.0E0
C
20     FORMAT(6F11.5)
C
C ITERATION FOR CRITICAL MASS FLOW RATE
C
      LOOP
C
C TEMPERATURE, ENTROPY, ENTHALPY, QUALITY, AND SPECIFIC VOLUME
C AT GUESSED PRESSURE
C
      TTH=T2OFP(REF,PTH)
      STH=SINMN
      HTH=H2OFTS(REF,TTH,STH)
      XTHR=XTH(REF,TTH,HTH)
      VTH=VFOFT(REF,TTH)+XTHR*VFGOFT(REF,TTH)
C
C VELOCITY AT NOZZLE THROAT FOR GUESSED PRESSURE
      UTH=SQRT(2*(HINMN-HTH)*25033.69673D0)
C
C MASS FLOW RATE
      MDOT=ATH*UTH/VTH*60
C OUTPUT STATEMENT
      WRITE(*,*) PTH,MDOT
C
C THROAT PRESSURE INCREMENT
      PTH=PTH-0.2E0
C
C EXIT QUALIFICATION
      IF (MDOT .LT. MDOTL) THEN
      WRITE(*,*) PINMN(K),PTH,MDOTL
      GOTO 30
      ENDIF
```

```
C
      MDOTL=MDOT
      END LOOP
C
30    CONTINUE
C
      PE=119.0D0
      SE=SINMN
C
C ITERATION LOOP FOR EXIT PRESSURE, AND VELOCITY
C
      LOOP
C
C TEMPERATURE, ENTHALPY, QUALITY, AND SPECIFIC VOLUME AT NOZZLE EXIT
C FOR GUESSED EXIT PRESSURE
C
      TE=T2OFP(REF,PE)
      HE=H2OFTS(REF,TE,SE)
      XE=XTH(REF,TE,HE)
      VE=VFOFT(REF,TE)+XE*VFGOFT(REF,TE)
C VELOCITY AT NOZZLE EXIT
      UE=SQRT(2*(HINMN-HE)*25033.69673D0)
C
C NOZZLE EXIT AREA CALCULATION
      AE=MDOTL*VE/UE/60
C NOZZLE THRUST
      F=MDOTL*UE/1930.2D0
C
C EXIT QUALIFICATION
      IF (AE .GT. AESET) THEN
      WRITE(*,20) PINMN(K),PTH,PE,MDOTL,F,UE
      GOTO 60
      END IF
C
C EXIT PRESSURE INCREMENT
      PE=PE+0.0001
C
      END LOOP
C
50    CONTINUE
C
C END OF FILE EXIT LOOP QUALIFICATION
      K=K+1
C     WRITE(*,*) K,I
      IF (K .EQ. I) GO TO 60
      GOTO 6
60    CONTINUE
      END
```

M.2 Program for Frozen Critical Mass Flow Calculation

```
C$NOEX
C$NOWA
C
C PROGRAM CRITFROZ.FOR
C
C THIS PROGRAM CALCULATES THE FROZEN CRITICAL MASS FLOW RATE, AND OUTLET
C PRESSURE OF THE NOZZLE FOR A GIVEN INLET PRESSURE AND QUALITY.
C
C VARIABLE DECLARATIONS
      REAL PINMN(100),XINMN(100),TINMN,SGINMN,SFINMN,SINMN,HINMN,TTH
      REAL XTHR,VGTH,VFTH,VTH,UTH,MDOT,MDOTL,PE,SE,TE,HE,XE,VGE,VFE
      REAL VE,UE,AE,F,HTH,STH,FROZW
      DOUBLE PRECISION ATH,AESET
      INTEGER I,K
      CHARACTER*4 REF
      REF='RR12'
      I=1
C NOZZLE AREA ASSIGNMENTS
      ATH=1.01787602D-3
      AESET=4.656625711D-3
      OPEN(UNIT=1,FILE='CRITDATA.PRN')
15    FORMAT(2F10.4)
C
      K=1
C CALL TO REFRIGERANT SUBROUTINES
      CALL RINIT(REF,IERR)
C FILE RETRIEVAL FROM EXTERNAL SOURCE
      OPEN(UNIT=2,FILE='OUTPUT.PRN')
      LOOP
      READ(UNIT=2,END=5,FMT=15) PINMN(I),XINMN(I)
      I=I+1
      ENDLOOP
5     ENDFILE(UNIT=2)
6     CONTINUE
C
C NOZZLE INLET TEMPERATURE, ENTROPY, AND ENTHALPY
      TINMN=T2OFP(REF,PINMN(K))
      SINMN=SFOFT(REF,TINMN)+XINMN(K)*SFGOFT(REF,TINMN)
      HINMN=H2OFTS(REF,TINMN,SINMN)
C
      MDOTL=0.0E0
      PTH=PINMN(K)-1.0E0
C
20    FORMAT(6F11.5)
C
C ITERATION FOR CRITICAL MASS FLOW RATE
C
      LOOP
C
C TEMPERATURE, QUALITY, ENTROPY, ENTHALPY, AND SPECIFIC VOLUME
C AT GUESSED THROAT PRESSURE
```

```
C
      TTH=T2OFP(REF,PTH)
      XTHR=XINMN(K)
      STH=SFOFT(REF,TTH)+XTHR*SFGOFT(REF,TTH)
      HTH=H2OFTS(REF,TTH,STH)
      VTH=VFOFT(REF,TTH)+XTHR*VFGOFT(REF,TTH)
C
C THROAT VELOCITY
      UTH=SQRT(2*(HINMN-HTH)*25033.69673D0)
C
C MASS FLOW RATE
      FROZW=ATH*UTH/VTH/144*60
C
C THROAT PRESSURE INCREMENT
      PTH=PTH-0.2E0
C
C EXIT QUALIFICATION
      IF (FROZW .LT. MDOTL) THEN
      WRITE(*,*) PINMN(K),PTH,MDOTL
      WRITE(1,*) PINMN(K),PTH,MDOTL
      GOTO 50
      ENDIF
C
      MDOTL=FROZW
      END LOOP
C
30    CONTINUE
C
      PE=PTH
      SE=SINMN
C
C ITERATION FOR NOZZLE EXIT PRESSURE
      LOOP
C TEMPERATURE, ENTHALPY, QUALITY, AND SPECIFIC VOLUME FOR
C GUESSED EXIT PRESSURE
      TE=T2OFP(REF,PE)
      HE=H2OFTS(REF,TE,SE)
      XE=XTHR
      VE=VFOFT(REF,TE)+XTHR*VFGOFT(REF,TE)
C
C EXIT VELOCITY
      UE=SQRT(2*(HINMN-HE)*25033.69673D0)
C
C NOZZLE EXIT AREA
      AE=MDOTL*VE/UE*144
C
C EXIT QUALIFICATION
      IF (AE .GT. AESET) THEN
      WRITE(1,20) PINMN(K),PTH,PE,MDOTL,F,UE
      WRITE(*,20) PINMN(K),PTH,PE,MDOTL,F,UE
      GOTO 50
      END IF
C
C EXIT PRESSURE INCREMENT
      PE=PE-0.2
C
```

```
      END LOOP
C
50    CONTINUE
C
      K=K+1
C     WRITE(*,*) K,I
      IF (K .EQ. I) GO TO 60
      GOTO 6
60    CONTINUE
      END
```

REFERENCES

1. Menegay, P., "Experimental Investigation of an Ejector as a Refrigerant Expansion Engine," MS Thesis, Virginia Polytechnic Institute and State University, 1991.
2. Menegay, P., "Data from Experimentation," Virginia Polytechnic Institute and State University, 1993.
3. Kornhauser, A.A., "The Use of an Ejector as a Refrigerant Expander," *Proceedings of the 1990 USNC/IIR-Purdue Refrigeration Conference*, Purdue University, 1990.
4. Ohta, J., Fujii, T., Akagawa, K., & Takenaka, N., "Performance and Flow Characteristics for Nozzles for Initially Subcooled Hot Water (Influence of Turbulence and Decompression Rate)," *International Journal of Multiphase Flow*, Vol. 19, 1993, pp. 125-36.
5. Akagawa, K., Fujii, T., Ohta, J., Inoue, K. & Taniguchi, K., "Performance Characteristics of Convergent-Divergent Nozzles for Subcooled Hot Water," *International Journal of the JSME Serial II*, Vol. 31, 1988b, pp. 718-26.
6. Reynolds, J., "Special R-12 Ejector," Croll Reynolds Co., Oct. 11, 1990.
7. Kornhauser, A.A., & Menegay, P., "Patent for Bubbly Flow Elements," Virginia Polytechnic Institute and State University, 1992.
8. Shaw, G.V., & Loomis, A.W., ed. Cameron Hydraulic Data, Ingersoll-Rand Company, New York, N.Y., 1951, p. 91.
9. Spotts, M.F., Design of Machine Elements, 4th Ed., Prentice-Hall, Englewood Cliffs, N.J., 1971, pp. 478-82.
10. Deutschman, A.D., Michels, & W.J., Wilson, C.E., Machine Design: Theory and Practice, Macmillan, New York, N.Y., 1975, pp. 815-7.
11. Measurements Group Inc., Catalog 500: Precision Strain Gages. January, 1993, pp. 4-10.
12. Micro-Measurements Instruction Bulletin B-129-4, "Surface Preparation for Strain Gage Bonding," Measurements Group Inc., Raleigh, N.C.
13. Micro-Measurements Instruction Bulletin B-130-9, "Strain Gage Installations with M-Bond 43-B, 600, and 610 Adhesive Systems," Measurements Group Inc., Raleigh, N.C.

14. Asea Brown Boveri Specification Sheet 4-11, "1330L Integral Orifice Flow Elements 1/2, 1, 1-1/2" Pipe Sizes," Asea Brown Boveri Kent-Taylor Co., Rochester, N.Y.
15. Daniel Flow Products Catalog H-1900, "Honed Flow Sections," Danial Flow Products, Inc., Houston, TX.
16. Harrison of Texas, Pipe Honing Company, Houston, TX.
17. ASME Research Committee on Fluid Meters, Fluid Meters: Their Theory and Application, ed. H.S. Bean, ASME, 1971, pp.180-1.
18. Stearns, R.F., Johnson, R.R., Jackson, R.M., Larson, C.A., Flow Measurement with Orifice Meters, D. Van Nostrand, New York, N.Y., 1951.
19. Omega Engineering, Inc., OMEGA Complete Temperature Measurement Handbook and Encyclopedia, Vol. 28, Technical Reference Section Z.
20. Data Translation Document UM-06160-E, "User Manual for DT2811," Data Translation, Inc., Marlboro, MA.
21. Schenck, H., Jr., Theories of Engineering Experimentation, McGraw-Hill, New York, N.Y., 1968.
22. Hy-Cal Engineering Bulletin PD-2311, "T/C Reference Block," Hy-Cal Engineering, El Monte, CA.
23. Anderson, J.D., Modern Compressible Flow with Historical Perspective, 2nd Ed., McGraw-Hill, New York, N.Y., 1990.
24. Moody, F.J., "A Pressure Pulse Model for Two-Phase Critical Flow and Sonic Velocity," *Journal of Heat Transfer*, Vol. 91-C, August, 1969, pp. 372-84.
25. Collingham, R.E., & Firey, J.C., "Velocity of Sound Measurements in Wet Steam," *Industrial Engineering and Chemical Process Design and Development*, Vol. 2, no. 3, July, 1963, pp. 197-202.
26. Dejong, V.J., & Firey, J.C., "Effect of Slip and Phase Change on Sound Velocity in Steam-Water Mixtures and the Relation to Critical Flow," *Industrial Engineering and Chemical Process Design and Development*, Vol. 7, no. 3, July, 1968, pp. 454-63.
27. Jung, D., & Radermacher, R., "Transport Properties and Surface Tension of Pure and Mixed Refrigerants," ASHRAE Transactions pt. 1, 1991, pp. 90-9.
28. Jones, J.B., & Hawkins, G.A., Engineering Thermodynamics: An Introductory Textbook, 2nd Ed., Wiley, New York, N.Y., 1986, p. 522.
29. Powell, R.L., et al. "Thermocouple Reference Tables Based on the IPTS-68," US Department of Commerce, NBS Monograph 125, March 1974, p. 183.

The vita has been removed from the scanned document